

Non-equilibrium Functional Renormalization for Driven-Dissipative Bose-Einstein Condensation

L. M. Sieberer^{1,2}, S. D. Huber^{3,4}, E. Altman^{4,5}, and S. Diehl^{1,2}

¹*Institute for Theoretical Physics, University of Innsbruck, A-6020 Innsbruck, Austria*

²*Institute for Quantum Optics and Quantum Information of the Austrian Academy of Sciences, A-6020 Innsbruck, Austria*

³*Theoretische Physik, Wolfgang-Pauli-Straße 27, ETH Zurich, CH-8093 Zurich, Switzerland*

⁴*Department of Condensed Matter Physics, Weizmann Institute of Science, Rehovot 76100, Israel and*

⁵*Department of Physics, University of California, Berkeley, CA 94720, USA*

(Dated: September 27, 2013)

We present a comprehensive analysis of critical behavior in the driven-dissipative Bose condensation transition in three spatial dimensions. Starting point is a microscopic description of the system in terms of a many-body quantum master equation, where coherent and driven-dissipative dynamics occur on an equal footing. An equivalent Keldysh real time functional integral reformulation opens up the problem to a practical evaluation using the tools of quantum field theory. In particular, we develop a functional renormalization group approach to quantitatively explore the universality class of this stationary non-equilibrium system. Key results comprise the emergence of an asymptotic thermalization of the distribution function, while manifest non-equilibrium properties are witnessed in the response properties in terms of a new, independent critical exponent. Thus the driven-dissipative microscopic nature is seen to bear observable consequences on the largest length scales. The absence of two symmetries present in closed equilibrium systems – underlying particle number conservation and detailed balance, respectively – is identified as the root of this new non-equilibrium critical behavior. Our results are relevant for broad ranges of open quantum systems on the interface of quantum optics and many-body physics, from exciton-polariton condensates to cold atomic gases.

PACS numbers: 67.25.dj,64.60.Ht,64.70.qj,67.85.Jk

I. INTRODUCTION

In recent years, there has been tremendous progress in realizing systems with many degrees of freedom, in which matter is strongly coupled to light.¹ This concerns vastly different experimental platforms: In ensembles of ultracold atoms, the immersion of a Bose-Einstein condensate (BEC) into an optical cavity has allowed to achieve strong matter-light coupling, and lead to the realization of open Dicke models.^{2–4} In the context of semiconductor quantum wells in optical cavities, non-equilibrium Bose condensation has been achieved^{5–7} – here the effective degrees of freedom, the exciton-polaritons, result from a strong hybridization of cavity light and excitonic matter degrees of freedom.^{1,8,9} Further promising platforms, which are at the verge of the transition to true many-body systems, are arrays of microcavities^{10–13} or trapped ions,^{14,15} but also optomechanical setups.^{16–18}

Those systems have three key properties in common. First, they are strongly driven by external fields, such as lasers, placing them far away from thermodynamic equilibrium even under stationary conditions. Equilibrium detailed balance conditions therefore are not generically present. Second, they exhibit the characteristics of both quantum optical setups, in that coherent and dissipative dynamics occur on an equal footing, but also genuine many-body systems, in that they dispose of a continuum of spatial degrees of freedom. Finally, a third characteristic is the absence of the conservation of particle number. In particular, the admixture of light opens up strong loss channels for the effective hybrid light-matter degrees of freedom. This makes it necessary to counterpoise these losses by continuous pumping mechanisms in order to achieve stable stationary flux equilibrium states. The pumping mechanisms can be either coherent or incoherent. In the latter case, e.g., sin-

gle particle pumping directly counteracts the incoherent single particle loss; once it starts to dominate over the losses, a second order phase transition results on the mean-field level, in close analogy to a laser threshold.

At this point a clear difference between the quantum optical single mode problem of a laser and a driven-dissipative many-body problem becomes apparent: While the inclusion of fluctuations in the laser case smears out the mean-field transition, in a system with a continuum of spatial degrees of freedom a genuine out-of-equilibrium second order phase transition with true universal critical behavior can be expected. The theoretical challenge is then to understand the universal phenomena that can emerge due to the many-body complexity in a non-equilibrium setting.

In this work we address this challenge, focusing on a key representative that shows all the above characteristics: The driven-dissipative Bose condensation transition, relevant to experiments with exciton-polariton condensates, or more generally to any driven-dissipative system equipped with a $U(1)$ symmetry of global phase rotations tuned to its critical point. We provide a comprehensive characterization of the resulting non-equilibrium critical behavior in three dimensions, extending and corroborating results presented recently.¹⁹ A key finding concerns the existence of a new critical exponent associated with the non-equilibrium drive. It describes universal decoherence at long distances, and is observable, e.g., in the single particle response, as probed in homodyne detection of exciton-polariton systems.²⁰ This provides evidence that the microscopic non-equilibrium character bears observable consequences up to the largest distances in driven Bose condensation. Furthermore, an asymptotic thermalization mechanism for the low frequency distribution function is found, reflected in an emergent symmetry at the Wilson-Fisher fixed point.

An important aspect of this article is to provide a de-

tailed exposition of our theoretical approach to open markovian many-body quantum systems, which may be applied and generalized to a vast variety of non-equilibrium situations, such as driven or driven-dissipative systems with different symmetries,^{21–24} driven-dissipative systems with disorder,²⁵ or even superfluid turbulence.^{26–29} We start from a second quantized description in terms of quantum master equations, with the goal of making the paper accessible to researchers working on the interface of quantum optics and many-body physics. Translating the master equation into a Keldysh real-time functional integral opens up the well-established toolbox of quantum field theory for the investigation of such systems. Here, we develop a functional renormalization group (FRG) approach based on the Wetterich equation³⁰ for the practical evaluation of the problem, which constitutes an exact reformulation of the many-body functional integral in terms of a functional differential equation. This method encompasses not only the critical physics as more conventional renormalization group (RG) approaches, but also non-universal many-body physics of a given problem. In particular, in this work we use it for the determination of the Ginzburg scale delimiting the extent of the critical domain as relevant for possible experimental observations, from a full numerical solution of the set of non-linear renormalization group equations.

The paper is organized as follows: We present our key results and sketch the resulting physical picture in the following section. A pedagogical introduction to our approach is provided in Sec. III, where we discuss the mapping of the master equation to an equivalent Keldysh functional integral. In this framework we reproduce the results from mean-field and Bogoliubov theory, and show how the physics of a semi-classical driven-dissipative Gross-Pitaevskii equation emerges naturally as a low frequency limit of the full quantum master equation. We highlight the additional challenges tied to the continuum of spatial degrees of freedom when it comes to the analysis of critical behavior, and show how they are properly addressed by means of the FRG approach. The precise manifestation of the non-equilibrium character of the problem is worked out in Sec. IV. A detailed comparison of our non-equilibrium versus more conventional equilibrium models shows that both situations can be distinguished by means of a symmetry which is only present in equilibrium and expresses detailed balance. Sec. V summarizes the computation of the flow equations, as well as the extraction of the universal behavior in terms of the set of critical exponents. It also presents in detail the hierarchical structure of criticality in non-equilibrium systems. In Sec. VII we discuss the numerical analysis of the flow equations. We conclude in Sec. VIII.

II. KEY RESULTS AND PHYSICAL PICTURE

Driven-dissipative Bose condensation transition – Driven open quantum systems are commonly modeled microscopically by means of quantum master equations or in terms of Keldysh functional integrals as shown below. However, critical dynamics is captured by an effective long-wavelength description, valid in the vicinity of a phase transition. According

to the arguments presented in Sec. III F below, we obtain such an effective model by dropping irrelevant (in the sense of the RG) terms in the microscopic description. On the other hand, the effective long-wavelength model must include effects such as particle diffusion that are not contained in the microscopic model but become important close to the critical point. As a result, the stochastic equation of motion for the order parameter of driven-dissipative Bose condensation may be cast in Langevin form,

$$i\partial_t\psi = \left[-(A - iD)\Delta - \mu - \frac{i}{2}(\gamma_l - \gamma_p) + (g - i\gamma_l)|\psi|^2 \right] \psi + \xi. \quad (1)$$

Such a dissipative stochastic Gross-Pitaevskii equation has been used as a model for exciton-polariton condensates.^{31–36} In addition to terms describing coherent dynamics, which are propagation $A = 1/(2m)$, the chemical potential μ and elastic two-body interactions g , it features dissipative contributions: Apart from diffusion D , we have single-particle loss and gain as well as two-body loss which occur at rates γ_l , γ_p , and γ_t , respectively. The different physical origin of coherent and dissipative dynamics is a key difference to the familiar models of dynamical critical phenomena³⁷ and underlies the existence of the new universal critical behavior described below. Loss and pump processes induce noise, which is taken into account by the Gaussian white noise source ξ with zero mean, $\langle \xi(t, \mathbf{x}) \rangle = 0$, and correlations

$$\langle \xi(t, \mathbf{x}) \xi^*(t', \mathbf{x}') \rangle = \frac{\gamma_l + \gamma_p}{2} \delta(t - t') \delta(\mathbf{x} - \mathbf{x}'). \quad (2)$$

Equation (1) admits for a time-independent homogeneous mean-field solution $|\psi_0|^2 = (\gamma_p - \gamma_l)/(2\gamma_t)$ if the single-particle pump rate γ_p exceeds the corresponding loss rate γ_l . The chemical potential is then given by $\mu = g|\psi_0|^2$. We see that the order parameter ψ_0 vanishes continuously as the effective single-particle pump rate $\gamma_p - \gamma_l$ goes to zero, which is the hallmark of a second order phase transition, leading us to expect universal critical behavior.

However, we emphasize that mean-field theory misses any kind of non-trivial critical behavior below the upper critical dimension $d_c = 4$ (while it becomes appropriate above). More precisely, it describes the physics at the non-interacting ‘‘Gaussian’’ fixed point with rational-valued, dimension-independent critical exponents, while in dimensions $d < 4$ the true critical behavior is governed by the interacting ‘‘Wilson-Fisher’’ fixed point with irrational and dimension-dependent exponents, see, e.g., Refs.^{38,39}. This non-trivial behavior is to be extracted here.

Universality and extent of the critical domain – Our FRG analysis confirms the expectation of universal critical behavior in the driven-dissipative Bose condensation transition. This is illustrated in Fig. 1 (cf. also Sec. VII), where the emergence of universality in a system tuned to the critical point is clearly visible: The flow of real and imaginary parts of the complex couplings (corresponding to Hamiltonian and dissipative contributions to the dynamics) are clearly attracted to their fixed points, irrespective of the initial conditions. We note that the persistence of a second order transition under

inclusion of fluctuations is not guaranteed in general, as witnessed by the Coleman-Weinberg (or Halperin-Lubensky-Ma) mechanism of fluctuation induced first order transitions.^{40,41}

An important non-universal aspect of the phase transition concerns the extent of the critical domain, which is delimited by the Ginzburg momentum scale k_G . Knowledge of this scale is a key ingredient for estimating experimental requirements. We find it to be given by (cf. Sec. VII)

$$k_G = \gamma_\Lambda \kappa_\Lambda / (2CD_\Lambda^2), \quad (3)$$

where $C \approx 14.8$ and γ_Λ , κ_Λ , and D_Λ are, respectively, the noise-strength, two-body loss rate and diffusion constant appearing in the description of the system at a mesoscopic scale Λ (see Sec. III G). Here we confirm this behavior quantitatively by a full numerical solution of the flow equations outside the critical domain, highlighting the capability of the FRG approach to compute universal and non-universal physics in a single framework.

Hierarchical shell structure of non-equilibrium criticality – A key result is the hierarchical structure, in which the non-equilibrium criticality is organized. The three shells contain different classes of critical exponents, respectively.

The innermost shell in this hierarchy contains the two independent exponents ν, η describing the static (spatial) critical behavior, which is present already in the classical $O(2)$ model.⁴² We find the static exponents to coincide with those of an *ab initio* computation of the classical $O(2)$ exponents at the same level of approximation. Thus, the non-equilibrium conditions do not modify the static critical behavior.

The intermediate shell contains the so-called dynamical exponent z , which describes the dynamical (temporal) critical behavior. This intermediate shell is already present in models for equilibrium dynamical criticality. Crucially, it extends the static critical behavior but does not modify it. In fact, there is a certain dynamical fine structure: the same static universality class splits up into various dynamical universality classes, classified in models A to F by Hohenberg and Halperin (HH).³⁷ Again, we find the dynamic exponents to coincide with the one of an *ab initio* computation for one of HH's models (model A) – the non-equilibrium conditions do not modify the dynamical critical behavior either. A stronger physical consequence of this finding is discussed in the next subsection.

The outer shell identified in¹⁹ is new, however. The new exponent η_r making up this shell physically describes universal decoherence as explained below. Crucially, it relates to the dynamical model A in the same pattern as model A relates to the classical $O(2)$ model: It adds a new shell, but does not “feed back” or modify the ones enclosed. This outer shell also contains a certain fine-structure as discussed below.

Asymptotic thermalization of the distribution function –

Regarding the intermediate shell of the hierarchy, we not only find z of model A unmodified by the non-equilibrium conditions, but also the emergence of an “equilibrium symmetry”, cf. Sec. IV. The symmetry is implied by the relation $\eta_z = \eta_\gamma$, where η_z and η_γ are the anomalous dimensions of the wave-function renormalization and the noise strength, respectively, cf. Sec. V. In turn, the presence of the symme-

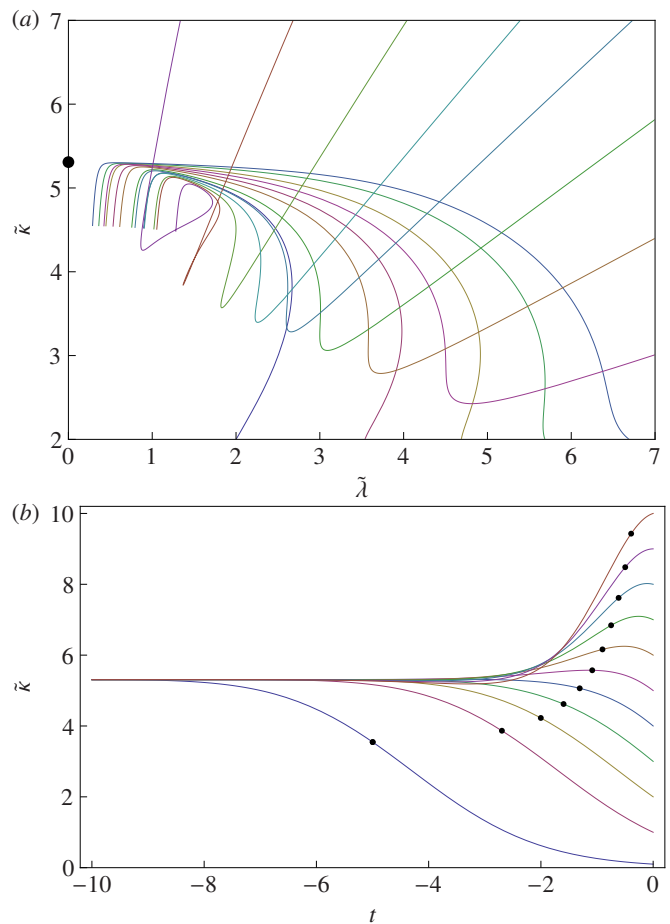


Figure 1. Emergence of universality: (a) The flow of the complex renormalized two-body coupling $\tilde{u}_2 = \tilde{\lambda} + i\tilde{\kappa}$ (see Sec. VI A) is attracted to the Wilson-Fisher fixed point $\tilde{u}_{2*} = i5.308$ irrespective of the initial value \tilde{u}_Λ . Fine-tuning of the initial values w_Λ of the dimensionless mass parameter results in trajectories that approach the fixed point (indicated by the black dot) before eventually being driven towards the symmetric phase with $w = 0$. We show numerical solutions to the flow equations for $r_{K\Lambda} = 10$, $r_{u_3\Lambda} = 1$, $\tilde{\kappa}_{3\Lambda} = 0.01$, and values of $\tilde{u}_{2\Lambda}$ lying on a rectangle with sides $\tilde{\lambda} \in [0, 10]$, $\tilde{\kappa} = 2, 10$ and $\tilde{\lambda} = 10, \tilde{\kappa} \in [2, 10]$. (b) Flow of $\tilde{\kappa}$ as a function of the dimensionless cutoff $t = \ln(k/\Lambda)$ for various starting values $\tilde{\kappa}_\Lambda$. Dots on the lines indicate the extent of the critical domain, which is set by the Ginzburg scale Eq. (129). Initial values are the same as in (a), apart from $\tilde{\kappa}_\Lambda = 0.1, 1, 2, \dots, 10$ and $r_{u_2\Lambda} = 10$.

try implies a fluctuation-dissipation theorem (FDT), or, more physically speaking, a detailed balance condition.

In order to better understand this aspect, consider an equilibrium problem with detailed balance. All subparts of the system are thus in equilibrium with each other. This means that we can choose an arbitrary bipartition of the system, average over or integrate out the degrees of freedom in one of them, and determine the temperature in the remaining part: No matter how the partition is chosen, the same temperature is found. In other words, temperature is partition invariant in an equilibrium system. This statement is easily translated into a RG language: The natural system partitions are the mo-

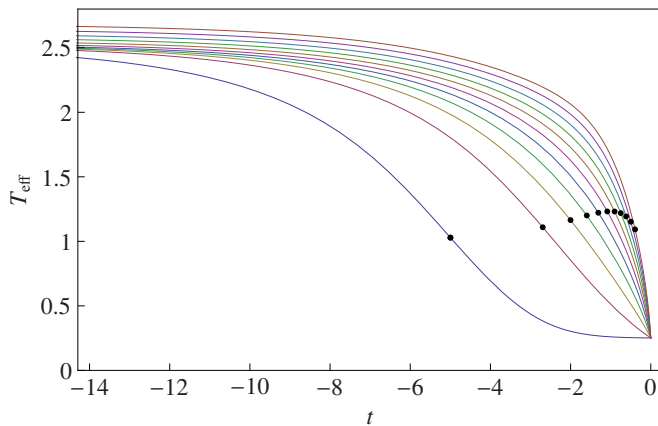


Figure 2. Scale dependence at criticality of the effective temperature $T_{\text{eff}} = \tilde{\gamma}/(4|Z|)$, where $\tilde{\gamma}$ denotes the dimensionless Keldysh mass and Z is the wave-function renormalization (see Secs. III G and VI A). For $t \rightarrow -\infty$ the effective temperature saturates to a constant value. Initial values are the same as in Fig. 1, (b).

mentum shells. Partition invariance of the temperature thus becomes a scale invariance of temperature under renormalization, which successively integrates out high momentum shells. The “equilibrium symmetry” expresses precisely this physical intuition.

In a non-equilibrium problem as ours, this property and the associated symmetry are manifestly absent in general, i.e., at arbitrary momentum scales. However, our results imply the emergence of this symmetry in the universal critical domain delimited by the Ginzburg scale. In order to quantify this observation, we compute the scale dependence of an effective temperature, entering the (non-equilibrium) FDT, cf. Sec. IV. Indeed, we find non-universal scale dependent behavior at high momentum scales, while becoming universal and scale independent within the Ginzburg domain, cf. Fig. 2. We may thus speak of an asymptotic low-frequency thermalization of the critical driven open system.

Independence of the new critical exponent and maximality of the extension – It is important to demonstrate the independence of the new exponent: At a second order phase transition, many critical exponents can be defined, each characterizing a different observable. However, only few of them are independent, i.e., cannot be expressed in terms of a smaller set by means of scaling relations.

In our FRG approach, the independence of the four above described exponents is reflected in the deep infrared behavior of the flow equations. More precisely, it is expressed in a block diagonal structure of the stability matrix encoding the universal behavior in the vicinity of the Wilson-Fisher fixed point, cf. Sec. VI: There are two blocks, and the lowest eigenvalue of each of them determines an independent critical exponent. In addition we have the independent anomalous dimension η and the dynamical exponent z . Moreover, a complementary argument can be given from the opposite, ultraviolet limit of the problem.

To this end, recall that any independent critical exponent must be related to a short-distance mass scale in the

problem.⁴³ Indeed, the length dimension of a spatial two-point correlation function in d dimensions is $\langle \phi^*(\mathbf{x})\phi(\mathbf{0}) \rangle \sim L^{2-d}$. This contrasts with the observed long-distance behavior $\sim |\mathbf{x}|^{2-d+\eta}$ with the so-called anomalous dimension η . The reason for this discrepancy must be rooted in a compensating short distance scale, so that indeed $\langle \phi^*(\mathbf{x})\phi(\mathbf{0}) \rangle \sim a^{-\eta} |\mathbf{x}|^{2-d+\eta} \sim L^{2-d}$. Therefore, to determine the number of independent critical exponents we only need to count the mass scales in the problem. The corresponding part of the action reads

$$\mathcal{S}_m = \int dt d^d \mathbf{x} \left[(\phi_c^*, \phi_q^*) \begin{pmatrix} 0 & \mu - i\kappa_1 \\ \mu + i\kappa_1 & i\gamma \end{pmatrix} \begin{pmatrix} \phi_c \\ \phi_q \end{pmatrix} + f (J_c^* \phi_q + J_q^* \phi_c + \text{c.c.}) \right], \quad (4)$$

with real parameters μ, κ_1, γ, f . κ_1 and f have direct counterparts in the classical $O(2)$ model, describing the tuning parameter for the phase transition and an external magnetic field, respectively. They give rise to the two critical exponents ν (characterizing the divergence of the correlation length) and η (the anomalous dimension of the static two-point function). γ is introduced in the theory of dynamical critical phenomena and is associated to the dynamical exponent in the purely relaxational model A of HH.³⁷ In the full non-equilibrium problem however, there is yet another mass scale μ . This scale is at the origin of the additional independent exponent identified in Ref.¹⁹.

There are two immediate implications of this discussion. First, we conclude that the extension of criticality is maximal, i.e., no more independent exponents will be found. This is due to general requirements on the mass matrix above: the off-diagonal elements must be hermitean conjugates; the lower diagonal must be anti-hermitean; and the upper diagonal must be zero due to the conservation of probability. Second, the case of a discrete Z_2 Ising symmetry rules out an imaginary mass term ($\kappa_1 = 0$), so that in this case no modification of the above kind of the known equilibrium criticality can occur in such systems. This concerns, for example, open Dicke models.^{2,3}

Non-Equilibrium character and fine-structure of the outer shell – Non-Equilibrium conditions are characterized by the absence of the equilibrium symmetry discussed in Sec. IV. In particular, the simultaneous presence of coherent (reversible) and dissipative (irreversible) couplings are not indicative of a distinction between equilibrium and non-equilibrium. However, as explained in Sec. IV, the symmetry implies a geometric constraint on the location of the couplings in the complex plane: In an equilibrium system, all couplings must lie on a single ray, cf. Fig. 3. No such constraint is present out-of-equilibrium.

As shown in Sec. VIC, this gives rise to a fine-structure in the outer shell, determining the drive exponent η_r . The latter is determined by the slowest flow of the couplings towards the imaginary axis (where the Wilson-Fisher fixed point is located), i.e., by the lowest eigenvalue in the corresponding block of the stability matrix. Clearly, the equilibrium situation with all couplings on a single ray is contained in the more general non-equilibrium case, as it may be viewed as

one of the eigenvectors of the more general situation. We find in Sec. VIC that the eigenvalue associated to the symmetry constrained equilibrium flow is not the smallest one. The lowest eigenvalue, therefore, manifestly describes non-equilibrium physics. The physical understanding of this finding can thus be seen as a consequence of the *independence* of coherent and dissipative dynamics, which generically gives rise to non-equilibrium conditions, where real and imaginary parts are not related to each other, as they result from different physical origins.

While this proves formally the non-equilibrium character, the equilibrium situation constructed in the above way may seem a bit academic. In fact, the locking of the ratios of all coherent vs. dissipative couplings amounts to an unrealistic fine-tuning. Indeed, there is a second, much more physical difference of our setting to the standard equilibrium Bose condensation transition, provided by the presence of an exact particle number conservation in the latter – and only the latter – case. It can be seen that the exact particle number conservation rules out a finite κ_1 mass term.⁴⁴ Therefore, the standard equilibrium Bose condensation transition only exhibits three independent exponents, and no counterpart to η_r . However, as an additional consequence of the exact particle number conservation, additional slow modes occur at criticality. They modify the *dynamical* exponent, which is given by the one of model E, instead of model A.

In summary, the differences between our driven and the conventional equilibrium Bose condensation transition concern both the value of the dynamical exponent and the existence of the drive exponent, and therefore are rather substantial.

Interpretation and observability of the new exponent –

The new critical exponent describes the universal flow behavior of all possible ratios of coherent vs. dissipative couplings (real vs. imaginary parts) to zero upon moving to larger and larger distances. In the competition of coherent and dissipative dynamics, loosely speaking dissipation always wins. Physically, this should be interpreted as a universal mechanism of decoherence. The new exponent therefore is subleading and not observable in the correlation functions of the system. However, it is directly observable in the single particle dynamical response (single particle retarded Green's function).

This dynamical response can be measured with any probe that couples directly to the field operator $\hat{\psi}(x)$, i.e., any probe that out-couples single particles from the system. This is the case, e.g., in the angle-resolved detection of leakage photons in exciton-polariton systems,²⁰ or in angle-resolved radio-frequency spectroscopy in ultra-cold atoms.⁴⁵ As we argue in Sec. VIC, the excitation spectrum close to the critical point is given by

$$\omega(q) \sim A_0 q^{z-\eta_r} - iD_0 q^z \sim A_0 q^{2.223} - iD_0 q^{2.121}, \quad (5)$$

where A_0 and D_0 are non-universal constants. This excitation spectrum leads to a broadened signal in the experiment, cf. Fig. 4. The new exponent η_r can be observed due to the different scaling with momentum of the location ($\sim q^{z-\eta_r}$) and the width ($\sim q^z$) of the measured peak. We note here, how-

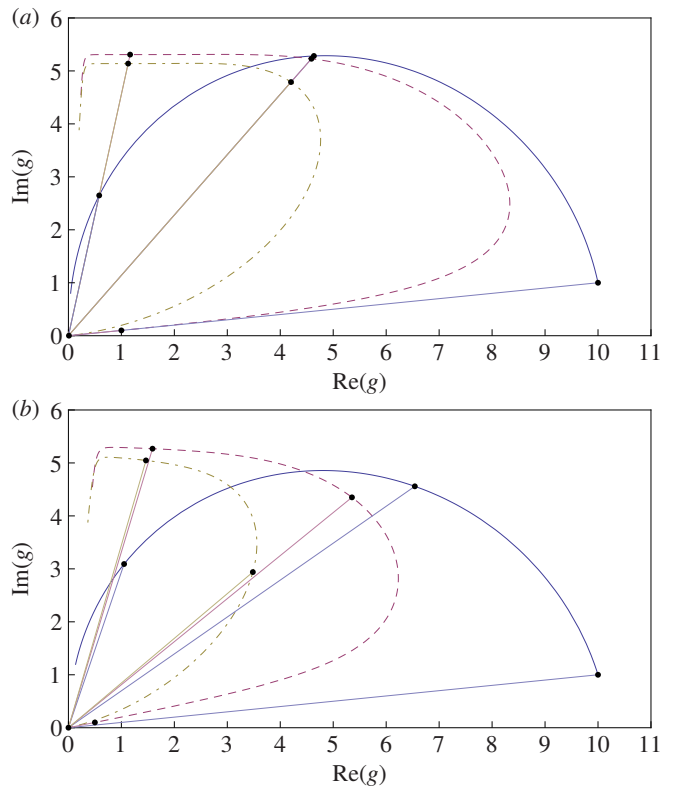


Figure 3. Equilibrium vs. non-equilibrium flow: Real and imaginary parts of various couplings defining the RG flow of the effective action. (a) The equilibrium flow is constrained by a symmetry expressing detailed balance, which fixes all couplings to lie on a single ray in the complex plane. (b) No such symmetry and geometric constraint is present out-of-equilibrium. This difference in symmetry, physically describing the independence of coherent and dissipative dynamics, underlies the non-equilibrium nature of the driven Bose criticality. In both cases the couplings approach the fixed point Eq. (106) but flow to the symmetric phase eventually. We show $g = 10K, \bar{u}$, and $10^{-1}\bar{u}_3$ (see Secs. III G and VI A for the definitions of these couplings) as solid, dashed, and dot-dashed lines respectively. Stages of the flow at $t = 0, -8$, and -16 are indicated with points on the trajectories). Initial values are (a) $r_\Lambda = 10, w_\Lambda = 0.01281$ and (b) $r_{K\Lambda} = 10, r_{u\Lambda} = 5, r_{u_3\Lambda} = 1, w_\Lambda = 0.01264$. In both cases we have $\bar{\kappa}_\Lambda = 0.1, \bar{\kappa}_{3\Lambda} = 0.01$, and $K_\Lambda = 1 + i0.1$.

ever, that technical noise and other uncertainties in the measurement setup will unavoidably also lead to a broadening of the spectrum. The small value of $\eta_r \approx 0.143$ thus challenges experiments to verify this prediction.

III. MODEL

Here we introduce the microscopic model in terms of a second quantized master equation, and discuss the transition to an equivalent description in terms of a markovian dissipative action in the Keldysh functional integral framework. In App. A we summarize a derivation of this action from a microscopic Hamiltonian system-bath setting, performing the identical approximations as in the master equation and therefore leading

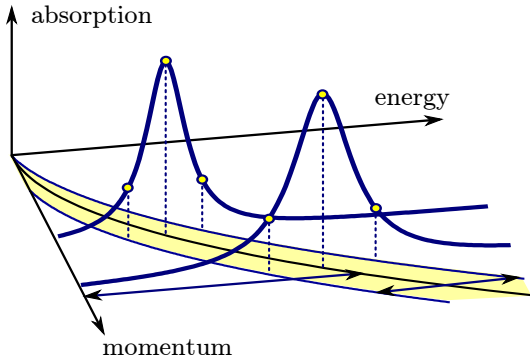


Figure 4. Illustration of the observability of the new exponent: The absorption peak for a measurement that observes the single particle dynamical response. The new exponent η_r reveals itself in a different scaling of the peak location and peak-width as a function of the momentum q .

to the identical physics. These considerations show in which sense the validity of the markovian dissipative action, as well as the independence of coherent and dissipative dynamics, relies on explicitly driving the system.

A. Master equation

Our model with particle loss and pumping is described microscopically by a many-body master equation that determines the time evolution of the system density operator (units are chosen such that $\hbar = 1$),

$$\partial_t \hat{\rho} = -i[\hat{H}, \hat{\rho}] + \mathcal{L}[\hat{\rho}]. \quad (6)$$

This equation incorporates both coherent dynamics generated by the Hamiltonian \hat{H} and dissipation that is subsumed in the action of the Liouville operator \mathcal{L} . The Hamiltonian \hat{H} describes interacting bosonic degrees of freedom of mass m and is given by (we use the shorthand $\int_{\mathbf{x}} = \int d^d \mathbf{x}$)

$$\hat{H} = \int_{\mathbf{x}} \hat{\psi}^\dagger(\mathbf{x}) \left(-\frac{\Delta}{2m} \right) \hat{\psi}(\mathbf{x}) + \frac{g}{2} \int_{\mathbf{x}} \hat{\psi}^\dagger(\mathbf{x})^2 \hat{\psi}(\mathbf{x})^2, \quad (7)$$

where $\hat{\psi}(\mathbf{x})$ are bosonic field operators. Note that we do not explicitly introduce any system chemical potential, as the density of the system will be fixed by the balance of pumping and losses. Two-body interactions are described by a density-density interaction with coupling constant g . In the following we shall be interested in dynamically stable systems which are characterized by a positive coupling constant $g > 0$. This modeling of interactions is valid on length scales which are not sufficient to resolve details of the microscopic interaction potential.

In our model, dissipative dynamics comes in the form of one-body pumping (p) and losses (l) as well as two-body losses (t). Accordingly, the Liouville operator can be decomposed into the sum of three terms $\mathcal{L} = \sum_{\alpha} \mathcal{L}_{\alpha}$ with $\alpha = p, l, t$

which have the common Lindblad structure

$$\mathcal{L}_{\alpha}[\hat{\rho}] = \gamma_{\alpha} \int_{\mathbf{x}} \left(\hat{L}_{\alpha}(\mathbf{x}) \hat{\rho} \hat{L}_{\alpha}^{\dagger}(\mathbf{x}) - \frac{1}{2} \{ \hat{L}_{\alpha}^{\dagger}(\mathbf{x}) \hat{L}_{\alpha}(\mathbf{x}), \hat{\rho} \} \right), \quad (8)$$

with local Lindblad or quantum jump operators $\hat{L}_{\alpha}(\mathbf{x})$ that create (p) and destroy (l) single particles; for $\alpha = t$ two particles are destroyed at the same instant in time, i.e., the quantum jump operators are given by

$$\hat{L}_p(\mathbf{x}) = \hat{\psi}^{\dagger}(\mathbf{x}), \quad \hat{L}_l(\mathbf{x}) = \hat{\psi}(\mathbf{x}), \quad \hat{L}_t(\mathbf{x}) = \hat{\psi}(\mathbf{x})^2. \quad (9)$$

These processes occur at rates γ_p , γ_l , and γ_t , respectively.

The net effect of single-particle pumping and losses is determined by the relative size of the respective rates: For $\gamma_p > \gamma_l$, there is an effective gain of single particles. Nevertheless, Eq. (6) leads (in a suitably chosen rotating frame, as we will show below) to a stationary state $\hat{\rho}_{ss}$ in which the gain of single particles is balanced by two-body losses. In this situation, a finite condensate amplitude builds up,

$$\langle \hat{\psi}(\mathbf{x}) \rangle_{ss} = \text{tr}(\hat{\psi}(\mathbf{x}) \hat{\rho}_{ss}) = \psi_0 \neq 0, \quad \gamma_p > \gamma_l. \quad (10)$$

That is, in stationary state the system is in a condensed phase in which the symmetry of the dynamics described by Eq. (6) under global $U(1)$ transformations of the field operators $\hat{\psi}(\mathbf{x}) \mapsto \hat{\psi}(\mathbf{x}) e^{i\phi}$ is broken. When the loss rate γ_l exceeds the pumping rate γ_p , on the other hand, no condensate emerges in stationary state, and the expectation value of the bosonic field operator is zero,

$$\langle \hat{\psi}(\mathbf{x}) \rangle_{ss} = 0, \quad \gamma_p \leq \gamma_l. \quad (11)$$

Equations (10) and (11) can be derived from the master equation (6) in mean-field approximation by making the ansatz of a coherent stationary state $\hat{\rho}_{\psi} = |\psi\rangle\langle\psi|$ where we assume that the amplitude in $|\psi\rangle = \frac{1}{\mathcal{N}} \exp\left(\psi \int_{\mathbf{x}} \hat{\psi}^{\dagger}(\mathbf{x})\right) |0\rangle$ is spatially homogeneous but possibly time-dependent. Proper normalization of the coherent state is ensured by the choice $\mathcal{N} = e^{V|\psi|^2}$ with the system volume V . The time-dependence of the condensate amplitude is determined by taking the time derivative on both sides of the equality $\psi = \text{tr}(\hat{\psi}(\mathbf{x}) \hat{\rho}_{\psi})$ and using the master equation (6), which results in

$$i\partial_t \psi = \left[g |\psi|^2 + \frac{i}{2} (\gamma_p - \gamma_l - 2\gamma_t |\psi|^2) \right] \psi. \quad (12)$$

For $\gamma_p > \gamma_l$ this equation allows for a solution of the form $\psi = \psi_0 e^{-i\mu t}$, where the condensate density is determined by the imaginary part of the term in brackets on the right-hand side (RHS) as

$$|\psi_0|^2 = \frac{\gamma_p - \gamma_l}{2\gamma_t}. \quad (13)$$

The parameter μ is then given by $\mu = g |\psi_0|^2$. We obtain the steady state density matrix of Eq. (10) by means of a transformation to a rotating frame with the unitary operator $\hat{U} = \exp(i\mu \hat{N} t)$ where the particle number operator is $\hat{N} = \int_{\mathbf{x}} \hat{\psi}^{\dagger}(\mathbf{x}) \hat{\psi}(\mathbf{x})$: We have $\hat{\rho}_{ss} = \hat{U} \hat{\rho}_{\psi} \hat{U}^{\dagger}$, which is indeed

time-independent, and recover Eqs. (10) and (11). Under the transformation to this rotating frame, the Hamiltonian acquires a contribution $-\mu\hat{N}$, whereas the Liouvillian \mathcal{L} remains invariant. In the following we will always be working in the rotating frame.

In summary, the steady state phase diagram of our model exhibits two phases: A symmetric one characterized by Eq. (11) and an ordered one where the global $U(1)$ symmetry is broken by a finite condensate amplitude Eq. (10) with definite phase. These two phases are separated by a continuous phase transition with order parameter ψ_0 . The transition is crossed by tuning the single-particle pumping rate from $\gamma_p < \gamma_l$ in the “symmetric” to $\gamma_p > \gamma_l$ in the “symmetry-broken” or “ordered” phase.

In the following we shall be interested in the critical behavior that is induced by tuning $\gamma_p - \gamma_l$ to zero. Powerful tools for investigating critical phenomena at a second order phase transition are provided by a multitude of variants of the RG. The particular flavor we employ here is the FRG in the formulation of Wetterich³⁰ (for reviews see Refs.⁴⁶⁻⁵¹). This method builds upon the use of functional integrals. Therefore, as a first step towards implementing a FRG investigation of our model, we will reformulate the physics that is encoded in the master equation (6) in terms of Keldysh functional integrals.⁵²

B. Keldysh functional integral

The Keldysh approach provides a means to tackle general non-equilibrium problems in the language of functional integrals. For the model at hand, the dynamics described by the master equation (6) can be represented equivalently as a Keldysh partition function (see App. A): By $\Psi_\sigma = (\psi_\sigma, \psi_\sigma^*)$ for $\sigma = +, -$ we denote Nambu spinors of fields on the forward- and backward-branch of the closed time contour, respectively. Then, collecting time and space in a single variable $X = (t, \mathbf{x})$ and using the abbreviation $\int_X = \int dt \int d^d \mathbf{x}$, the Keldysh partition function reads

$$\mathcal{Z}[J_+, J_-] = \int \mathcal{D}[\Psi_+, \Psi_-] e^{iS[\Psi_+, \Psi_-] + i \int_X (J_+^\dagger \Psi_+ - J_-^\dagger \Psi_-)}. \quad (14)$$

The fields $J_\sigma = (j_\sigma, j_\sigma^*)$ are external sources inserted here for the purpose of calculating correlation functions of the bosonic fields in the usual manner by means of functional differentiation. When they are set to zero, $J_+ = J_- = 0$, the partition function reduces to unity,⁵² i.e., we have the normalization $\mathcal{Z}[0, 0] = 1$. While the Keldysh approach can in principle be utilized to study time evolution, here we are assuming translational invariance in time, as appropriate for the investigation of steady state properties.

In complete analogy to the separation of coherent and dissipative contributions to the time evolution of the density operator in Eq. (6), the action \mathcal{S} in the functional integral Eq. (14) can be decomposed as $\mathcal{S} = \mathcal{S}_H + \mathcal{S}_D$ into a Hamiltonian part \mathcal{S}_H and a part \mathcal{S}_D corresponding to the dissipative Liouvillian \mathcal{L} in the master equation. The former is given by (from now

on we will use units such that $2m = 1$)

$$\mathcal{S}_H = \sum_{\sigma=\pm} \sigma \int_X \left[\psi_\sigma^* (i\partial_t + \Delta + \mu) \psi_\sigma - \frac{g}{2} (\psi_\sigma^* \psi_\sigma)^2 \right]. \quad (15)$$

As a general rule (see App. A), normally ordered operators in Eq. (6) acting on the density matrix $\hat{\rho}$ from the left (right) result in corresponding fields on the $\sigma = +$ ($\sigma = -$) contour. Consequently, the commutator with the Hamiltonian in Eq. (6) is transferred into the two contributions to Eq. (15) with a relative minus sign.

The same rule applies to the dissipative part in the master equation (6). Passing from the Liouvillian \mathcal{L} on to a dissipative action \mathcal{S}_D , quantum jump operators \hat{L}_α are replaced by corresponding jump fields $L_{\alpha,\sigma}$ on the $\sigma = +$ ($\sigma = -$) contour. (In App. A we will discuss regularization issues related to normal ordering of Lindblad operators.) As above we have the three contributions $\mathcal{S}_D = \sum_\alpha \mathcal{S}_\alpha$ that are due to single-particle pumping (p) and losses (l) as well as two-body losses (t). The form of the jump fields can directly be inferred from Eq. (9) as

$$L_{p,\sigma} = \psi_\sigma^*, \quad L_{l,\sigma} = \psi_\sigma, \quad L_{t,\sigma} = \psi_\sigma^2. \quad (16)$$

Then, for the dissipative parts of the action we find the expression

$$\mathcal{S}_\alpha = -i\gamma_\alpha \int_X \left[L_{\alpha,+} L_{\alpha,-}^* - \frac{1}{2} (L_{\alpha,+}^* L_{\alpha,+} + L_{\alpha,-}^* L_{\alpha,-}) \right]. \quad (17)$$

As we can see, the transition from a description of a specific problem in terms of a master equation to one in terms of Keldysh functional integrals, reduces to the application of simple rules. For our model, Eqs. (14), (15) and (17) provide us with a convenient starting point for the investigation of the steady state phase transition described in the previous section.

While the translation rules from the master equation to the Keldysh functional integral are most simply applied in a basis of fields ψ_\pm that can be ascribed to the forward and backward branches of the Keldysh contour, subsequently we will find it advantageous to introduce so-called classical and quantum fields, given by the symmetric and anti-symmetric combinations

$$\begin{pmatrix} \phi_c \\ \phi_q \end{pmatrix} = M \begin{pmatrix} \psi_+ \\ \psi_- \end{pmatrix}, \quad M = \frac{1}{\sqrt{2}} \begin{pmatrix} 1 & 1 \\ 1 & -1 \end{pmatrix}. \quad (18)$$

Condensation is described by a time-independent, homogeneous expectation value of the fields on the $\sigma = \pm$ contours, $\langle \psi_+(X) \rangle = \langle \psi_-(X) \rangle = \psi_0$, cf. Eq. (10). In the basis of classical and quantum fields, this is expressed as $\langle \phi_c(X) \rangle = \phi_0 = \sqrt{2}\psi_0$, $\langle \phi_q(X) \rangle = 0$, i.e., only ϕ_c can condense (and, therefore, become a “classical” variable), whereas ϕ_q is a purely fluctuating field with zero expectation value by construction.

By means of the transformation Eq. (18), the inverse propagator, determined by the quadratic part of the action, is cast in the characteristic causality structure⁵² with retarded, advanced, and Keldysh components P^R , P^A , and P^K , respectively (in the following we will denote the two-body coupling

constant and loss rate by, respectively, $\lambda = g/2$ and $\kappa = \gamma_l/2$,

$$S = \int_X \left\{ (\phi_c^*, \phi_q^*) \begin{pmatrix} 0 & P^A \\ P^R & P^K \end{pmatrix} \begin{pmatrix} \phi_c \\ \phi_q \end{pmatrix} + i4\kappa\phi_c^*\phi_c\phi_q^*\phi_q \right. \\ \left. - [(\lambda + i\kappa)(\phi_c^{*2}\phi_c\phi_q + \phi_q^{*2}\phi_c\phi_q) + \text{c.c.}] \right\}. \quad (19)$$

The inverse retarded and advanced single-particle Green's functions are given by $P^R = P^{A\dagger} = i\partial_t + \Delta + \mu + i\kappa_1$ where $\kappa_1 = (\gamma_l - \gamma_p)/2$. For the Keldysh component of the inverse propagator we have $P^K = i\gamma$, where $\gamma = \gamma_l + \gamma_p$ is the sum of single-particle pumping and loss rates – both of them increase the noise level in the system.

The spectrum of single-particle excitations is encoded in the poles of the retarded propagator in frequency-momentum space or, equivalently, in the zeros of the inverse propagator. Solving $P^R(Q) = 0$ for ω , where $Q = (\omega, \mathbf{q})$ collects the frequency and spatial momentum, we obtain the dispersion relation ($q = |\mathbf{q}|$)

$$\omega = q^2 - \mu - i\kappa_1. \quad (20)$$

For $\kappa_1 > 0$ (i.e., $\gamma_p < \gamma_l$) the pole is located in the lower complex half-plane, and the effective loss rate κ_1 takes the role of an inverse lifetime. One has single-particle excitations that decay exponentially in time, a situation that is well-known from the general theory of the analytic structure of correlation functions.⁵³ As κ_1 is tuned to negative values (i.e., as we cross the phase transition), however, the pole Eq. (20) is shifted into the upper complex half-plane, signaling an instability. After crossing this threshold, the system develops a condensate, and the proper analytical structure of the retarded propagator is restored only by taking the tree-level shifts due to the condensate into account. We will discuss the corresponding modifications of the dispersion relation Eq. (20) below in Sec. III D.

Inversion of the 2×2 matrix in Eq. (19) yields the propagator with retarded, advanced, and Keldysh components,

$$G = \begin{pmatrix} G^K & G^R \\ G^A & 0 \end{pmatrix}. \quad (21)$$

The components along with their respective usual diagrammatic representation⁵² are given by

$$G^R(Q) = 1/P^R(Q) = \text{---}\text{---}\text{---}, \\ G^A(Q) = 1/P^A(Q) = \text{---}\text{---}\text{---}, \\ G^K(Q) = -P^K / (P^R(Q)P^A(Q)) = \text{---}\text{---}\text{---}, \quad (22)$$

which shows that the poles of $G(Q)$ are determined solely by the zeros of $P^R(Q)$ and $P^A(Q)$. The Keldysh component P^K of the inverse propagator enters the expression for $G^K(Q)$ multiplicatively. Therefore, even in a situation where P^K is a polynomial in frequency and/or momentum, it can not give rise to further poles in the propagator $G(Q)$.

In the Keldysh formalism, elastic two-body collisions and two-body losses are treated on an equal footing: Both appear in the action Eq. (19) as quartic vertices, however, with a real coupling constant λ in the case of elastic collisions and

a purely imaginary coupling constant $i\kappa$ for two-body losses. The vertices in Eq. (19) can further be distinguished by the number of quantum fields they contain: We have the so-called classical vertex $-\frac{1}{2} \int_X [(\lambda + i\kappa)\phi_c^{*2}\phi_c\phi_q + \text{c.c.}]$ which contains only one quantum field and three classical fields, and two quantum vertices: The first one $i2\kappa \int_X \phi_c^*\phi_c\phi_q^*\phi_q$ containing two and the second one $-\frac{1}{2} \int_X [(\lambda + i\kappa)\phi_q^{*2}\phi_c\phi_q + \text{c.c.}]$ containing three quantum fields. Diagrammatically, these vertices are depicted as

$$\begin{array}{ccc} \begin{array}{c} \phi_q^* \quad \phi_c^* \\ \diagdown \quad \diagup \\ \lambda + i\kappa \\ \diagup \quad \diagdown \\ \phi_c^* \quad \phi_c \end{array} & , & \begin{array}{c} \phi_q^* \quad \phi_c^* \\ \diagdown \quad \diagup \\ i\kappa \\ \diagup \quad \diagdown \\ \phi_c^* \quad \phi_c \end{array} & , & \begin{array}{c} \phi_q^* \quad \phi_c^* \\ \diagdown \quad \diagup \\ \lambda + i\kappa \\ \diagup \quad \diagdown \\ \phi_c^* \quad \phi_c \end{array} \end{array} \quad (23)$$

The fact that there are no vertices consisting only of classical fields is a manifestation of causality in the Keldysh framework.⁵² Below we will find that only the classical vertex is relevant (in the sense of the RG) once the system is tuned close to the phase transition.

C. Effective action

Having established a description of our model in terms of a Keldysh functional integral, we proceed by introducing the concept of the effective action,³⁹ which is central to the FRG. It is also a convenient starting point for a discussion of the phase transition on the mean-field level (see Sec. III D).

In equilibrium statistical physics, the effective action Γ is related to the free energy as a functional of a space-dependent order parameter, and the equilibrium state is determined as the order parameter configuration that minimizes Γ . In the present context of non-equilibrium statistical physics, however, we do not have a sensible notion of a free energy. In fact, already the Keldysh partition function Eq. (14) reduces for vanishing external sources to a representation of unity $\mathcal{Z}[0, 0] = 1$, independently of the parameters that characterize the action.⁵² Still, the Keldysh effective action, defined analogously to its equilibrium counterpart as the Legendre transform of the generating functional for connected correlation functions, is a very useful object. From Γ we can derive, e.g., field equations that determine the stationary configurations of classical and quantum fields $\Phi_\nu = (\phi_\nu, \phi_\nu^*)$, $\nu = c, q$. On a more formal level, Γ is the generating functional of one-particle irreducible vertices.³⁹ Most importantly for our model, however, the FRG provides us with a means of calculating critical exponents for the phase transition by studying the RG flow of Γ as a function of an infrared cutoff k .

Our starting point for introducing the effective action is the generating functional Eq. (14) for correlation functions, expressed in the basis of classical and quantum fields Φ_ν , i.e., the action is given by Eq. (19), and we introduce classical and quantum sources $J_\nu = (j_\nu, j_\nu^*)$ with $\nu = c, q$ according to the Keldysh rotation

$$\begin{pmatrix} j_c \\ j_q \end{pmatrix} = M \begin{pmatrix} j_+ \\ j_- \end{pmatrix}, \quad (24)$$

where the matrix M is defined in Eq. (18). For the generating functional \mathcal{W} for connected correlation functions and \mathcal{Z} we have the relation

$$\mathcal{W}[J_c, J_q] = -i \ln \mathcal{Z}[J_c, J_q]. \quad (25)$$

The idea is now to express \mathcal{W} , which is a functional of the external sources J_ν , in terms of the corresponding field expectation values $\bar{\Phi}_\nu = \langle \Phi_\nu \rangle|_{J_c, J_q} = \delta \mathcal{W} / \delta J_\nu$. The passage to these new variables is accomplished by means of a Legendre transform

$$\Gamma[\bar{\Phi}_c, \bar{\Phi}_q] = \mathcal{W}[J_c, J_q] + \int_X (J_c^\dagger \bar{\Phi}_c + J_q^\dagger \bar{\Phi}_q). \quad (26)$$

The difference between the action \mathcal{S} and the effective action Γ results from the inclusion of both statistical and quantum fluctuations in the latter. This becomes apparent in the representation of Γ as a functional integral,⁴⁶

$$e^{i\Gamma[\bar{\Phi}_c, \bar{\Phi}_q]} = \int \mathcal{D}[\delta\bar{\Phi}_c, \delta\bar{\Phi}_q] e^{iS[\bar{\Phi}_c + \delta\bar{\Phi}_c, \bar{\Phi}_q + \delta\bar{\Phi}_q]}, \quad (27)$$

which holds for the equilibrium states that obey $\delta\Gamma/\delta\bar{\Phi}_c = \delta\Gamma/\delta\bar{\Phi}_q = 0$ at vanishing external sources $J_c = J_q = 0$. The most straightforward way of evaluating the functional integral Eq. (27) approximately is by performing a perturbative expansion around the configuration that minimizes the action \mathcal{S} . To zeroth order this corresponds to mean-field theory, an approach we will discuss in the following section. In the FRG, the fluctuations $\delta\bar{\Phi}_\nu$ are included stepwise by introducing an infrared regulator which suppresses fluctuations with momenta less than an infrared cutoff scale k . A short review of this method, adapted to the Keldysh framework, is provided in Sec. III E. We will apply it to our model in Sec. V.

D. Mean-field theory

In Sec. III A we identified the exact balance between single-particle losses and pumping as the transition point, cf. Eqs. (10) and (11). Here we will derive this result from the Keldysh functional integral Eq. (27), again employing a mean-field approximation. We will then proceed by calculating the excitation spectrum above the stationary mean-field by treating quadratic fluctuations in a Bogoliubov (tree-level) expansion. While this issue can equally well be addressed in the master equation formalism of Sec. III A, in going beyond the mean-field approximation by perturbative methods we will make a first encounter with infrared divergences. Proper treatment of these requires RG methods, which are well-established and elegantly formulated in terms of functional integrals.

Mean-field theory corresponds to an approximate evaluation of the functional integral in Eq. (27) in which fluctuations around the classical fields are completely neglected. In the present context, by classical fields we mean spatially homogeneous solutions to the classical field equations

$$\frac{\delta\mathcal{S}}{\delta\phi_c^*} = 0, \quad \frac{\delta\mathcal{S}}{\delta\phi_q^*} = 0. \quad (28)$$

As already mentioned above, there are no terms in the action Eq. (19) that have zero power of both ϕ_q^* and ϕ_q . The same is obviously true for $\delta\mathcal{S}/\delta\phi_c^*$. Therefore, the first equation (28) is solved by $\phi_q = 0$. Inserting this condition in the second equation (28), we have

$$\left[\mu + i\kappa_1 - (\lambda - i\kappa)\phi_0^*\phi_0 \right] \phi_0 = 0. \quad (29)$$

The solution for $\rho_0 = \phi_0^*\phi_0$ is determined by the imaginary part of Eq. (29): For $\kappa_1 \geq 0$, in the symmetric phase, the classical field is zero, $\rho_0 = 0$, whereas for $\kappa_1 < 0$ we have a finite condensate density $\rho_0 = -\kappa_1/\kappa$. In a second step, the parameter μ is determined by the real part of Eq. (29) as $\mu = -\lambda\kappa_1/\kappa$.

Quadratic fluctuations around the mean-field order parameter can be investigated in a Bogoliubov or tree-level expansion: We set $\phi_c = \phi_0 + \delta\phi_c$, $\phi_q = \delta\phi_q$ in the action Eq. (19) and expand the resulting expression to second order in the fluctuations $\delta\phi_\nu$. The poles of the retarded propagator (which is now a 2×2 matrix in the space of Nambu spinors $\delta\Phi_\nu = (\delta\phi_\nu, \delta\phi_\nu^*)$) are then³¹ ($q = |\mathbf{q}|$)

$$\omega_{1,2}^R = -i\kappa\rho_0 \pm \sqrt{q^2(q^2 + 2\lambda\rho_0) - (\kappa\rho_0)^2}. \quad (30)$$

Real and imaginary parts of both branches are shown in Fig. 5 in panels (a) and (b), respectively. Due to the tree-level shifts $\propto \rho_0$ the instability of Eq. (20) for $\kappa_1 < 0$ is lifted: Both poles are located in the lower complex half-plane, indicating a physically stable situation with decaying single-particle excitations. For $\kappa = 0$, Eq. (30) reduces to the usual Bogoliubov result,⁵⁴ where for $q \rightarrow 0$ the dispersion is phononic, $\omega_{1,2}^R = \pm cq$, with speed of sound $c = \sqrt{2\lambda\rho_0}$ whereas particle-like behavior $\omega_{1,2}^R \sim q^2$ is recovered at high momenta. Here, due to the presence of two-body loss $\kappa \neq 0$, the dispersion is strongly modified: While at high momenta the dominant behavior is still given by $\omega_{1,2}^R \sim q^2$, at low momenta we obtain purely diffusive non-propagating modes $\omega_1^R \sim -i\frac{\lambda}{\kappa}q^2$ and $\omega_2^R \sim -i2\kappa\rho_0$. In particular, for $q = 0$ we have $\omega_1^R = 0$: This is a diffusive Goldstone mode,^{31,33,55} associated with the spontaneous breaking of the global $U(1)$ symmetry in the ordered phase. The existence of such a mode is not bound to the mean-field approximation but rather an exact property of the theory guaranteed by the $U(1)$ invariance of the effective action, even in the present case of a driven-dissipative condensate.

The discussion of our model on the mean-field level has illustrated some of the benefits of the Keldysh approach: Not only have we gained a simple physical picture of the phase transition as a condensation instability in the retarded and advanced propagators, but were we able to investigate excitations in both the symmetric and ordered phases quite straightforwardly. Mean-field theory, however, while providing us with a good qualitative understanding of the stationary state physics of our model far away from the phase transition, has major shortcomings when it comes to the discussion of critical phenomena. In particular, the critical exponents that can be extracted from an analysis of quadratic fluctuations around the mean-field configuration are not indicative of the universality class of the phase transition, as they correspond to the RG

flow in the vicinity of a non-interacting (or Gaussian) fixed point. Critical behavior at the phase transition, however, is encoded in the RG flow in the vicinity of an interacting (or Wilson-Fisher) fixed point.

In a many-body system, excitations and their interactions get dressed due to scattering from other particles. The mean-field results of this section can be taken as the starting point for a calculation of the effective dressed parameters in a perturbative expansion. In the functional integral Eq. (27), this amounts to an expansion in the number of loops around the mean-field configuration. To lowest (one-loop) order, the correction $\Delta\lambda$ to the real part of the bare classical vertex (the first diagram in Eq. (23)) reads ($v_d = (2^{d+1}\pi^{d/2}\Gamma(d/2))^{-1}$)

$$\begin{aligned} \Delta\lambda &= \text{diagram} + \dots \\ &= -\frac{v_d\gamma(\lambda^2 + \kappa^2)^2}{\lambda\kappa} \int_{q_{\text{IR}}}^{\infty} \frac{dq}{q^{5-d}}, \end{aligned} \quad (31)$$

where the elements appearing in the diagram are defined in Eqs. (31) and (22) (here, however, lines correspond to propagators of fluctuations $\delta\Phi_\nu$ and acquire an additional 2×2 matrix structure in Nambu space) and the ellipsis indicate that all diagrams with four external legs and one closed loop corresponding to a single internal momentum integration have to be included. In the integrand we have only kept the dominant contribution for $q \rightarrow 0$ and we have introduced an infrared cutoff q_{IR} in order to regularize the divergence at low momenta. Such infrared divergences, however, appear not only in our specific example of the loop correction to λ , but rather are characteristic of perturbative expansions in symmetry broken phases. They are due to the presence of a massless Goldstone mode, which results in a pole of the retarded and advanced propagators at $\omega = q = 0$. This problem is even enhanced as we approach the phase transition: Then both modes become degenerate, with also the second mode $\omega_2^R \sim -i2\kappa\rho_0$ for $q \rightarrow 0$ becoming massless. A method that allows us to go beyond mean-field theory, therefore, has to provide for a proper treatment of infrared divergences. In the FRG, this is achieved by effectively introducing a mass term $\propto k^2$ in the inverse propagators by hand. In consequence, the integrand in Eq. (31) is replaced by $\int_{q_{\text{IR}}}^{\infty} dq q^{d-1} / (q^2 + k^2)^2$ and we may safely set q_{IR} to zero since the effective mass k^2 acts as an infrared cutoff. The resulting loop-corrected coupling is a function of this cutoff, $\lambda = \lambda(k)$, and we obtain the fully dressed or renormalized coupling by following the RG flow of the running coupling $\lambda(k)$ for $k \rightarrow 0$. This procedure can be implemented efficiently by introducing the cutoff in the functional integral Eq. (27). We will discuss how this is done in practice for the present non-equilibrium problem⁵⁶⁻⁵⁹ in the following section. Critical exponents can then be extracted from the flow of the critical system, i.e., when κ_1 is fine-tuned to zero.

So far we have discussed only corrections to the bare interaction vertices due to the inclusion of loop diagrams. However, also the propagators appearing in these diagrams are themselves renormalized. In particular, the inverse propaga-

tor can be written as $P(Q) - \Sigma(Q)$, i.e., as the sum of the bare inverse propagator $P(Q)$ and a self-energy correction $\Sigma(Q)$.³⁹ The self-energy contribution to the retarded propagator is represented diagrammatically as

$$\Sigma^R(Q) = \text{diagram 1} + \text{diagram 2} \quad (32)$$

where effective cubic couplings appear in the second diagram. These are obtained upon expanding the interaction vertex around the field expectation value. Due to momentum conservation, the first diagram does not depend on the external momentum $Q = (\omega, \mathbf{q})$ and gives a correction to the constant part of the inverse propagator, i.e., the so-called mass terms. Since the coupling $\lambda + i\kappa$ associated with the vertex appearing in this diagram is complex, both the real and imaginary masses, μ and κ_1 , are affected by the loop correction. The second diagram in Eq. (32) gives a frequency- and momentum-dependent contribution to the self-energy. Symmetry under spatial rotations implies that it depends only on the modulus of the momentum and we may write $\Sigma^R(Q) = \Sigma^R(\omega, q^2)$. For small ω and q^2 we can expand $\Sigma^R(\omega, q^2) \approx \Sigma^R(0, 0) + \omega\partial_\omega\Sigma^R(0, 0) + q^2\partial_{q^2}\Sigma^R(0, 0)$. Transforming back to the time domain and real space, the derivatives of the self-energy with respect to frequency and momentum give corrections to the coefficients of ∂_t and Δ in the inverse propagators, which are again complex valued. An imaginary part of the coefficient of the Laplacian corresponds to an effective diffusion constant due to the interaction with other particles. A complex prefactor of the time derivative, on the other hand, has significant consequences for the physical interpretation of all other couplings, as we will discuss in detail in later sections.

E. FRG approach for the Keldysh effective action

The transition from the action \mathcal{S} to the effective action Γ consists in the inclusion of both statistical and quantum fluctuations in the latter (see Eq. (27)). In the FRG, the functional integral over fluctuations is carried out stepwise by introducing an infrared regulator which suppresses fluctuations with momenta less than an infrared cutoff scale k .⁴⁶ This is achieved by adding to the action in Eq. (14) a term

$$\Delta\mathcal{S}_k = \int_X (\phi_c^*, \phi_q^*) \begin{pmatrix} 0 & R_{k,\bar{K}}(-\Delta) \\ R_{k,\bar{K}}^*(-\Delta) & 0 \end{pmatrix} \begin{pmatrix} \phi_c \\ \phi_q \end{pmatrix} \quad (33)$$

with a cutoff function $R_{k,\bar{K}}$ which will be specified below in Sec. III G. We denote the resulting cutoff-dependent Keldysh partition function and generating functional for connected correlation functions by, respectively, \mathcal{Z}_k and \mathcal{W}_k . The effective running action Γ_k is then defined as the modified Legendre transform

$$\begin{aligned} \Gamma_k[\bar{\Phi}_c, \bar{\Phi}_q] &= \mathcal{W}_k[J_c, J_q] \\ &+ \int_X (J_c^\dagger \bar{\Phi}_c + J_q^\dagger \bar{\Phi}_q) - \Delta\mathcal{S}_k[\bar{\Phi}_c, \bar{\Phi}_q]. \end{aligned} \quad (34)$$

The subtraction of ΔS_k on the RHS guarantees that the only difference between the functional integral representations for Γ and Γ_k is the inclusion of the cutoff term in the latter,

$$e^{i\Gamma_k[\bar{\Phi}_c, \bar{\Phi}_q]} = \int \mathcal{D}[\delta\bar{\Phi}_c, \delta\bar{\Phi}_q] e^{iS[\bar{\Phi}_c + \delta\bar{\Phi}_c, \bar{\Phi}_q + \delta\bar{\Phi}_q] + i\Delta S_k[\delta\bar{\Phi}_c, \delta\bar{\Phi}_q]}. \quad (35)$$

Physically, Γ_k can be viewed as the effective action for averages of fields over a coarse-graining volume with size $\sim k^{-d}$.

We choose the form of the cutoff term ΔS_k such that it modifies the inverse retarded and advanced propagators: Comparing Eqs. (19) and (33), we see that associated with the action $S + \Delta S_k$ are the regularized retarded and advanced inverse propagators $P^R(Q) + R_{k, \bar{K}}^*(q^2)$ and $P^A(Q) + R_{k, \bar{K}}(q^2)$ respectively, whereas the Keldysh part P^K of the inverse propagator remains unchanged. In other words, by introducing the cutoff ΔS_k we manipulate the spectrum of single-particle excitations, which is encoded in the zeros of the inverse propagators $P^{R/A}(Q)$ or, equivalently, in the poles of the propagators Eq. (22). At the transition, these poles are determined by Eq. (20) with $\kappa_1 = 0$, i.e., we have a pole at $\omega = q = 0$. As we have pointed out in the paragraph following Eq. (31), this leads to infrared divergences that drive critical behavior. For the regularized propagators, on the other hand, we have $G^R(\omega = 0, q^2 = 0) = 1/R_{k, \bar{K}}^*(0)$ and $G^A(\omega = 0, q^2 = 0) = 1/R_{k, \bar{K}}(0)$ which are finite for

$$R_{k, \bar{K}}(q^2) \sim k^2, \quad q \rightarrow 0. \quad (36)$$

To regulate infrared divergences, it is sufficient to introduce the cutoff function in the retarded and advanced inverse propagators, as becomes clear from the discussion following Eq. (22).

We have seen that the effective action Γ_k defined by Eq. (35) has an infrared-finite loop expansion. Its main usefulness, however, lies in the fact that it interpolates between the action S for $k \rightarrow \Lambda$ where Λ is an ultraviolet cutoff scale, and the full effective action Γ for $k \rightarrow 0$. This is ensured by the requirements on the cutoff function⁵⁷

$$\begin{aligned} R_{k, \bar{K}}(q^2) &\sim \Lambda^2, & k \rightarrow \Lambda, \\ R_{k, \bar{K}}(q^2) &\rightarrow 0, & k \rightarrow 0, \end{aligned} \quad (37)$$

where under the condition that Λ exceeds all energy scales in the action by far, for $k \rightarrow \Lambda$ we may evaluate the functional integral Eq. (35) in a stationary phase approximation. Then, to leading order we find $\Gamma_\Lambda \sim S$. The evolution of Γ_k from this starting point in the ultraviolet to the full effective action in the infrared for $k \rightarrow 0$ is described by an exact flow equation^{30,46}

$$\partial_k \Gamma_k = \frac{i}{2} \text{Tr} \left[\left(\Gamma_k^{(2)} + \bar{R}_k \right)^{-1} \partial_k \bar{R}_k \right], \quad (38)$$

where $\Gamma_k^{(2)}$ and R_k denote, respectively the second variations of the effective action and the cutoff ΔS_k and will be specified in Sec. III G. The flow equation provides us with an alternative but fully equivalent formulation of the functional integral

Eq. (35) as a functional differential equation. Like the functional integral, the flow equation can not be solved exactly. It is, however, amenable to various systematic approximation strategies. Here we will perform an expansion of the effective action Γ_k in canonical scaling dimensions, keeping only those couplings which are – in the sense of the RG – relevant or marginal at the phase transition. The classification of couplings into relevant, marginal, and irrelevant ones will be the subject of the following section.

F. Canonical power counting

For $k \rightarrow \Lambda$ the effective action Γ_k is determined by the action S . As the infrared cutoff k is lowered, the couplings appearing in S are renormalized and additional couplings – arbitrarily many, in principle – are generated in the course of the RG flow. It is, therefore, necessary to find a reasonable and computationally manageable truncation for the number of couplings that we will take into account in the RG. For the study of critical phenomena, a suitable ordering principle is provided by the classification of couplings according to their canonical scaling dimension, and we will choose an ansatz for the effective action that contains only couplings which are relevant or marginal according to canonical power counting.³⁹ In the following we will briefly review this procedure.

At second order phase transitions, physical quantities exhibit scaling behavior, which means that they depend on the distance from the phase transition (in our case this distance is measured by κ_1) in a power-law fashion $\sim \kappa_1^\tau$, with an in general non-integer exponent τ . In order to study critical behavior in the RG, we investigate the RG flow starting from the action fine-tuned to criticality, i.e., with $\kappa_1 = 0$, and approach the critical point by lowering k . Then, scaling behavior of a physical quantity g shows up as power-law dependence $g \sim k^\theta$ on k for $k \rightarrow 0$ with a critical exponent θ . In other words, phase transitions are associated to scaling solutions of the RG flow (not all scaling solutions correspond to phase transitions⁶⁰), or – equivalently – fixed points of the flow of rescaled couplings $\tilde{g} = k^\theta g$. The dominant contribution to the exponent θ associated to a coupling g is determined by its physical dimension measured in units of momentum k , i.e., the canonical scaling dimension or engineering dimension $[g]$ (we have $[k] = 1$). Anticipating that deviations from canonical scaling will be small (see Sec. VI), let us study the flow of the dimensionless two-body elastic collision coupling $\tilde{\lambda} = \lambda/k$ (we will see below that $\tilde{\lambda}$ is indeed dimensionless). In Sec. III D we saw that the flow of λ is generated by the loop diagrams Eq. (31). Then, to the flow of the dimensionless variable $\tilde{\lambda}$ we have an additional contribution due to the engineering dimension,

$$\partial_t \tilde{\lambda} = -\tilde{\lambda} + \text{loop diagrams}, \quad (39)$$

where we are taking the derivative with respect to the dimensionless logarithmic scale $t = \ln(k/\Lambda)$ which is zero for $k = \Lambda$ and goes to $-\infty$ for $k \rightarrow 0$. The loop contribution to the flow of $\tilde{\lambda}$ is of order $\tilde{\lambda}^2, \tilde{\lambda}\tilde{\kappa}, \tilde{\kappa}^2$ and higher in the dimensionless two-body couplings $\tilde{\lambda}, \tilde{\kappa}$. We find, therefore, a trivial fixed point

$\partial_t \tilde{\lambda} = 0$ for $\tilde{\lambda}_* = \tilde{\kappa}_* = 0$. The flow for small $\tilde{\lambda}$ in the vicinity of this Gaussian fixed point is determined by the canonical scaling contribution on the RHS of Eq. (39) and is directed towards higher values of $\tilde{\lambda}$, i.e., the coupling $\tilde{\lambda}$ is relevant at the Gaussian fixed point. For increasing $\tilde{\lambda}$, the loop contributions become important and balance canonical scaling at a second fixed point. This non-trivial Wilson-Fisher fixed point at finite $\tilde{\lambda}_*, \tilde{\kappa}_*$ corresponds to the phase transition in the interacting system, and for small deviations $\tilde{\lambda} - \tilde{\lambda}_*$ the flow is attracted to $\tilde{\lambda}_*$.

The described scenario changes drastically for a coupling with negative canonical scaling dimension, i.e., when instead of the prefactor -1 for the first term on the RHS in Eq. (39) we had a positive integer. Such a coupling is irrelevant at the Gaussian fixed point, which means that its flow is attracted to the fixed point. We can, therefore, as a starting point for a systematic expansion in the relevance of couplings, set all irrelevant couplings to zero. Unlike perturbative expansions, the inclusion of irrelevant couplings in higher orders in the expansion in canonical scaling dimensions results not only in enhanced quantitative accuracy, but rather refines our picture of the phase transition, as it involves higher order vertices and a refined treatment of the momentum dependence of propagators.⁶¹

We proceed by determining the engineering dimensions of the couplings appearing in the action Eq. (19). The scaling dimensions are not uniquely determined by the requirement that the action is dimensionless, $[S] = 0$: Still we have the freedom of assigning different scaling dimensions to the classical ϕ_c and quantum fields ϕ_q . We exploit this freedom in order to impose a scaling dimension upon the Keldysh component of the inverse propagator in Eq. (19) that is the same as in finite-temperature thermodynamic equilibrium,⁵² i.e., we require $[\gamma] = 0$. Then, denoting the dynamical exponent by $[\partial_t] = z$ we find, from the quadratic part of the action and in d dimensions,

$$z = [\mu] = [\kappa_1] = 2, \quad [\phi_c] = \frac{d-2}{2}, \quad [\phi_q] = \frac{d+2}{2}. \quad (40)$$

The different scaling dimensions of classical and quantum fields result in different behavior of the complex couplings associated with the classical and quantum vertices Eq. (23) under renormalization, even though their values at $k = \Lambda$ are the same. In particular, for a local vertex that contains n_c classical and n_q quantum fields, the canonical scaling dimension of the corresponding coupling is

$$[\lambda_{n_c, n_q}] = d + 2 - n_c[\phi_c] - n_q[\phi_q]. \quad (41)$$

We observe that all couplings λ_{n_c, n_q} with $n_q > 2$ ($n_q \geq 1$ is required by causality^{52,53}) or $n_c > 5$ are irrelevant. The coupling $\lambda_{3,1}$ associated with the classical quartic vertex has engineering dimension $4 - d$, i.e., its upper critical dimension is $d = 4$ and, in the case of interest $d = 3$, it is relevant with canonical scaling dimension equal to unity. All other quartic couplings are irrelevant, as are sextic couplings with $n_q > 1$. The classical three-body coupling $\lambda_{5,1}$ is marginal and we will include it (with both real and imaginary parts) in our ansatz for Γ_k , even

though it is not present in the action \mathcal{S} . Higher order couplings λ_{n_c, n_q} with $n_c + n_q > 6$ are irrelevant.

As we have seen, we can gain first insight into critical properties of our model by means of simple dimensional analysis. We will exploit this discussion as a guideline for our choice of an ansatz for the functional form of the effective action close to criticality in the following section. In particular, our ansatz will include only classical vertices and as a result it is equivalent to a Langevin equation of the form of Eq. (1).⁵²

G. Truncation

In three dimensional classical $O(N)$ -symmetric models, already the inclusion of non-irrelevant couplings gives a satisfactory description of critical phenomena.⁴⁶ As we will show below, static critical properties of our non-equilibrium phase transition are described by such a model with $N = 2$. Therefore, in the following, we will as well restrict ourselves to the inclusion of relevant and marginal couplings in the ansatz for the effective action, i.e., according to the discussion of the previous section, we choose a truncation of the form

$$\Gamma_k = \int_X \left[(\vec{\phi}_c^*, \vec{\phi}_q^*) \begin{pmatrix} 0 & \bar{D}^A \\ \bar{D}^R & i\bar{\gamma} \end{pmatrix} \begin{pmatrix} \vec{\phi}_c \\ \vec{\phi}_q \end{pmatrix} - \left(\frac{\partial \bar{U}}{\partial \vec{\phi}_c} \vec{\phi}_q + \frac{\partial \bar{U}^*}{\partial \vec{\phi}_c^*} \vec{\phi}_q^* \right) \right]. \quad (42)$$

(Here, all couplings depend on the infrared cutoff scale k . However, for the sake of keeping the notation simple, we will not state this dependence explicitly.) All terms involving derivatives are contained in $\bar{D}^R = iZ^* \partial_t + \bar{K}^* \Delta$ and $\bar{D}^A = \bar{D}^{R\dagger}$. In contrast to the action Eq. (19), however, we allow for complex coefficients $Z = Z_R + iZ_I$ and $\bar{K} = \bar{A} + i\bar{D}$: Due to the presence of complex couplings $\lambda + ik$ in the classical action, imaginary parts of Z and \bar{K} will be generated in the RG flow as indicated at the end of Sec. III D, even though they are zero initially at $k \rightarrow \Lambda$.

A complex prefactor Z of the time derivative – often referred to as wave-function renormalization – obscures the physical interpretation of the other complex couplings: The field equation $\delta\Gamma_k / \delta\vec{\phi}_q^* = 0$ contains $iZ^* \partial_t \vec{\phi}_c = -\bar{K}^* \Delta \vec{\phi}_c + \dots$. The physical meaning of the gradient coefficient \bar{K} becomes clear only after division by Z^* , i.e., in the form $i\partial_t \vec{\phi}_c = -(A - iD) \Delta \vec{\phi}_c + \dots$ where we introduced the decomposition $K = \bar{K}/Z = A + iD$ into real and imaginary parts. In this form, the interpretation of A and D as encoding propagation and diffusion of particles is apparent. Similar considerations hold for the other couplings in Eq. (42), and we will elaborate on this point in Sec. IV D.

In our truncation containing only non-irrelevant contributions, the only momentum-independent couplings we keep are the Keldysh and spectral masses, $\bar{\gamma}$ and $\bar{u}_1 = -\bar{\mu} + i\bar{\kappa}_1$ respectively, as well as the classical quartic and sextic couplings (i.e., those vertices containing only one quantum field). These are included in the part in Eq. (42) that involves the potential \bar{U} , which is a function of the $U(1)$ invariant $\bar{\rho}_c = \vec{\phi}_c^* \vec{\phi}_c$ and given by

$$\bar{U}(\bar{\rho}_c) = \bar{u}_1 (\bar{\rho}_c - \bar{\rho}_0) + \frac{1}{2} \bar{u}_2 (\bar{\rho}_c - \bar{\rho}_0)^2 + \frac{1}{6} \bar{u}_3 (\bar{\rho}_c - \bar{\rho}_0)^3, \quad (43)$$

where both $\bar{u}_2 = \bar{\lambda} + i\bar{\kappa}$ and $\bar{u}_3 = \bar{\lambda}_3 + i\bar{\kappa}_3$ are complex. In the symmetric phase, we keep $\bar{u}_1 \neq 0$ as a running coupling and set $\bar{\rho}_0 = 0$, whereas in the ordered phase we set the masses to zero, $\bar{u}_1 = 0$, and regard the condensate amplitude as a running coupling, $\bar{\rho}_0 \neq 0$. Then, the parameterization Eq. (43) corresponds to an expansion of the potential around its minimum in both the symmetric and ordered phases. It ensures that the field equations $\delta\Gamma_k/\delta\bar{\phi}_c^* = 0, \delta\Gamma_k/\delta\bar{\phi}_q^* = 0$ are solved by $\bar{\rho}_c = 0$ and $\bar{\rho}_c = \bar{\rho}_0$ in the symmetric and ordered phases respectively (in both cases we have $\bar{\phi}_q = \bar{\phi}_q^* = 0$) for all values of k .

In what follows we will find it advantageous to introduce renormalized fields $\phi_c = \bar{\phi}_c, \phi_q = Z\bar{\phi}_q$. With this choice the complex wave-function renormalization Z that multiplies the time derivative in Eq. (42) is absorbed in the field variables and we can write the effective action in the form

$$\Gamma_k = \int_X \Phi_q^\dagger \left[i\sigma_z \left(\partial_t \Phi_c + \frac{\delta\mathcal{U}_D}{\delta\Phi_c^*} \right) - \frac{\delta\mathcal{U}_H}{\delta\Phi_c^*} + i\frac{\gamma}{2}\Phi_q \right]. \quad (44)$$

The renormalized Keldysh mass is $\gamma = \bar{\gamma}/|Z|^2$. For the variational derivatives with respect to the classical fields we are using the notation $\delta/\delta\Phi_c^* = (\delta/\delta\phi_c^*, \delta/\delta\phi_c)^T$, and the renormalized potential functionals that encode unitary and dissipative terms respectively, read

$$\begin{aligned} \frac{\delta\mathcal{U}_H}{\delta\Phi_c^*} &= (-A\Delta + U'_H)\Phi_c, \\ \frac{\delta\mathcal{U}_D}{\delta\Phi_c^*} &= (-D\Delta + U'_D)\Phi_c, \end{aligned} \quad (45)$$

where A and D are the real and imaginary parts of the renormalized gradient coefficient $K = \bar{K}/Z = A + iD$. Primes denote derivatives with respect to $\rho_c = \phi_c^* \phi_c$ of the real and imaginary parts of the renormalized potential $U = \bar{U}/Z = U_H + iU_D$, which is given by

$$U(\rho_c) = u_1(\rho_c - \rho_0) + \frac{1}{2}u_2(\rho_c - \rho_0)^2 + \frac{1}{6}u_3(\rho_c - \rho_0)^3 \quad (46)$$

with renormalized couplings $u_1 = \bar{u}_1/Z = -\mu + i\kappa_1, u_2 = \bar{u}_2/Z = \lambda + i\kappa$, and $u_3 = \bar{u}_3/Z = \lambda_3 + i\kappa_3$. The inclusion of the classical three-body coupling u_3 adds the vertex

$$(47)$$

to the building blocks Eqs. (22) and (31).

As we have already indicated, the first variational derivative of the effective action yields field equations that determine the stationary state values of the classical and quantum fields. In the ordered phase, these are constant in space and time and read $\phi_{c|\text{ss}} = \phi_{c^*|\text{ss}} = \sqrt{\bar{\rho}_0}$ (our choice of a real condensate amplitude does not cause a loss of generality) and

$\phi_{q|\text{ss}} = \phi_{q^*|\text{ss}} = 0$. Then, the scale-dependent inverse connected propagator is given by the second variational derivative of the effective action,³⁹ evaluated in stationary state. We will carry out this variational derivative in a basis of real fields, which we introduce by decomposing the classical and quantum fields into real and imaginary parts according to $\phi_\nu = \frac{1}{\sqrt{2}}(\chi_{\nu,1} + i\chi_{\nu,2})$ for $\nu = c, q$. The inverse propagator at the scale k is then given by

$$P_{ij}(Q)\delta(Q - Q') = \frac{\delta^2\Gamma_k}{\delta\chi_i(-Q)\delta\chi_j(Q')}\Big|_{\text{ss}}. \quad (48)$$

Here the indices i, j enumerate the four components of the field vector

$$\chi(Q) = (\chi_{c,1}(Q), \chi_{c,2}(Q), \chi_{q,1}(Q), \chi_{q,2}(Q))^T. \quad (49)$$

Analogous to the inverse propagator in the action Eq. (19), the inverse propagator at the scale k is structured into retarded, advanced, and Keldysh blocks,

$$P(Q) = \begin{pmatrix} 0 & P^A(Q) \\ P^R(Q) & P^K \end{pmatrix}. \quad (50)$$

However, here these blocks are themselves 2×2 matrices. (This additional Nambu structure emerges in the ordered phase.) We have explicitly

$$\begin{aligned} P^R(Q) &= \begin{pmatrix} -Aq^2 - 2\lambda\rho_0 & i\omega - Dq^2 \\ -i\omega + Dq^2 + 2\kappa\rho_0 & -Aq^2 \end{pmatrix} = P^A(Q)^\dagger, \\ P^K &= i\gamma\mathbb{1}. \end{aligned} \quad (51)$$

These expressions can be used to deduce the dispersion relation for single-particle excitations. It is determined by solving

$$\det P(Q) = \det(P^R(Q))\det(P^A(Q)) = 0 \quad (52)$$

for ω . Due to the second relation Eq. (51), two of the four solutions to Eq. (52) are complex conjugate. The zeros of the determinant of the retarded inverse propagator encode the two branches

$$\omega_{1,2}^R = -iDq^2 - i\kappa\rho_0 \pm \sqrt{Aq^2(Aq^2 + 2\lambda\rho_0) - (\kappa\rho_0)^2}, \quad (53)$$

which differ from the mean-field expression Eq. (30) by the contribution $-iDq^2$ due to the explicit inclusion of a diffusion term in our truncation, and by the appearance of the scale dependent gradient coefficient A . The diffusive Goldstone mode is now characterized by the low-momentum behavior $\omega_1^R \sim -i\left(D + A\frac{\lambda}{\kappa}\right)q^2$, whereas for the ‘‘massive’’ (the mass is purely imaginary) mode we reproduce the form of the mean-field expression $\omega_2^R \sim -i2\kappa\rho_0$ – however, in a scale-dependent version with all couplings running in the course of the RG. In this way, structural properties such as Goldstone’s theorem are preserved during the flow. The dispersion relation Eq. (53) is depicted in Fig. 5.

We proceed by specifying the cutoff function $R_{k,\bar{K}}$ which appears in Eq. (33). We will work with an optimized cutoff⁶²

$$R_{k,\bar{K}}(q^2) = -\bar{K}(k^2 - q^2)\theta(k^2 - q^2), \quad (54)$$

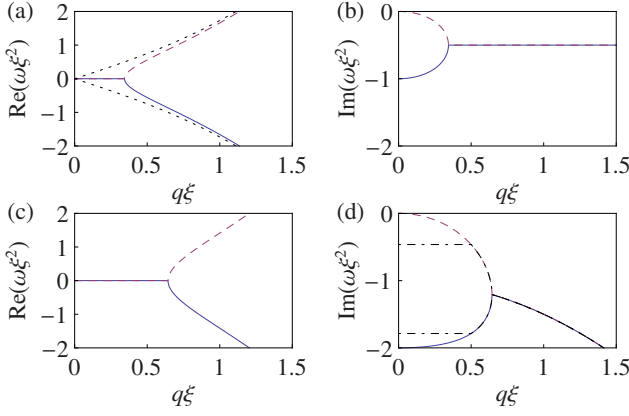


Figure 5. Dispersion relation of single-particle excitations in the ordered phase. Frequencies and momenta are measured in units of the healing length $\xi = 1/\sqrt{\lambda\rho_0}$. (a) and (b): The Goldstone and massive modes Eq. (30), obtained in mean-field approximation, are shown as, respectively, dashed and solid lines for $\kappa = \lambda/2$. For small momenta both modes are purely diffusive and non-propagating. The dotted lines in (a) correspond to the usual Bogoliubov dispersion relations for $\kappa = 0$. (c) and (d): Dispersion relations Eq. (53) with gradient coefficients A, D that are generated upon renormalization. (d) For finite D , the damping rate grows $\propto q^2$ for large q . The regularized dispersion relations, where aq^2 is replaced by $p_a(q^2)$ for $a = A, D$ (cf. Eq. (57)), are shown as a dash-dotted lines. Here we chose parameters $A = 1, D = 1/2, \kappa = \lambda, k = 1/(2\xi)$. The dashed lines in panels a) and c) are standard Bogoliubov modes in the absence of diffusive contributions.

which obviously meets the requirements Eqs. (36) and (37). The regularized propagator, which appears in the loop diagrams that generate the RG flow, reads

$$G(Q) = (P(Q) + R_k(Q))^{-1}, \quad (55)$$

where the 4×4 matrix $R_k(Q)$ is defined in analogy to the inverse propagator Eq. (48) as the second variational derivative of the cutoff Eq. (33) with respect to the real fields Eq. (49),

$$R_{k,ij}(q^2)\delta(Q - Q') = \frac{\delta^2 \Delta S_k}{\delta\chi_i(-Q)\delta\chi_j(Q')}. \quad (56)$$

Due to the cutoff $R_k(Q)$ in the denominator in Eq. (55), the poles of $G(Q)$ are given by Eq. (53), however, with Aq^2 and Dq^2 replaced by $p_A(q^2)$ and $p_D(q^2)$ respectively, where the function $p_a(q^2)$ for $a = A, D$ reads

$$p_a(q^2) = aq^2 - R_{k,a}(q^2) = \begin{cases} ak^2 & \text{for } q^2 < k^2, \\ aq^2 & \text{for } q^2 \geq k^2. \end{cases} \quad (57)$$

The thus modified dispersion relations are finite for $q \rightarrow 0$, i.e., infrared divergences of loop diagrams are regularized. In the panel d) in Fig. 5 the regularized dispersion relations are shown as dashed-dotted lines.

In Sec. III we introduced most of the ingredients for an FRG investigation of the steady state phase transition of our model. Before we present the explicit flow equations in Sec. V, we will discuss the relation between our non-equilibrium model

and other models that exhibit dynamical critical phenomena and have been studied in the literature. These models, however, relax towards a thermal equilibrium state by construction.

IV. RELATION TO EQUILIBRIUM DYNAMICAL MODELS

In this section, we work out the precise relation of the driven-dissipative model (DDM) to model A (MA) with $N = 2$ components of HH.³⁷ We emphasize that these considerations rely on the power counting introduced in Sec. III F, which is valid near a critical point only.

Originally, MA was formulated in terms of a Langevin equation for a non-conserved, coarse-grained order parameter. It provides for a phenomenological description of the relaxational dynamics of the order parameter subject to stochastic fluctuations, which are introduced necessarily as a consequence of the coarse-graining over a volume of extent k_{cg}^{-d} : The effects of fluctuations with momenta q greater than the coarse-graining scale k_{cg} are included by introducing random noise sources in the evolution equation.

For our model, coarse-graining amounts to integrating out fluctuations with momenta q greater than k_{cg} in the functional integral Eq. (35),⁴⁶ which results in an effective action Γ_{cg} that can be regarded as the starting point of a phenomenological description in the spirit of HH, i.e., we may interpret it as the action $\mathcal{S}_{\text{cg}} = \Gamma_{\text{cg}}$ for slow modes with momenta $q < k_{\text{cg}}$.

In MA it is assumed that the critical dynamics of the order parameter is purely dissipative and its stationary state is thermodynamic equilibrium which manifests itself in a FDT³⁷ relating the order parameter retarded response and correlation functions. The FDT can be derived as a consequence of a specific ‘‘equilibrium symmetry’’ of the action which is related to time reversal and expresses detailed balance.^{63–65} Thermodynamic equilibrium, therefore, does not imply the dynamics to be purely dissipative, but rather that additional coherent dynamics must be compatible with the equilibrium symmetry. The resulting extension of Model A with reversible mode couplings (MAR) differs from the DDM only in the obedience of the symmetry. As universality classes are fully characterized by the spatial dimensionality and symmetries of a system, however, this opens up the possibility of novel critical behavior in the DDM.

In the remainder of this section we specify the equilibrium symmetry and discuss its consequences for the form of the action $\mathcal{S}_{\text{cg}}^{\text{MAR}}$ for MAR on the coarse-graining scale k_{cg} and the truncation Γ_k^{MAR} for an FRG investigation of the critical properties of this model. We present the FDT and indicate how this specific relation between correlations and response can emerge in the DDM in the IR. Finally we give a simple geometric interpretation of the restriction that the symmetry poses on the couplings that parameterize the effective action, and specify the submanifolds in the coupling space for the DDM that correspond to MA and MAR.

A. Model A with $N = 2$ and reversible mode couplings

We specify the equilibrium symmetry in terms of fields $\tilde{\Phi}_\nu$, which are related to the bare fields $\bar{\Phi}_\nu$ of Eq. (42) via

$$\tilde{\Phi}_c = \bar{\Phi}_c, \quad \tilde{\Phi}_q = \frac{Z_{R,\text{cg}} - \bar{r}Z_{I,\text{cg}}}{1 + \bar{r}^2} (\bar{r}\mathbb{1} + i\sigma_z) \bar{\Phi}_q, \quad (58)$$

where $Z_{R,\text{cg}}$ and $Z_{I,\text{cg}}$ denote the real and imaginary parts of the wave-function renormalization at the coarse-graining scale k_{cg} and \bar{r} is a real parameter, the physical meaning of which will become clear in the following. The symmetry transformation is denoted by \mathcal{T} and reads^{63–65}

$$\begin{aligned} \mathcal{T} \tilde{\Phi}_c(t, \mathbf{x}) &= \sigma_x \tilde{\Phi}_c(-t, \mathbf{x}), \\ \mathcal{T} \tilde{\Phi}_q(t, \mathbf{x}) &= \sigma_x \left(\tilde{\Phi}_q(-t, \mathbf{x}) + \frac{i}{2T} \partial_t \tilde{\Phi}_c(-t, \mathbf{x}) \right). \end{aligned} \quad (59)$$

It includes complex conjugation (in the form of multiplication with the Pauli matrix σ_x) and time reversal; T is the temperature. As outlined above, we construct the action for MAR as follows: We identify the effective action Eq. (42) at the coarse-graining scale k_{cg} with the action for low-momentum modes, $\mathcal{S}_{\text{cg}} = \Gamma_{\text{cg}}$, and enforce thermodynamic equilibrium by requiring invariance of \mathcal{S}_{cg} under the transformation \mathcal{T} , which results in

$$\begin{aligned} \mathcal{S}_{\text{cg}}^{\text{MAR}} &= \int_X \bar{\Phi}_q^\dagger \left[(Z_{R,\text{cg}} \sigma_z - iZ_{I,\text{cg}} \mathbb{1}) i \partial_t \bar{\Phi}_c \right. \\ &\quad \left. + (i\sigma_z - \bar{r}\mathbb{1}) \frac{\delta \tilde{\mathcal{U}}_{D,\text{cg}}}{\delta \bar{\Phi}_c^*} + i \frac{\tilde{\gamma}_{\text{cg}}}{2} \bar{\Phi}_q \right]. \end{aligned} \quad (60)$$

(See Sec. B for details of the derivation.) The action $\mathcal{S}_{\text{cg}}^{\text{MAR}}$ contains coherent dynamics in the form of $\tilde{\mathcal{U}}_{H,\text{cg}} = \bar{r} \tilde{\mathcal{U}}_{D,\text{cg}}$, i.e., the parameter \bar{r} plays the role of the common fixed ratio between coherent and dissipative couplings. This relation ensures compatibility of coherent dynamics with the equilibrium symmetry. We note that here, crucially, both the irreversible and the reversible dynamics have the same physical origin, being generated by the same functional $\tilde{\mathcal{U}}_{D,\text{cg}}$. This is motivated in the frame of a phenomenological, effective model for relaxation dynamics in the absence of explicit drive.

However, not only the values of the couplings encoding coherent dynamics are restricted by the symmetry, but also the Keldysh mass $\tilde{\gamma}_{\text{cg}}$ is determined by the temperature that appears in the symmetry transformation as

$$\tilde{\gamma}_{\text{cg}} = \frac{4}{1 + \bar{r}^2} (Z_{R,\text{cg}} - \bar{r}Z_{I,\text{cg}})^2 T. \quad (61)$$

Finally we note that Eq. (60) includes MA with effectively purely dissipative dynamics as a special case: Indeed we can derive the action for MA in the same way as we derived the action for MAR from the truncation for the DDM, i.e., by enforcing an additional symmetry. Requiring invariance of $\mathcal{S}_{\text{cg}}^{\text{MAR}}$ under complex conjugation of the fields,

$$C \tilde{\Phi}_\nu = \sigma_x \tilde{\Phi}_\nu, \quad (62)$$

we find the additional constraint $\bar{r} = -Z_{I,\text{cg}}/Z_{R,\text{cg}}$ (see Sec. B), reducing the number of independent parameters further. Then, after rescaling the quantum fields with Z_{cg} it becomes apparent that this model describes purely dissipative dynamics as we will show in Sec. IV D.

B. Truncation for MAR

We proceed by specifying the truncation for a FRG analysis of MAR. Here it is crucial to note that the transformation \mathcal{T} Eq. (59) not only leaves the action Eq. (60) invariant, but is actually a symmetry of the full theory,⁶⁴ i.e., of the effective action. Then, if the cutoff $\Delta \mathcal{S}_k$ in Eq. (35) is \mathcal{T} -invariant as well (this is indeed the case for the choice Eq. (33)), also the scale-dependent effective action Γ_k^{MAR} must obey the symmetry. This requirement implies restrictions on the RG flow: Invariance of the effective action on all scales is guaranteed by the ansatz

$$\begin{aligned} \Gamma_k^{\text{MAR}} &= \int_X \bar{\Phi}_q^\dagger \left[(Z_R \sigma_z - iZ_I \mathbb{1}) i \partial_t \bar{\Phi}_c \right. \\ &\quad \left. + (i\sigma_z - \bar{r}\mathbb{1}) \frac{\delta \tilde{\mathcal{U}}_D}{\delta \bar{\Phi}_c^*} + i \frac{\tilde{\gamma}}{2} \bar{\Phi}_q \right], \end{aligned} \quad (63)$$

which follows by enforcing the symmetry on the truncation Eq. (42) (see Sec. B for details). We note in particular that compatibility of coherent and dissipative dynamics is conserved in the RG flow. In contrast to the DDM, here the Keldysh mass is not an independent running coupling, as it is linked to the wave-function renormalization $Z = Z_R + iZ_I$ by the Ward identity of the symmetry Eq. (59),

$$\tilde{\gamma} = \frac{Z_R - \bar{r}Z_I}{Z_{R,\text{cg}} - \bar{r}Z_{I,\text{cg}}} \tilde{\gamma}_{\text{cg}}. \quad (64)$$

In comparison to the DDM, therefore, MAR is described by a reduced number of couplings: Our truncation Eq. (42) for the DDM is parameterized by a vector of couplings

$$\bar{\mathbf{g}} = (Z, \bar{K}, \bar{\rho}_0, \bar{u}_1, \bar{u}_2, \bar{u}_3, \tilde{\gamma})^T, \quad (65)$$

where $Z, \bar{K}, \bar{u}, \bar{u}_3$ are complex whereas $\bar{\rho}_0, \tilde{\gamma}$ are positive real numbers. In MAR, the real parts of the complex couplings in the functional $\tilde{\mathcal{U}}$ are determined by imaginary ones and the ratio \bar{r} . Additionally the Keldysh mass is related to the wave-function renormalization via Eq. (64), so that a reduced set of couplings,

$$\bar{\mathbf{g}}_{\text{MAR}} = (Z, \bar{r}, \bar{D}, \bar{\rho}_0, \bar{k}_1, \bar{k}, \bar{k}_3)^T, \quad (66)$$

is sufficient to fully specify the truncation Eq. (63). In the purely dissipative MA, finally, the symmetry Eq. (62) determines \bar{r} in terms of the wave-function renormalization Z as $\bar{r} = -Z_I/Z_R$ (see Sec. B), excluding the former from the list of independent running couplings. The truncation for MA, therefore, is described by

$$\bar{\mathbf{g}}_{\text{MA}} = (Z, \bar{D}, \bar{\rho}_0, \bar{k}_1, \bar{k}, \bar{k}_3)^T. \quad (67)$$

We emphasize that MAR is a formal model which will help to prove and sharpen the non-equilibrium character of the DDM. However, it rests on an artificial fine-tuning of and imaginary parts. The physically realistic model which the DDM should be compared to is model E, which describes the equilibrium Bose condensation transformation. It has three independent exponents only, its dynamical exponent deviates from MA due to an additional slow diffusive mode related to particle number conservation.

C. Fluctuation-dissipation theorem

In the following we will show that the symmetry Eq. (59) implies a classical FDT for MAR.^{63–65} If we regard the full propagators of the theory as the $k \rightarrow 0$ limits of the RG flow of scale-dependent propagators, we may say that the FDT holds for MAR (and, *a fortiori*, for MA) for all $0 < k < k_{\text{cg}}$. Below we will see that this is not the case for the driven-dissipative system we consider. There the equilibrium symmetry is not present at mesoscopic scales but rather emergent for the system at criticality in the infrared for $k \rightarrow 0$. As a result, thermalization sets in only at low frequencies and long wavelengths.

As indicated at the beginning of the preceding section, the transformation \mathcal{T} Eq. (59) is a symmetry of the full theory. In particular, for correlation functions we have

$$\langle \tilde{\phi}_\nu(t, \mathbf{x}) \tilde{\phi}_\nu^*(t', \mathbf{x}') \rangle = \langle \mathcal{T} \tilde{\phi}_\nu(t', \mathbf{x}') \mathcal{T} \tilde{\phi}_\nu^*(t, \mathbf{x}) \rangle, \quad (68)$$

along with corresponding relations for anomalous and higher correlation functions. Here expectation values are defined as

$$\langle \dots \rangle \equiv \int \mathcal{D}[\Phi_c, \Phi_q] \dots e^{iS_{\text{cg}}^{\text{MAR}}[\Phi_c, \Phi_q]}. \quad (69)$$

The relation Eq. (68) implies a FDT: For the particular choice of correlations between quantum fields $\nu = \nu' = q$ which vanish by construction of the Keldysh functional integral,^{52,53} we find

$$0 = \langle \tilde{\phi}_q(t, \mathbf{x}) \tilde{\phi}_q^*(t', \mathbf{x}') \rangle = \langle \mathcal{T} \tilde{\phi}_q(t, \mathbf{x}) \mathcal{T} \tilde{\phi}_q^*(t', \mathbf{x}') \rangle. \quad (70)$$

Inserting here explicit expressions for the \mathcal{T} -transformed fields and performing a Fourier transformation, we obtain the classical FDT

$$\tilde{G}^K(\omega, \mathbf{q}) = \frac{2T}{\omega} (\tilde{G}^R(\omega, \mathbf{q}) - \tilde{G}^A(\omega, \mathbf{q})). \quad (71)$$

Such a relation is in general not valid in the DDM. It is, however, emergent for the critical system in the long-wavelength limit: In the basis $\hat{\phi}_c = \phi_c, \hat{\phi}_q = i(Z/|Z|)\phi_q$ we have for the inverse propagators at the scale k (for convenience we are working here in the symmetric phase) $\hat{P}^R(\omega, \mathbf{q}) = i|Z|(\omega - \xi^*(q)) = \hat{P}^A(\omega, \mathbf{q})^\dagger$ where $\xi(q) = Kq^2 + u_1$ (note that here the renormalized quantities appear) and $\hat{P}^K = \hat{P}^K$. With these inverse propagators we form the ratio

$$\frac{\omega}{2} \frac{\hat{P}^K}{\hat{P}^R(Q) - \hat{P}^A(Q)} = \frac{\bar{\gamma}}{4|Z|} \frac{\omega}{\omega - \text{Re} \xi(q)}, \quad (72)$$

which would equal the temperature if a FDT were valid.⁶⁶ As we will see in Sec. VI C, the effective action for the critical system becomes purely dissipative for $k \rightarrow 0$. In particular we have $\text{Re} \xi(q) \rightarrow 0$ so that Eq. (72) indeed reduces to an FDT with an effective temperature

$$T_{\text{eff}} = \frac{\bar{\gamma}}{4|Z|}. \quad (73)$$

Note that for purely dissipative dynamics Eq. (64) implies that the ratio $\bar{\gamma}/|Z|$ is a constant of the RG flow. For the DDM the emergence of an FDT with T_{eff} manifests itself in the relation Eq. (113) between the anomalous dimensions of $\bar{\gamma}$ and Z valid at the fixed point. The flow of $\bar{\gamma}/(4|Z|)$ is shown in Fig. 2.

D. Geometric interpretation of the equilibrium symmetry

For our truncation of the effective action Γ_k^{MAR} , the relation $\tilde{\mathcal{U}}_H = \bar{r}\tilde{\mathcal{U}}_D$ between the real and imaginary parts of the functional $\tilde{\mathcal{U}} = \tilde{\mathcal{U}}_H + i\tilde{\mathcal{U}}_D$ implies that the couplings parameterizing $\tilde{\mathcal{U}}_H$ and $\tilde{\mathcal{U}}_D$ share a common ratio \bar{r} of real to imaginary parts

$$\bar{r} = \frac{\bar{A}}{\bar{D}} = \frac{\bar{\lambda}_1}{\bar{\kappa}_1} = \frac{\bar{\lambda}}{\bar{\kappa}} = \frac{\bar{\lambda}_3}{\bar{\kappa}_3}. \quad (74)$$

The same applies to the renormalized couplings, however, with a different value r : With $z = -Z_I/Z_R$ we have

$$r = \frac{A}{D} = \frac{\lambda_1}{\kappa_1} = \frac{\lambda}{\kappa} = \frac{\lambda_3}{\kappa_3} = \frac{\bar{r} - z}{1 + \bar{r}z}. \quad (75)$$

This can be visualized conveniently in the complex plane, where the ratio of real to imaginary parts contains the same information as the argument of a complex number (the argument is $\tan(1/r)$): The renormalization of a complex coupling \bar{g} with Z corresponds to a rescaling $|\bar{g}| = |\bar{g}|/|Z|$ of the modulus and a rotation of the phase by the argument of Z , $\arg g = \arg \bar{g} - \arg Z$. The condition Eq. (74) corresponding to MAR is depicted in Fig. 6 (b): All bare⁶⁷ couplings lie on a single ray. In the purely dissipative case with $r = 0$ and $\bar{r} = z$, which is shown in Fig. 6 (a), this ray is perpendicular to Z . As a result, in this case the renormalized couplings are purely imaginary. Generally, only the renormalized quantities allow for an immediate physical interpretation: A and D describe propagation and diffusion of particles, respectively, while λ (λ_3) and κ (κ_3) are two-body (three-body) elastic collisions and loss. In the generic driven-dissipative case, we have no *a priori* relations between these couplings because they are due to different physical mechanisms: Dissipative couplings describe local incoherent single particle pump and loss, as well as local two-body loss. On the other hand, unitary dynamics is given by coherent propagation and elastic collisions. Geometrically, the physical couplings point in different directions in the first quadrant of the complex plane (see Fig. 6 (c)), the latter restriction being due to the physical stability of the system (see Sec. III A).

This concludes our discussion of the relation of the driven-dissipative model to thermodynamic equilibrium models. In the following section we will proceed to derive explicit flow equations for the couplings Eq. (65).

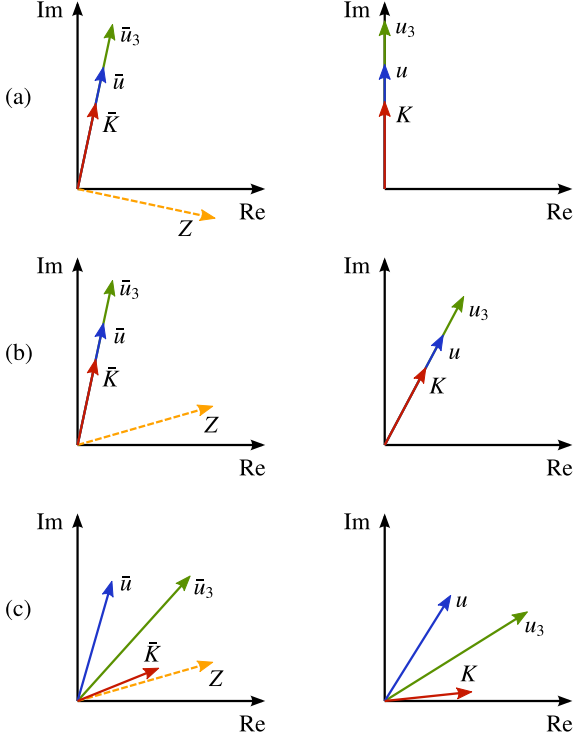


Figure 6. Visualization of the renormalization with Z . Left column: Bare couplings. Right column: Renormalized couplings. The renormalization of a complex coupling \bar{g} corresponds to a rescaling $|g| = |\bar{g}|/|Z|$ of the modulus and a rotation of the phase by the argument of Z , $\arg g = \arg \bar{g} - \arg Z$. (a) When all bare couplings lie on a single ray that is perpendicular to Z , the renormalized couplings are purely imaginary as in MA. (b) Deviations from the right angle incorporate MA with compatible reversible mode-couplings. (c) In a generic non-equilibrium situation there is no fixed relation between the arguments of the various couplings.

V. NON-EQUILIBRIUM FRG FLOW EQUATIONS

In the following we discuss how the functional differential equation Eq. (38) for the effective action is reduced to a set of ordinary differential equations by virtue of the ansatz Eq. (42) for Γ_k . First we derive the flow equation for the effective potential, i.e., the part of the effective action that involves all momentum-independent couplings. Then we proceed to specify the flow of the inverse propagator which determines flow equations for the wave-function renormalization Z and the gradient coefficient \bar{K} . In the FRG, we approach the critical point from the ordered (symmetry-broken) side of the transition. This allows us to capture the leading divergences of two-loop effects in a calculation that is formally one-loop⁴⁶ by means of diagrams like the second one in Eq. (32) in the spirit of the background field method in gauge theories.⁶⁸

We denote the truncation Eq. (42), evaluated for homogeneous, i.e., space- and time-independent “background fields” by

$$\Gamma_{k,cq} = -\Omega \left(\bar{U}' \bar{\rho}_{cq} + \bar{U}'' \bar{\rho}_{qc} - i\bar{\gamma} \bar{\rho}_q \right), \quad (76)$$

(the subscript cq indicates that we have classical and quantum background fields) where Ω is the quantization volume and the $U(1)$ invariant combinations of fields are $\bar{\rho}_{cq} = \bar{\phi}_c^* \bar{\phi}_q = \bar{\rho}_{qc}^*$ and $\bar{\rho}_q = \bar{\phi}_q^* \bar{\phi}_q$. This representation of $\Gamma_{k,cq}$ implies that the flow equation for the potential \bar{U}' can be obtained from Eq. (38) by taking the derivative with respect to $\bar{\rho}_{cq}$ and setting the quantum background fields to their stationary value (which is zero) afterwards,

$$\partial_t \bar{U}' = -\frac{1}{\Omega} \left[\partial_{\bar{\rho}_{cq}} \partial_t \Gamma_{k,cq} \right]_{\bar{\phi}_q = \bar{\phi}_q^* = 0}, \quad (77)$$

where the dimensionless RG flow parameter t is related to the cutoff scale k via $t = \ln(k/\Lambda)$. The flow equation for the renormalized potential follows straightforwardly by taking the scale derivative of the relation $\bar{U} = ZU$, which results in

$$\partial_t \bar{U}' = Z(-\eta_Z U' + \partial_t U'), \quad (78)$$

where we introduced the anomalous dimension of the wave-function renormalization,

$$\eta_Z = -\partial_t Z/Z. \quad (79)$$

Then, using $\partial_{\bar{\rho}_{cq}} = Z \partial_{\rho_{cq}}$, the flow equation for the renormalized potential can be written as

$$\partial_t U' = \eta_Z U' + \zeta', \quad \zeta' = -\frac{1}{\Omega} \left[\partial_{\rho_{cq}} \partial_t \Gamma_{k,cq} \right]_{\phi_q = \phi_q^* = 0}. \quad (80)$$

We proceed by specifying the projection prescriptions that allow us to derive the flow of the couplings u_n in the ordered phase from the flow equation (80). Taking the scale derivatives of the relation $u_n = U^{(n)}(\rho_0)$ we find

$$\partial_t u_n = \left(\partial_t U^{(n)} \right) (\rho_0) + U^{(n+1)}(\rho_0) \partial_t \rho_0. \quad (81)$$

Based on the power-counting arguments of Sec. III F, our truncation includes terms up to cubic order in the $U(1)$ invariants, i.e., for derivatives of the effective potential of the order of $n \geq 4$ we have $U^{(n)} = 0$. The flow equations for the quartic and sextic couplings are then given by (the RHS of these equations determine the so-called β -functions)

$$\partial_t u_2 = \beta_{u_2} = \eta_Z u_2 + u_3 \partial_t \rho_0 + \partial_{\rho_c} \zeta' \Big|_{\text{ss}}, \quad (82)$$

$$\partial_t u_3 = \beta_{u_3} = \eta_Z u_3 + \partial_{\rho_c}^2 \zeta' \Big|_{\text{ss}}, \quad (83)$$

where according to Eq. (81) in ζ' we specify the classical background field ρ_c it to its stationary value $\rho_c|_{\text{ss}} = \rho_0$. As we have seen above (cf. Secs. III A and III D, the latter is determined by the dissipative part of the field equation, i.e., by the condition $\text{Im} U'(\rho_0) = 0$. Taking here the derivative with respect to the RG parameter t , we find

$$\partial_t \rho_0 = -(\text{Im} \partial_t U')(\rho_0) / \text{Im} U''(\rho_0) = -\text{Im} \zeta' \Big|_{\text{ss}} / \kappa. \quad (84)$$

Having thus specified the flow equations for the couplings that parameterize the potential U , we proceed to the Keldysh mass $\bar{\gamma}$, which is the coefficient of the term that is proportional to

the quantum $U(1)$ invariant $\bar{\rho}_q$ in Eq. (76). We obtain the flow equation for $\bar{\gamma}$ as

$$\partial_t \bar{\gamma} = -\frac{i}{\Omega} \left[\partial_{\bar{\rho}_q} \partial_t \Gamma_{k,cq} \right]_{\text{ss}}. \quad (85)$$

For the renormalized Keldysh mass, which is related to the bare one via $\gamma = \bar{\gamma}/|Z|^2$, we have (the transformation from bare to renormalized fields implies $\partial_{\bar{\rho}_q} = |Z|^2 \partial_{\rho_q}$)

$$\partial_t \gamma = \beta_\gamma = 2\eta_{ZR}\gamma + \zeta_\gamma, \quad \zeta_\gamma = -\frac{i}{\Omega} \left[\partial_{\rho_q} \partial_t \Gamma_{k,cq} \right]_{\text{ss}}. \quad (86)$$

While the flow of $\Gamma_{k,cq}$ (i.e., the flow equation evaluated at homogeneous background fields) yields flow equations for all momentum-independent couplings, we have to consider the flow of the inverse propagator

$$\partial_t \bar{P}_{ij}(Q) \delta(Q - Q') = \left[\frac{\delta^2 \partial_t \Gamma_k}{\delta \bar{\chi}_i(-Q) \delta \bar{\chi}_j(Q')} \right]_{\text{ss}}, \quad (87)$$

in order to derive flow equations for the wave-function renormalization Z and the gradient coefficient \bar{K} . The retarded component of the inverse propagator in the presence of real stationary background fields $\bar{\phi}_c = \bar{\phi}_c^* = \bar{\phi}_0$ reads

$$\bar{P}^R(Q) = \begin{pmatrix} -iZ_I\omega - \bar{K}_R q^2 - 2\bar{\lambda}\bar{\rho}_0 & iZ_R\omega - \bar{K}_I q^2 \\ -iZ_R\omega + \bar{K}_I q^2 + 2\bar{\kappa}\bar{\rho}_0 & -iZ_I\omega - \bar{K}_R q^2 \end{pmatrix}, \quad (88)$$

Then, for the kinetic coefficient \bar{K} we choose from the flow equation (87) the elements of the inverse propagator that do not have mass-like contributions⁴⁶ $2\bar{\lambda}\bar{\rho}_0$ and $2\bar{\kappa}\bar{\rho}_0$,

$$\partial_t \bar{K} = -\partial_{q^2} \left(\partial_t \bar{P}_{22}^R(Q) + i\partial_t \bar{P}_{12}^R(Q) \right) \Big|_{Q=0}. \quad (89)$$

The flow equation for the wave-function renormalization Z as specified below, on the other hand, mixes massive and massless components symmetrically

$$\partial_t Z = -\frac{1}{2} \partial_\omega \text{tr} \left[(\mathbb{1} + \sigma_y) \partial_t \bar{P}^R(Q) \right] \Big|_{Q=0}. \quad (90)$$

This choice allows for the locking of the flows of the Keldysh mass and Z as implied by the emergence of the symmetry Eq. (59) in the purely dissipative IR regime (see Sec. VI). Finally, the flow equation for the renormalized coefficient K follows by straightforward differentiation of its definition $K = \bar{K}/Z$ in terms of bare quantities. We find

$$\partial_t K = \beta_K = \eta_Z K + \partial_t \bar{K}/Z. \quad (91)$$

The truncation Eq. (42) is parameterized in terms of the couplings Eq. (65). Renormalization of the fields with Z leads to a description in terms of $\mathbf{g} = (K, \rho_0, u, u_2, u_3, \gamma)^T$ (where we omit the mass u_1 : as indicated above we approach the critical point from the ordered phase, i.e., we parameterize the effective action in terms of the stationary condensate density ρ_0 instead of the mass u_1). In this section we derived the β -functions for these renormalized couplings, i.e., we have specified a closed set of flow equations $\partial_t \mathbf{g} = \beta_{\mathbf{g}}(\mathbf{g})$ from which Z can be completely eliminated (the anomalous dimension η_Z entering the β -functions can again be expressed in terms of the couplings \mathbf{g} alone). More explicit expressions for the β -functions are provided in App. C 3).

VI. SCALING SOLUTIONS

As one considers an effective description of a system at a continuous phase transition at longer and longer scales (which is equivalent to following the RG flow to smaller values of k), physical observables and the couplings that describe the system exhibit scaling behavior. The search for such scaling solutions to the flow equations is facilitated by introducing rescaled dimensionless (in the sense of the canonical power counting introduced in Sec. III F) couplings which remain constant, i.e., by searching for a fixed point of the flow equations of these rescaled couplings instead. In the following section we introduce such rescaled couplings and derive the corresponding flow equations.

A. Scaling form of the flow equations

As a first step we trade the real parts of K , u_2 , and u_3 for the ratios of real to imaginary parts

$$r_K = A/D, \quad r_{u_2} = \lambda/\kappa, \quad r_{u_3} = \lambda_3/\kappa_3, \quad (92)$$

which measure the relative strength of coherent and dissipative dynamics. As we will show below, at criticality all these ratios flow to zero signaling decoherence. Their flow is given by

$$\partial_t r_K = \beta_{r_K} = \frac{1}{D} (\beta_A - r_K \beta_D), \quad (93)$$

$$\partial_t r_{u_2} = \beta_{r_{u_2}} = \frac{1}{\kappa} (\beta_\lambda - r_{u_2} \beta_\kappa), \quad (94)$$

$$\partial_t r_{u_3} = \beta_{r_{u_3}} = \frac{1}{\kappa_3} (\beta_{\lambda_3} - r_{u_3} \beta_{\kappa_3}). \quad (95)$$

(The β -functions for the real and imaginary parts of K , u_2 , and u_3 are specified in App. C 2, see Eq. (C34).) We proceed by introducing a dimensionless mass term

$$w = \frac{2\kappa\rho_0}{k^2 D}, \quad (96)$$

the flow equation of which mixes contributions from the β -functions of ρ_0 , κ , and D , and reads

$$\partial_t w = \beta_w = -(2 - \eta_D) w + \frac{w}{\kappa} \beta_\kappa + \frac{2\kappa}{k^2 D} \beta_{\rho_0}, \quad (97)$$

where the anomalous dimension of D is defined as

$$\eta_D = -\partial_t D/D. \quad (98)$$

Finally we replace the quartic and sextic couplings by dimensionless ones. For a momentum-independent n -body coupling u_n we can construct a corresponding dimensionless coupling by means of the relation

$$\tilde{u}_n = \frac{k^{(d-2)n-d}}{D^n} \left(\frac{\gamma}{2} \right)^{n-1} u_n. \quad (99)$$

The flow equations for the imaginary parts $\tilde{\kappa}$ and $\tilde{\kappa}_3$ of the dimensionless quartic and sextic couplings, therefore, are given by

$$\partial_t \tilde{\kappa} = \beta_{\tilde{\kappa}} = -\left(4 - d - 2\eta_D + \eta_\gamma\right) \tilde{\kappa} + \frac{k^{-4+d}\gamma}{2D^2} \beta_\kappa, \quad (100)$$

$$\partial_t \tilde{\kappa}_3 = \beta_{\tilde{\kappa}_3} = -\left(6 - 2d - 3\eta_D + 2\eta_\gamma\right) \tilde{\kappa}_3 + \frac{k^{-6+2d}\gamma^2}{4D^3} \beta_{\kappa_3}, \quad (101)$$

and include contributions from the anomalous dimension

$$\eta_\gamma = -\partial_t \gamma / \gamma. \quad (102)$$

Thus we are left with six dimensionless running couplings, which we collect in vectors $\mathbf{r} = (r_K, r_{u_2}, r_{u_3})^T$ and $\mathbf{s} = (w, \tilde{\kappa}, \tilde{\kappa}_3)^T$. Their flow equations form a closed set,

$$\partial_t \mathbf{r} = \beta_{\mathbf{r}}(\mathbf{r}, \mathbf{s}), \quad \partial_t \mathbf{s} = \beta_{\mathbf{s}}(\mathbf{r}, \mathbf{s}). \quad (103)$$

The β -functions on the RHS of these equations contain the anomalous dimensions η_Z, η_D , and η_γ , which in turn can be expressed as functions of the running couplings \mathbf{r} and \mathbf{s} alone. We note in passing that according to the discussion of Sec. IV D, the equilibrium model MAR is described by $r_K = r_{u_2} = r_{u_3} = r$, i.e.,

$$\mathbf{r}_{\text{MAR}} = r(1, 1, 1)^T \quad (104)$$

(MA is realized for the special case $r = 0$). Inserting the same value r for all three ratios in the respective β -functions we find $\beta_{r_K} = \beta_{r_{u_2}} = \beta_{r_{u_3}}$, which shows that for MAR the common ratio is preserved by the flow as it should be.

Our analysis of the flow equations (103) will proceed in two steps: First we will search for fixed points \mathbf{r}_* and \mathbf{s}_* , which are solutions to the algebraic equations

$$\beta_{\mathbf{r}}(\mathbf{r}_*, \mathbf{s}_*) = \beta_{\mathbf{s}}(\mathbf{r}_*, \mathbf{s}_*) = \mathbf{0}. \quad (105)$$

In Sec. VI B we briefly discuss the trivial Gaussian fixed point and then turn to the Wilson-Fisher fixed point that describes the critical system in VI C). Second we will solve the full flow equations numerically and provide our results in Sec. VII. While already the linearized flow equations in the vicinity of the Wilson-Fisher fixed point encode universal physics at the phase transition and determine the asymptotic flow of the system for $k \rightarrow 0$ (or $t \rightarrow -\infty$), the numerical integration of the full flow equations provides us with information on non-universal aspects such as the extent of the scaling regime.

B. Gaussian fixed point

All β -functions vanish on the manifold of Gaussian fixed points which is parameterized by $\mathbf{s}_* = \mathbf{0}$ and $\mathbf{r}_* \in \mathbb{R}^3$. We note that the combination of vanishing imaginary parts $\tilde{\kappa}_*$ and $\tilde{\kappa}_{3*}$ of the quartic and sextic couplings and arbitrary finite ratios of real to imaginary parts implies that also the real parts of \tilde{u}_{2*} and \tilde{u}_{3*} are zero on this fixed point manifold. In a linearization

of the flow equations around $\mathbf{s}_* = \mathbf{0}$, the fluctuation contributions vanish and the scaling behavior is determined solely by the canonical scaling dimensions, implying in particular that the Gaussian fixed point is unstable (for small values $\mathbf{s} \neq \mathbf{s}_*$ the flow is directed away from the fixed point) and, therefore, physically not relevant. Non-trivial scaling behavior at criticality is governed by the Wilson-Fisher fixed point which we will discuss in the next section.

C. Wilson-Fisher fixed point: critical behavior

As discussed in Sec. IV, our driven-dissipative model reduces to MA when we set the real parts of all renormalized couplings to zero, cf. Fig. 6, i.e., for $\mathbf{r} = \mathbf{0}$. It is well-known that MA exhibits a non-trivial Wilson-Fisher fixed point,³⁷ and indeed we find this fixed point at

$$\begin{aligned} \mathbf{r}_* &= (r_{K_*}, r_{u_*}, r_{u'_*}) = \mathbf{0}, \\ \mathbf{s}_* &= (w_*, \tilde{\kappa}_*, \tilde{\kappa}'_*) = (0.475, 5.308, 51.383). \end{aligned} \quad (106)$$

The values of the coupling \mathbf{s}_* are identical to those obtained in an equilibrium classical $O(2)$ model from functional RG calculations at the same level of truncation.⁴⁶ We note that this fixed point is also contained in the subspace of couplings corresponding to MAR, which is characterized by Eq. (104), i.e., the phase transitions in both the equilibrium and non-equilibrium models are described by the same fixed point. Critical behavior, however, is determined by the RG flow in the vicinity of the fixed point. Here the non-equilibrium setting adds two more independent directions, thereby opening up the possibility for deviations from equilibrium criticality as we will now show.

The asymptotic flow for $k \rightarrow 0$ of the critical system is determined by a linearization of the flow equations in the deviations $\delta \mathbf{s} \equiv \mathbf{s} - \mathbf{s}_*$, $\delta \mathbf{r} \equiv \mathbf{r}$ from the fixed point. In the linear regime the two sectors corresponding to \mathbf{s} and \mathbf{r} decouple as described by the block diagonal stability matrix

$$\partial_t \begin{pmatrix} \delta \mathbf{r} \\ \delta \mathbf{s} \end{pmatrix} = \begin{pmatrix} N & 0 \\ 0 & S \end{pmatrix} \begin{pmatrix} \delta \mathbf{r} \\ \delta \mathbf{s} \end{pmatrix}, \quad (107)$$

where the 3×3 submatrices S and N are given by

$$S = \nabla_{\mathbf{s}}^T \beta_{\mathbf{s}} \Big|_{\mathbf{r}=\mathbf{r}_*, \mathbf{s}=\mathbf{s}_*} = \begin{pmatrix} -1.620 & 0.088 & 0.005 \\ -3.183 & 0.290 & 0.036 \\ -15.374 & -42.249 & 2.183 \end{pmatrix}, \quad (108)$$

$$N = \nabla_{\mathbf{r}}^T \beta_{\mathbf{r}} \Big|_{\mathbf{r}=\mathbf{r}_*, \mathbf{s}=\mathbf{s}_*} = \begin{pmatrix} 0.053 & 0.059 & 0.032 \\ 0 & -0.053 & 0.196 \\ 0.498 & -2.327 & 1.973 \end{pmatrix}. \quad (109)$$

The matrix N would be identically zero in the absence of anomalous additions to the canonical scaling dimensions (note that the ratios \mathbf{r} have canonical scaling dimension zero), or even if coherent and dissipative couplings would exhibit identical anomalous scaling. The non-vanishing of this block thus indicates a different universal behavior of these two types of couplings. Due to the decoupling of the flows of \mathbf{r} and \mathbf{s} we

	ν	η	z	η_r
$O(2)$	0.716	0.039		
MA	0.716	0.039	2.121	
MAR	0.716	0.039	2.121	0.101
DDM	0.716	0.039	2.121	0.143

Table I. Results for the correlation length exponent ν , the anomalous dimension η , the dynamical critical exponent z , and the decoherence exponent η_r in our truncation.

may discuss the linearized flow of each set of couplings separately.

In the matrix S we find one negative eigenvalue s_1 corresponding to the correlation length exponent $\nu = -1/s_1 = 0.716$ (our findings for critical exponents are summarized in Tab. I), and two complex conjugate eigenvalues $s_{2,3} = 1.124 \pm i0.622$ with positive real parts (indicating that these directions are stable). The imaginary parts are known artifacts of this level of truncation for the $O(2)$ model and vanish upon inclusion of higher order terms in the effective potential.⁶⁹

The scaling behavior of the couplings Z, D , and γ is determined by the values of the respective anomalous dimensions at the fixed point. In addition we define the anomalous dimension for the bare kinetic coefficient \bar{K} as

$$\eta = -\partial_t \bar{K} / \bar{K} = \frac{1}{1 + r_K^2} \left[r_K^2 \bar{\eta}_A + \bar{\eta}_D - i r_K (\bar{\eta}_A - \bar{\eta}_D) \right], \quad (110)$$

where the representation in terms of $\bar{\eta}_A$ and $\bar{\eta}_D$ follows from the definition of these quantities in Eq. (C32). At the fixed point η takes the value

$$\eta = 0.039, \quad (111)$$

which is again the result for the anomalous dimension of the classical $O(2)$ model in $d = 3$ dimensions at the same level of truncation⁴⁶ and agrees well with results from more accurate calculations.⁷⁰ In summary, the static critical behavior coincides precisely with the one of the classical $O(2)$ model, implying that the dynamical critical exponent η_Z effectively does not enter the corresponding equations. This can be seen as follows: Inserting $\mathbf{r} = \mathbf{0}$ in the expressions for the anomalous dimensions, we find

$$\eta_{ZR} = -\eta_\gamma, \quad \eta_{ZI} = 0. \quad (112)$$

(We note that this holds for all values of the static couplings \mathbf{s} , i.e., it is always realized in MA.) These relations ensure that η_{ZR} and η_γ compensate each other in all flow equations.⁷¹ Moreover they imply that the ratio $\bar{\gamma}/|Z|$ appearing on the RHS of the fluctuation-dissipation relation Eq. (72) approaches a constant value at the fixed point: According to the definition of the anomalous dimensions Eqs. (79) and (102), close to the fixed point the flow of Z and γ is described by $Z \sim k^{-\eta_Z}$ (note that η_Z is real so that this behavior indeed describes algebraic scaling and does not contain oscillatory parts) and $\gamma \sim k^{-\eta_\gamma}$ with η_Z and η_γ evaluated at \mathbf{r}_* and \mathbf{s}_* . Thus we find $\bar{\gamma}/|Z| = |Z| \gamma \sim k^{-\eta_Z - \eta_\gamma} = \text{const.}$, i.e.,

the symmetry Eq. (59), which manifests itself in this quantity approaching a constant value (cf. Eq. (73)), emerges in the IR without imposing it in the microscopic model. In other words, the driven-dissipative system obeys a classical FDT in the long-wavelength limit (see Fig. 2). At the fixed point we find the value

$$\eta_Z = -\eta_\gamma = 0.161. \quad (113)$$

Let us now consider the upper left block N of the stability matrix. It has three positive eigenvalues,

$$n_1 = 0.101, \quad n_2 = 0.143, \quad n_3 = 1.728, \quad (114)$$

which indicates that the ratios \mathbf{r} are attracted to their fixed point value zero. The corresponding eigenvectors are

$$\mathbf{u}_1 = \begin{pmatrix} 0.022 \\ 0.109 \\ 0.994 \end{pmatrix}, \quad \mathbf{u}_2 = \frac{1}{\sqrt{3}} \begin{pmatrix} 1 \\ 1 \\ 1 \end{pmatrix}, \quad \mathbf{u}_3 = \begin{pmatrix} 0.802 \\ 0.469 \\ 0.370 \end{pmatrix}. \quad (115)$$

The smallest of the eigenvalues determines the scaling behavior of \mathbf{r} in the deep IR. In order to see this let us expand \mathbf{r} in the basis of eigenvectors of the matrix N ,

$$\mathbf{r} = \sum_{i=1}^3 \mathbf{u}_i c_i. \quad (116)$$

The coefficients in this expansion are given by $c_i = \mathbf{v}_i \cdot \mathbf{r}$, where \mathbf{v}_i are the left eigenvectors of N (the latter is not symmetric and its left and right eigenvectors, therefore, are not equal), normalized such that $\mathbf{u}_i \cdot \mathbf{v}_j = \delta_{ij}$. The asymptotic behavior of the flow of the so-called scaling fields⁵³ c_i is given by $c_i \sim e^{n_i t} = k^{n_i}$, which implies that for \mathbf{r} we indeed find

$$\mathbf{r} \sim \mathbf{u}_1 k^{n_1} = \mathbf{u}_1 k^{-\eta_r}, \quad (117)$$

with only subdominant contributions in the directions of \mathbf{u}_2 and \mathbf{u}_3 . This leads us to identify the decoherence exponent

$$\eta_r = -n_1 = -0.101. \quad (118)$$

From the scaling behavior of the ratios \mathbf{r} we may infer the one of the coherent couplings. For the coefficient of coherent propagation A , in particular, we have

$$A = r_K D \sim k^{n_1 - \eta_D} = k^{-\eta_A}. \quad (119)$$

Then, with the anomalous dimension of the diffusion coefficient D at the fixed point,

$$\eta_D = -0.121, \quad (120)$$

we obtain the value

$$\eta_A = -0.223. \quad (121)$$

Let us discuss the consequences of this result for the effective dispersion relation of long-wavelength excitations, which is encoded in the running inverse propagator Eq. (48). Once

the cutoff scale k becomes smaller than the external momentum q , the effective infrared cutoff is given by q instead of k .⁷² Then, in the dispersion relation Eq. (53), which we rewrite here in terms of the scaling variables introduced in Sec. VI A as

$$\omega_{1,2}^R = Dq^2 \left[-i(1 + w/2) \pm \sqrt{r_K^2 + r_K r_u w - (w/2)^2} \right], \quad (122)$$

we may insert the scaling forms $A \sim A_0 q^{-\eta_A}$ and $D \sim D_0 q^{-\eta_D}$. For $q \rightarrow 0$ both modes are purely diffusive with $\omega_1^R \sim -iD_0 q^{2-\eta_D}$ and $\omega_2^R \sim -iD_0 q^{2-\eta_D} (1 + w_*)$, and for the dynamical critical exponent z which is defined via the relation $\omega^R \sim -iq^z$ we find the value

$$z = 2 - \eta_D = 2.121. \quad (123)$$

Above the purely diffusive IR regime, when $w \ll r_K, r_u$, the dispersion relation simplifies to

$$\omega_{1,2}^R \sim (-iD \pm Dr_K) q^2 \sim -iD_0 q^{2.121} \pm A_0 q^{2.223}, \quad (124)$$

i.e., coherent propagation and diffusion contributions scale differently with the momentum q . The observable consequences of this finding are discussed in Sec. II.

Before moving on to a numerical integration of the flow equations in the next section, we briefly contrast our findings with the equilibrium case of MAR. There, analyzing the stability of the fixed point Eq. (106) we have to take into account only one direction $r = r_K = r_{u_2} = r_{u_3}$, and we find (as $r_* = 0$ we have $\delta r \equiv r$)

$$\partial_t \begin{pmatrix} \delta r \\ \delta s \end{pmatrix} = \begin{pmatrix} R & 0 \\ 0 & S \end{pmatrix} \begin{pmatrix} \delta r \\ \delta s \end{pmatrix} \quad (125)$$

where the matrix S is the same as above and the element R is given by the ‘‘middle’’ eigenvalue Eq. (114) of the stability matrix N in the non-equilibrium problem,

$$R = \partial_r \beta_r \Big|_{r=r_*, s=s_*} = n_2, \quad (126)$$

i.e., also in the equilibrium setting we find decoherence at the longest scales, however, with a value of the decoherence exponent that is different from the one in non-equilibrium. Let us finally remark that in the linearized regime, the fact that MAR is contained as a special case in the non-equilibrium problem, becomes visible in the form of the second eigenvector Eq. (115) which realizes the constraint Eq. (104).

VII. NUMERICAL INTEGRATION OF FLOW EQUATIONS

In the previous section we have seen that the flow equations Eq. (103) entail non-trivial critical behavior governed by the Wilson-Fisher fixed point Eq. (106). While these results were based on an analysis of the linearized flow equations in the vicinity of the fixed point, we will now turn to a numerical integration of the full non-linear equations. On the one hand, this serves to illustrate the concept of universality: Independently from the initial values $\mathbf{r}_\Lambda, \tilde{\kappa}_\Lambda$, and $\tilde{\kappa}_{3\Lambda}$ at the mesoscopic

starting point of the RG flow, critical behavior can be induced by a proper fine-tuning of w_Λ and becomes apparent in the approach of the RG flow to the scaling solution. Apart from that, the availability of the full flow in the framework of the FRG allows us to extract non-universal aspects. In particular, we will give an estimate of the Ginzburg scale, i.e., the scale that separates the region of non-universal flow from the universal scaling regime and thus is important for determining experimental requirements on the necessary frequency resolution.

Our approach for finding numerical solutions to the flow equations that exhibit critical behavior is as follows: We choose initial values $\mathbf{r}_\Lambda, \tilde{\kappa}_\Lambda$, and $\tilde{\kappa}_{3\Lambda}$ at the mesoscopic scale $k = \Lambda$ ($t = 0$), which are appropriate for the description of the model introduced in Sec. III. This model contains two-body elastic interactions and loss, while three-body terms are contained only in an effective low-momentum description, implying $\tilde{\kappa}_\Lambda \approx 1$ and $\tilde{\kappa}_{3\Lambda} \ll 1$. The diffusion constant D is very small in the microscopic description, so that $r_{K\Lambda} \gg 1$ initially, while for the two-body terms we have $r_{u_2\Lambda} \approx 1$. The latter generate the three-body couplings and we assume that $r_{u_3\Lambda} \approx 1$ as well. For such a choice of initial values, there is a critical value $w_\Lambda = w_c$ so that the resulting RG trajectories $\mathbf{r}(t)$ and $\mathbf{s}(t)$ approach the scaling solution, i.e., the fixed point, for $k \rightarrow 0$ ($t \rightarrow -\infty$). Any solution obtained by *numerically* integrating the flow equations with w_Λ fine-tuned to w_c , however, eventually always flows away from the fixed point, as due to limited accuracy the solution develops a non-zero component in the unstable direction of the fixed point at some stage. For all solutions shown in the figures we choose w_Λ slightly below w_c , so that the trajectory at large RG ‘‘times’’ t flows to the symmetric phase with $w = 0$.

When such a near-critical trajectory approaches the scaling solution, the couplings \mathbf{s} flow towards their fixed point values \mathbf{s}_* on a scale $1/\text{Re } s_{2,3} \approx 1$ determined by the eigenvalues $s_{2,3}$ of the stability matrix S , cf. Fig. 7, and stay there for a long ‘‘time’’ t_s . Depending on how close w_Λ is to w_c , this duration is typically $t_s = 10$ to 20 which corresponds to several orders of magnitude in k/Λ . During t_s the ratios \mathbf{r} decay according to Eq. (116), i.e., as the sum of three exponentials, with decay rates given by the eigenvalues Eq. (114) of the stability matrix N . In order to extract these eigenvalues from the numerical solution, we consider the flow of the coefficients $c_i \sim e^{n_i t}$ in the expansion of \mathbf{r} in the basis of eigenvectors of N Eq. (116). Figure 7 shows $c_{1,2}$ along with exponential fits, which reproduce the eigenvalues $n_{1,2}$ to satisfactory accuracy.

An important result of the previous section is the scaling relation Eq. (113) between the anomalous dimensions η_Z and η_γ of the wave-function renormalization and the Keldysh mass respectively, which implies that when evaluated along a critical trajectory, the value of $-\eta_\gamma$ approaches the one of the real part η_{ZR} of η_Z , while the imaginary part η_{ZI} flows to zero. This prediction – physically implying asymptotic thermalization – is verified numerically in Fig. 8.

As the anomalous dimensions η_a of $a = Z, D$, and γ are functions of the renormalized dimensionless couplings \mathbf{r} and \mathbf{s} alone and not the quantities a themselves, we get the solutions to the flow equations $\partial_t a = -\eta_a a$ simply by exponentiating the integrals of the anomalous dimensions along RG trajectories

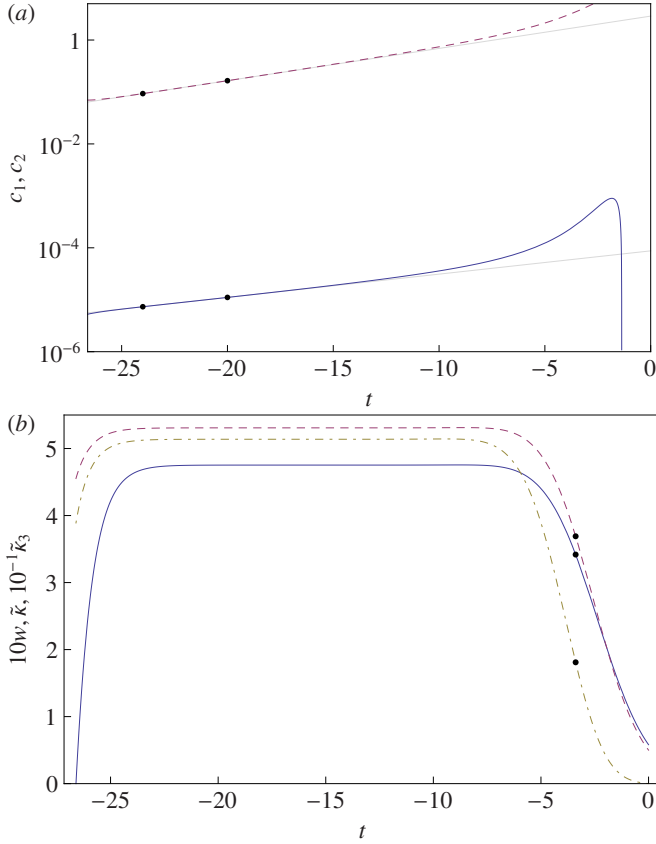


Figure 7. (a) The flow of c_1 (solid line) describes the vanishing of coherent dynamics. A fit with $c_1 = a_1 t + n_1$ in the region $t \in [-24, -20]$ (the points $t = -24$ and $t = -20$ are highlighted by dots on the trajectory) yields the slope $a_1 = 0.10$ in agreement with smallest eigenvalue $n_1 = -\eta_r$ of the stability matrix Eq. (109). We also show the evolution of the coefficient c_2 (dashed line). For the evolution of c_2 , the slope of a linear fit is $a_2 = 0.14$ and reproduces the eigenvalue n_2 . In the scaling region, the coefficient c_3 drops to very small values $\lesssim 10^{-11}$ on a scale $1/n_3 \approx 0.6$. The exponential decay of the components of \mathbf{r} is in this range still dominated by the contribution stemming from c_2 . (b) The couplings \mathbf{s} are close to the fixed point values \mathbf{s} , in the range from $t \approx -5$ to $t \approx -25$. A measure for the extent of the universal domain is given by the Ginzburg scale Eq. (128) which here takes the value $t_G \approx -3.4$. Initial conditions for both (a) and (b) are $r_{\kappa\Lambda} = r_{u\Lambda} = 10$, $r_{u_3\Lambda} = 1$, $w_\Lambda \approx 0.05810$, $\tilde{\kappa} = 0.5$, and $\tilde{\kappa}_3 = 0.01$.

$\mathbf{r}(t)$ and $\mathbf{s}(t)$, i.e.,

$$a(t) = a_\Lambda e^{-\int_0^t dr' \eta_a}. \quad (127)$$

In this way we obtain the trajectories of K shown in Fig. 3 and the flow of the effective temperature $T_{\text{eff}} = \bar{\gamma}/(4|Z|) = \gamma|Z|/4$ which according to the discussion in Sec. IV C at low frequencies approaches a constant value as illustrated in Fig. 2.

The near-critical trajectories we consider in this section illustrate the concept of universality in that they show how details of the microscopic model, which determine the initial conditions of the RG flow, are lost as we lower $k \rightarrow 0$, where all of these trajectories converge towards the scaling solution, cf. Fig. 1. However, a distinctly non-universal feature of these

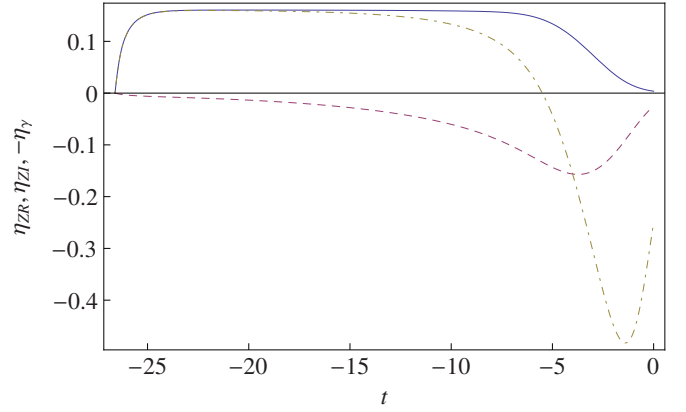


Figure 8. Anomalous dimensions η_{ZR} (solid), η_{ZI} (dashed), and $-\eta_\gamma$ (dot-dashed) for the solution of Fig. 7. From $t \approx -5$ to $t \approx -25$, where the values of \mathbf{s} are close to the scaling solution, η_{ZR} takes the constant value Eq. (113), while η_{ZI} decays to zero. The value of $-\eta_\gamma$ approaches the one of η_{ZR} so that Eq. (113) is satisfied at late “times” t . Eventually, as the trajectory is driven away from the fixed point and enters the symmetric phase with $w = 0$, the anomalous dimensions drop to zero.

trajectories is the point where the crossover to the universal regime takes place, which is known as the Ginzburg scale.³⁹ Physically, the Ginzburg scale marks the breakdown of mean-field theory as we approach the fluctuation-dominated critical region. In a perturbative estimate in the symmetric phase, we compare the bare distance from the phase transition κ_1 to the corresponding one-loop correction. Demanding these quantities to be of the same order of magnitude yields¹⁹

$$\kappa_{1G} = \frac{1}{D_\Lambda^3} \left(\frac{\gamma_\Lambda \kappa_\Lambda}{2C} \right)^2, \quad (128)$$

where C is a numerical constant (we find $C = 2\pi$ if we set the bare value κ_{1G} exactly equal to its one-loop correction). Expressing κ_{1G} through a momentum scale as $\kappa_{1G} = D_\Lambda k_G^2$ we find Eq. (3), and for the dimensionless RG “time” $t_G = \ln(k_G/\Lambda)$, in terms of the dimensionless two-body loss rate $\tilde{\kappa}$ introduced in Sec. VI A, we have

$$t_G = \ln(\tilde{\kappa}_\Lambda/C). \quad (129)$$

Fitting this logarithmic dependence to numerically obtained trajectories in Fig. 1, we find $C \approx 14.8$. The Ginzburg scale delimits also the region where the driven-dissipative system obeys a FDT and the ratio $T_{\text{eff}} = \bar{\gamma}/(4|Z|)$ saturates to a constant value as shown in Fig. 2.

VIII. CONCLUSIONS

We have studied the nature of Bose criticality in driven open systems. To this end, starting from a description of the microscopic physics in terms of a many-body quantum master equation, we have developed and put into practice a FRG approach based on a Keldysh functional integral reformulation

of the quantum master equation for the quantitative determination of the universality class. The absence of an exact particle number conservation and the detailed balance condition were seen to underly the existence of a new and independent critical exponent governing universal decoherence, while the distribution function shows asymptotic thermalization despite the microscopic driven nature of the system.

This work is just a first step in the exploration of non-equilibrium critical behavior. Key questions for future studies concern the status of critical points in lower dimensionality as, e.g., relevant for current exciton-polariton systems. It is also a key issue to investigate different symmetries beyond the $O(2)$ case. For example, Heisenberg models realized with ensembles of trapped ions may exhibit $O(3)$ symmetry.⁷³ Furthermore, given the fact that many light-matter systems are pumped coherently as opposed to the incoherent pump considered here, it will be important to understand the impact of the coherent driven on potential criticality in these classes of systems. Finally, it is an intriguing question whether driven open systems which realize non-equilibrium counterparts of quantum criticality can be identified. In the long run, it remains to be seen whether a classification of non-equilibrium criticality with similarly clear structure as familiar from equilibrium dynamical criticality³⁷ can be reached.

ACKNOWLEDGMENTS

We thank J. Berges, M. Buchhold, I. Carusotto, T. Gasenzer, A. Imamoglu, J. M. Pawłowski, A. Rosch, U. C. Täuber, A. Tomadin, C. Wetterich, and P. Zoller for stimulating discussions. This work was supported by the Austrian Science Fund (FWF) through the START Grant No. Y 581-N16, the SFB FoQuS (FWF Project No. F4006-N16) (LMS, SD), and the ISF under Grant No. 1594/11 (EA).

Appendix A: Markovian dissipative action

1. Translation table: Master equation vs. Keldysh functional integral

Here we specify the relation between second quantized master equation and the equivalent Keldysh functional integral, defined with a markovian dissipative action. In particular, we review how the presence of external driving underlies the validity of the master equation and markovian dissipative action. We start from a master equation governing the time evolution of a system density matrix,

$$\partial_t \hat{\rho} = -i [\hat{H}_s, \hat{\rho}] + \kappa \left(\hat{L} \hat{\rho} \hat{L}^\dagger - \frac{1}{2} \{ \hat{L}^\dagger \hat{L}, \hat{\rho} \} \right). \quad (\text{A1})$$

Here, \hat{H}_s is a system Hamiltonian generating the unitary evolution and \hat{L} is a Lindblad operator making up the dissipative part of the Liouvillian. For simplicity we consider only a single dissipative channel. The generalization to several channels as in Eq. (6), realized through the coupling to several

baths, is straightforward. Equation (A1) results from a more general system-bath setting, $\hat{H}_{\text{tot}} = \hat{H}_s + \hat{H}_b + \hat{H}_{sb}$ (\hat{H}_b and \hat{H}_{sb} are a quadratic bath Hamiltonian with a continuum of frequencies and a system-bath Hamiltonian linear in the bath operators, respectively) under the following three assumptions: (i) the system-bath coupling $\sqrt{\gamma(\omega)}$ is weak compared to a typical scale ω_0 in the system (or, by energy conservation, in the bath) indicating, e.g., the level spacing in an atom (Born approximation $\gamma(\omega)/\omega_0 \ll 1$) (ii) the frequency dependence of the system-bath coupling is negligible over the bandwidth ϑ of the bath centered around ω_0 , implying δ -correlations in the time domain (Markov approximation $\gamma(\omega) \approx \text{const.}$), and (iii) the system is *driven with an external field with frequency ν* to bridge the large energy separation of the levels, $(\nu - \omega_0) / (\nu + \omega_0) \ll 1$. This makes it possible to work in the rotating wave approximation, in which only the detuning $\Delta = \nu - \omega_0$ occurs as a physical scale, while all fast terms involving $\nu + \omega_0$ are dropped. From this consideration, it is clear that the master equation is an accurate description of strongly driven systems coupled to an environment. A typical realization in quantum optics is an atom with two relevant levels separated by ω_0 , connected by an external laser drive with frequency ν , which is detuned from resonance by $\Delta = \nu - \omega_0$. Only the laser drive makes the excited level accessible and gives rise to two-level dynamics such as Rabi oscillations, with frequency determined by the laser intensity. The excited level is unstable and can undergo spontaneous emission by coupling to the radiation field, providing for the reservoir – this mechanism is physically completely independent of the coherent dynamics. Alternatively but fully equivalent to the operator formalism, the above approximations can be performed in a Keldysh path integral setting (see below). In this way, the physics of a given quantum master equation becomes amenable to quantum field theoretical approaches, which is particularly useful for bosonic and fermionic driven-dissipative many-body systems. Here the starting point is the Keldysh partition function

$$\mathcal{Z} = \int \mathcal{D}[a^*, a, b^*, b] e^{-i\mathcal{S}_{\text{tot}}[a^*, a, b^*, b]}, \quad (\text{A2})$$

which results from a ‘‘Trotterization’’ of the Hamiltonian dynamics (after normal ordering) acting on the density matrix in the integrated form of the von Neumann equation in the basis of coherent states; in this process, the second quantized system and bath field operators, \hat{a}_i (the index i denotes both position and internal indices, such as different particle species) and \hat{b}_μ (μ labels the bath modes and will be chosen a continuous index below) respectively, are mapped to time-dependent complex valued fields in the action

$$\mathcal{S}_{\text{tot}} = \sum_{\sigma=\pm} \sigma \int dt \left(\sum_i a_{i,\sigma}^*(t) i \partial_t a_{i,\sigma}(t) + \sum_\mu b_{\mu,\sigma}^*(t) i \partial_t b_{\mu,\sigma}(t) - H_{\text{tot},\sigma}(t) \right), \quad (\text{A3})$$

where $H_{\text{tot},\sigma}(t)$ is a quasilocal polynomial of these fields. The relative minus sign for the evolution on the forward (+) and

backward (-) contours clearly reflects the commutator structure in the von Neumann equation of motion for the system-bath density operator above. We have omitted an imaginary regularization term ensuring convergence of the functional integral^{52,53} for simplicity, as it does not affect any of the next steps. Integrating out the harmonic bath variables using approximations (i) – (iii) and considering for the moment Lindblad operators \hat{L} which are linear in the system field operators, we arrive at the following effective Markovian dissipative action:

$$\mathcal{S} = \sum_{\sigma} \sigma \int dt \left(\sum_i a_{i,\sigma}^*(t) i \partial_t a_{i,\sigma}(t) - H_{s,\sigma}(t) \right) - i\kappa \left[L_+(t) L_-^*(t) - \frac{1}{2} (L_+^*(t) L_+(t) + L_-^*(t) L_-(t)) \right]. \quad (\text{A4})$$

While the relative minus sign for the system Hamiltonian H_s on the + and - contours preserve the commutator structure, the dissipative terms clearly reflect the temporally local Lindblad structure of Eq. (A1). We thus arrive at a simple translation rule for bosonic⁷⁴ master equations into the corresponding Keldysh functional integral: (i) the temporal derivative terms can be read off from the last equation; (ii) for all (normal ordered) operators on the right (left) of the density matrix, introduce a contour index + (-) and write down the Markovian dissipative action. The linear Lindblad operators we consider here are not affected by normal ordering. For the more general case of Lindblad operators that are quasilocal polynomials in the system field operators, operator ordering can be tracked by a suitable temporal regularization procedure as elaborated in the next section.

2. Derivation in the Keldysh setting

Here we present a derivation of the Markovian dissipative action in the \pm basis for arbitrary (non-linear) Lindblad jump operators, which allows for the most direct comparison with the master equation. In particular, we pay special attention to the question how the operator ordering in the master equation is reflected in the path integral formulation. We leave the system action unspecified, requiring only the property that after proper rotating frame transformation the evolution of the system is much slower than the correlation time of the bath $\tau_c = 1/\vartheta$ (broadband bath). The action of the bath is, in the \pm basis,

$$\mathcal{S}_b = \sum_{\mu} \int dt dt' \left(b_{\mu,+}^*(t), b_{\mu,-}^*(t) \right) \times \begin{pmatrix} G_{\mu}^{++}(t, t') & G_{\mu}^{+-}(t, t') \\ G_{\mu}^{-+}(t, t') & G_{\mu}^{--}(t, t') \end{pmatrix}^{-1} \begin{pmatrix} b_{\mu,+}(t') \\ b_{\mu,-}(t') \end{pmatrix}. \quad (\text{A5})$$

The Green's functions for the oscillators of the bath are assumed to be in thermal equilibrium and read

$$\begin{aligned} G_{\mu}^{+-}(t, t') &= -i\bar{n}(\omega_{\mu}) e^{-i\omega_{\mu}(t-t')}, \\ G_{\mu}^{-+}(t, t') &= -i(\bar{n}(\omega_{\mu}) + 1) e^{-i\omega_{\mu}(t-t')}, \\ G_{\mu}^{++}(t, t') &= \theta(t-t') G_{\mu}^{-+}(t, t') + \theta(t'-t) G_{\mu}^{+-}(t, t'), \\ G_{\mu}^{--}(t, t') &= \theta(t'-t) G_{\mu}^{-+}(t, t') + \theta(t-t') G_{\mu}^{+-}(t, t'). \end{aligned} \quad (\text{A6})$$

The linear coupling between system and the bath is (note that the case of several dissipative channels and local baths as in Eq. (6) can be implemented by adding appropriate indices to the L_{σ} and $b_{\mu,\sigma}$ and summing over these indices)

$$\mathcal{S}_{sb} = \sum_{\mu} \sqrt{\gamma_{\mu}} \int dt \left(L_+^*(t) b_{\mu,+}(t) + L_+ b_{\mu,+}^*(t) - L_-^*(t) b_{\mu,-}(t) - L_- b_{\mu,-}^*(t) \right), \quad (\text{A7})$$

where L_{\pm} correspond to the quantum jump operators which are typically quasilocal polynomials of the system's creation and annihilation operators. To be consistent with the derivation of the path integral, we require the jump operators to have been normal ordered before the Trotter decomposition giving rise to the path integral. The partition function is of the general form

$$\mathcal{Z} = \int \mathcal{D}[a^*, a, b^*, b] e^{i(\mathcal{S}_s[a^*, a] + \mathcal{S}_b[b^*, b] + \mathcal{S}_{sb}[a^*, a, b^*, b])}, \quad (\text{A8})$$

Now we integrate out the bath via completion of the square which results in an effective action \mathcal{S}_{eff} for the system degrees of freedom. The contribution $\mathcal{S}_{\text{eff},\mu}$ of the μ th mode to the effective action reads

$$\begin{aligned} \mathcal{S}_{\text{eff},\mu} &= \gamma_{\mu} \int dt dt' (L_+^*(t), -L_-^*(t)) \\ &\quad \times \begin{pmatrix} G_{\mu}^{++}(t, t') & G_{\mu}^{+-}(t, t') \\ G_{\mu}^{-+}(t, t') & G_{\mu}^{--}(t, t') \end{pmatrix} \begin{pmatrix} L_+(t') \\ -L_-(t') \end{pmatrix}. \end{aligned} \quad (\text{A9})$$

The signs for the operators on the - contour comes from the backward integration in time. Thus the mixed terms will occur with an overall - sign, while the ++ and -- terms come with an overall +. Summing over all the modes μ we obtain the effective action for the field variables of the subsystem due to the coupling to the bath. We now take the continuum limit of densely lying bath modes, centered around some central frequency ω_0 and with bandwidth ϑ . That is, we substitute the sum over the modes with an integral in the energy Ω weighted by a (phenomenologically introduced) density of states $\nu(\Omega)$ of the bath $\sum_{\mu} \gamma_{\mu} \simeq \int_0^{\infty} d\Omega \gamma(\Omega) \nu(\Omega)$, and obtain

$$\begin{aligned} \mathcal{S}_{\text{eff}} &= - \int_{\omega_0 - \vartheta}^{\omega_0 + \vartheta} d\Omega \gamma(\Omega) \nu(\Omega) \int dt d\tau (L_+^*(t), -L_-^*(t)) \\ &\quad \times \begin{pmatrix} G_{\Omega}^{++}(\tau) & G_{\Omega}^{+-}(\tau) \\ G_{\Omega}^{-+}(\tau) & G_{\Omega}^{--}(\tau) \end{pmatrix} \begin{pmatrix} L_+(t - \tau) \\ -L_-(t - \tau) \end{pmatrix}, \end{aligned} \quad (\text{A10})$$

where in addition we have used the translation invariance of the bath Green's function, $G_{\Omega}^{\alpha\beta}(t, t') = G_{\Omega}^{\alpha\beta}(t - t')$ to suitably

shift the integration variables. We consider the various terms separately. In doing the Markov approximation, we use (a) that by assumption it is possible to choose a rotating frame in which the evolution of the system is slow compared to the scales in the bath, $\omega_{\text{sys}} \ll \omega_0, \vartheta$. In this case, a zeroth order temporal derivative approximation for the jump operators is appropriate. This gives rise to a *temporally local* form of the markovian dissipative action. However, for the evaluation of tadpole diagrams for this action, ambiguities due to a tempo-

rally local vertex arises. In these diagrams – and only in these – it is then important to specify the proper regularization of the system's Green's function at equal time arguments. To keep track of this, we indicate the sign of the next time step in the approximated jump operators by $t_{\pm\delta} = t \pm \delta t$. In step (b) below, we assume that the density of states and the coupling of the system to bath are well approximated as constant over the relevant reservoir width,

$$\begin{aligned}
& - \int dt L_+^*(t) \int d\tau \int_{\omega_0-\vartheta}^{\omega_0+\vartheta} \frac{d\Omega}{2\pi} \gamma(\Omega) \nu(\Omega) G_{\Omega}^{+-}(\tau) L_-(t-\tau) = i \int dt L_+^*(t) \int d\tau \int_{\omega_0-\vartheta}^{\omega_0+\vartheta} \frac{d\Omega}{2\pi} \gamma(\Omega) \nu(\Omega) \bar{n}(\Omega) e^{-i\Omega\tau} L_-(t-\tau) \\
& \stackrel{(a)}{\approx} i \int dt L_+^*(t) \int d\tau \int_{\omega_0-\vartheta}^{\omega_0+\vartheta} \frac{d\Omega}{2\pi} \gamma(\Omega) \nu(\Omega) \bar{n}(\Omega) e^{-i\Omega\tau} L_-(t-\delta) \stackrel{(b)}{\approx} i \int dt L_+^*(t) \gamma \nu \int d\tau \int_{\omega_0-\vartheta}^{\omega_0+\vartheta} \frac{d\Omega}{2\pi} \bar{n}(\Omega) e^{-i\Omega\tau} L_-(t-\delta) \\
& \approx i \int dt L_+^*(t) \gamma \nu \int_{-\infty}^{\infty} d\Omega \bar{n}(\Omega) \delta(\Omega - \omega_0) L_-(t-\delta) = i\kappa\bar{n} \int dt L_+^*(t) L_-(t-\delta),
\end{aligned} \tag{A11}$$

where we have shifted the frequency integration domain by $-\omega_0$ and taken the limit $\vartheta \rightarrow \infty$, as well as $\kappa = \gamma\nu$ and $\bar{n} = \bar{n}(\omega_0)$. Further note the relation to the operator formalism $\int_{-\infty}^{\infty} \frac{d\Omega}{2\pi} \bar{n}(\Omega) e^{-i\Omega\tau} = \langle \hat{b}^\dagger(\tau) \hat{b}(0) \rangle$. Similarly,

$$- \int dt L_-^*(t) \int d\tau \int_{\omega_0-\vartheta}^{\omega_0+\vartheta} \frac{d\Omega}{2\pi} \gamma(\Omega) \nu(\Omega) G_{\Omega}^{-+}(\tau) L_+(t-\tau) \approx i\kappa(\bar{n} + 1) \int dt L_-^*(t) L_+(t-\delta) \tag{A12}$$

and $\int_{-\infty}^{\infty} \frac{d\Omega}{2\pi} (\bar{n}(\Omega) + 1) e^{-i\Omega\tau} = \langle \hat{b}(\tau) \hat{b}^\dagger(0) \rangle$. For the terms on the forward contour, we obtain

$$\begin{aligned}
& \int dt L_+^*(t) \int d\tau \int_{\omega_0-\vartheta}^{\omega_0+\vartheta} \frac{d\Omega}{2\pi} \gamma(\Omega) \nu(\Omega) G_{\Omega}^{++}(\tau) L_+(t-\tau) \\
& = -i \int dt L_+^*(t) \int d\tau \int_{\omega_0-\vartheta}^{\omega_0+\vartheta} \frac{d\Omega}{2\pi} \gamma(\Omega) \nu(\Omega) [\theta(\tau) (\bar{n}(\Omega) + 1) + \theta(-\tau) \bar{n}(\Omega)] e^{-i\Omega\tau} L_+(t-\tau) \\
& \stackrel{(a)}{\approx} -i \int dt L_+^*(t) \int d\tau \int_{\omega_0-\vartheta}^{\omega_0+\vartheta} \frac{d\Omega}{2\pi} \gamma(\Omega) \nu(\Omega) [\theta(\tau) (\bar{n}(\Omega) + 1) + \theta(-\tau) \bar{n}(\Omega)] e^{-i\Omega\tau} L_+(t-\delta) \\
& \stackrel{(b)}{\approx} -i \int dt L_+^*(t) \gamma \nu \left[\int d\tau \theta(\tau) \int_{\omega_0-\vartheta}^{\omega_0+\vartheta} \frac{d\Omega}{2\pi} (\bar{n}(\Omega) + 1) e^{-i\Omega\tau} + \int d\tau \theta(-\tau) \int_{\omega_0-\vartheta}^{\omega_0+\vartheta} \frac{d\Omega}{2\pi} \bar{n}(\Omega) e^{-i\Omega\tau} \right] L_+(t-\delta) \\
& \approx -i \int dt \left\{ \left[\frac{1}{2} \kappa (\bar{n} + 1) - i\delta E_1 \right] L_+^*(t) L_+(t-\delta) + \left(\frac{1}{2} \kappa \bar{n} + i\delta E_2 \right) L_+^*(t) L_+(t+\delta) \right\}.
\end{aligned} \tag{A13}$$

In the last line we have used

$$\begin{aligned}
& \int d\tau \theta(\tau) \int_{\omega_0-\vartheta}^{\omega_0+\vartheta} \frac{d\Omega}{2\pi} (\bar{n}(\Omega) + 1) e^{-i\Omega\tau} L_+(t-\delta) \\
& \approx \int_{-\infty}^{\infty} \frac{d\Omega}{2\pi} (\bar{n}(\Omega) + 1) \left(\pi \delta(\Omega - \omega_0) - i\mathcal{P} \frac{1}{\Omega - \omega_0} \right) L_+(t-\delta) \\
& = \left[\frac{1}{2} \kappa (\bar{n} + 1) - i\delta E_1 \right] L_+(t-\delta)
\end{aligned} \tag{A14}$$

and

$$\begin{aligned}
& \int d\tau \theta(-\tau) \int_{\omega_0-\vartheta}^{\omega_0+\vartheta} \frac{d\Omega}{2\pi} \bar{n}(\Omega) e^{-i\Omega\tau} L_+(t-\delta) \\
& = \int d\tau \theta(\tau) \int_{\omega_0-\vartheta}^{\omega_0+\vartheta} \frac{d\Omega}{2\pi} \bar{n}(\Omega) e^{+i\Omega\tau} L_+(t+\delta) \\
& \approx \int_{-\infty}^{\infty} \frac{d\Omega}{2\pi} \bar{n}(\Omega) \left(\pi \delta(\Omega - \omega_0) - i\mathcal{P} \frac{1}{\Omega - \omega_0} \right) L_+(t+\delta) \\
& = \left(\frac{1}{2} \kappa \bar{n} + i\delta E_2 \right) L_+(t+\delta).
\end{aligned} \tag{A15}$$

Importantly, note the sign change in the regularization of the time argument upon reversal of integration direction. This

gives a hint which operator ‘‘comes first’’ in the coarse grained evolution where the bath has been integrated out, and reflects the fact that in the corresponding master equation, the ‘‘cooling’’ dissipation terms $\sim (\bar{n} + 1)$ are normal ordered in the jump operators ($\sim \hat{L}^\dagger \hat{L}$), while the ‘‘heating’’ terms $\sim \bar{n}$ are anti-normal ordered ($\sim \hat{L} \hat{L}^\dagger$). Similarly, we obtain on the backward contour,

$$\begin{aligned} & \int dt L_-^*(t) \int d\tau \int_{\omega_0 - \theta}^{\omega_0 + \theta} \frac{d\Omega}{2\pi} \gamma(\Omega) \nu(\Omega) G_{\Omega}^{--}(\tau) L_-(t - \tau) \\ & \approx -i \int dt \left\{ \left[\frac{1}{2} \kappa (\bar{n} + 1) + i\delta E_1 \right] L_-^*(t) L_-(t + \delta) \right. \\ & \quad \left. + \left[\frac{1}{2} \kappa \bar{n} - i\delta E_2 \right] L_-^*(t) L_-(t - \delta) \right\}, \quad (\text{A16}) \end{aligned}$$

where the changes in the signs relative to the forward term emerge from the reverse signs in the θ -functions. In summary, we obtain the following dissipative contribution to the action:

$$\begin{aligned} S_d = i\kappa \int dt & \left\{ (\bar{n} + 1) \left[L_-^*(t) L_+(t - \delta) \right. \right. \\ & \quad \left. \left. - \frac{1}{2} (L_+^*(t) L_+(t - \delta) + L_-^*(t) L_-(t + \delta)) \right] \right. \\ & \quad \left. + \bar{n} \left[L_+^*(t) L_-(t - \delta) - \frac{1}{2} (L_+^*(t) L_+(t + \delta) + L_-^*(t) L_-(t - \delta)) \right] \right\}. \quad (\text{A17}) \end{aligned}$$

In addition, there is a ‘‘Lamb shift’’ which reads

$$\begin{aligned} S_L = - \int dt & [\delta E_1 (-L_+^*(t) L_+(t - \delta) + L_-^*(t) L_-(t + \delta)) \\ & + \delta E_2 (L_+^*(t) L_+(t + \delta) - L_-^*(t) L_-(t - \delta))]. \quad (\text{A18}) \end{aligned}$$

This gives a contribution to the coherent dynamics which has the same physical origin as the dissipative dynamics. However, typically there is a dominant independent Hamiltonian contribution, such that the effective Hamiltonian parameters after the Lamb shift renormalization are properly regarded as independent of the Liouvillian ones.

Appendix B: Symmetry constraints on the action and truncation for MAR

In this section we derive the action Eq. (60) and the truncation Eq. (63) for MAR. Our starting point is the truncation Eq. (42) appropriate for the driven-dissipative model on which we impose invariance under the equilibrium symmetry transformation Eq. (59). This leads to Eq. (63) which reduces to the action Eq. (60) when we set $k = k_{\text{cg}}$.

In terms of the bare spinors $\tilde{\Phi}_\nu$, the truncation for the DDM can be written as

$$\begin{aligned} \Gamma_k = \int_X \tilde{\Phi}_q^\dagger & \left[(Z_R \sigma_z - iZ_I \mathbb{1}) i\partial_t \tilde{\Phi}_c \right. \\ & \left. - \frac{\delta \tilde{\mathcal{U}}_H}{\delta \tilde{\Phi}_c^*} + i\sigma_z \frac{\delta \tilde{\mathcal{U}}_D}{\delta \tilde{\Phi}_c^*} + i\frac{\tilde{\gamma}}{2} \tilde{\Phi}_q \right]. \quad (\text{B1}) \end{aligned}$$

We perform the change of basis Eq. (58) and obtain for the contributions in the sum $\Gamma_k = \Gamma_{\text{dyn},k} + \Gamma_{H,k} + \Gamma_{D,k} + \Gamma_{\text{reg},k}$ the expressions

$$\Gamma_{\text{dyn},k} = i \frac{\bar{r} Z_R + Z_I}{Z_{R,\text{cg}} - \bar{r} Z_{I,\text{cg}}} \int_X \tilde{\Phi}_q^\dagger \sigma_z \partial_t \tilde{\Phi}_c, \quad (\text{B2})$$

$$\Gamma_{H,k} = \frac{i}{Z_{R,\text{cg}} - \bar{r} Z_{I,\text{cg}}} \int_X \tilde{\Phi}_q^\dagger \sigma_z \left(\bar{r} \frac{\delta \tilde{\mathcal{U}}_D}{\delta \tilde{\Phi}_c^*} - \frac{\delta \tilde{\mathcal{U}}_H}{\delta \tilde{\Phi}_c^*} \right), \quad (\text{B3})$$

$$\Gamma_{D,k} = -\frac{1}{Z_{R,\text{cg}} - \bar{r} Z_{I,\text{cg}}} \int_X \tilde{\Phi}_q^\dagger \left(\frac{\delta \tilde{\mathcal{U}}_D}{\delta \tilde{\Phi}_c^*} + \bar{r} \frac{\delta \tilde{\mathcal{U}}_H}{\delta \tilde{\Phi}_c^*} \right), \quad (\text{B4})$$

and

$$\begin{aligned} \Gamma_{\text{reg},k} = \frac{i}{Z_{R,\text{cg}} - \bar{r} Z_{I,\text{cg}}} \int_X \tilde{\Phi}_q^\dagger & \left((Z_R - \bar{r} Z_I) i\partial_t \tilde{\Phi}_c \right. \\ & \left. + \frac{1 + \bar{r}^2}{Z_{R,\text{cg}} - \bar{r} Z_{I,\text{cg}}} \frac{\tilde{\gamma}}{2} \tilde{\Phi}_q \right). \quad (\text{B5}) \end{aligned}$$

Both $\Gamma_{\text{dyn},k}$ and $\Gamma_{D,k}$ are symmetric under the transformation Eq. (59). Demanding the remaining contributions $\Gamma_{H,k}$ and $\Gamma_{\text{reg},k}$ to be invariant we find that a term of the form of Eq. (B3) is actually forbidden by the symmetry, i.e., we must have $\Gamma_{H,k} = 0$, which is satisfied for $\tilde{\mathcal{U}}_H = r\tilde{\mathcal{U}}_D$. For the regularization term $\Gamma_{\text{reg},k}$ we obtain the additional constraint Eq. (64). All these requirements are implemented in the truncation Eq. (63) which is easily seen to reduce to Eq. (60) for $k = k_{\text{cg}}$.

If in addition to the equilibrium symmetry we demand invariance under complex conjugation of the fields Eq. (62) as is the case for MA, we find the condition $\Gamma_{\text{dyn},k} = 0$. This is met for all $0 < k < k_{\text{cg}}$ if $\bar{r} = -Z_I/Z_R$.

Appendix C: Non-Equilibrium FRG flow equations

Here we present details of the derivation of the non-equilibrium FRG flow equations in Sec. V. To start with, we rewrite the flow equation (38) such that only renormalized quantities appear on the RHS,

$$\partial_t \Gamma_k = \frac{i}{2} \text{Tr} \left[(\Gamma_k^{(2)} + R_k)^{-1} \tilde{\partial}_t R_k \right]. \quad (\text{C1})$$

The second functional derivatives appearing under the trace on the RHS are taken with respect to renormalized real fields Eq. (49). These can be written in terms of the bare ones as $\chi(Q) = z\tilde{\chi}(Q)$, where the matrix z is given by

$$z = \mathbb{1} \oplus R^\dagger \begin{pmatrix} Z & 0 \\ 0 & Z^* \end{pmatrix} R = \begin{pmatrix} Z_R & -Z_I \\ Z_I & Z_R \end{pmatrix}. \quad (\text{C2})$$

The linear transformation from bare to renormalized fields implies for functional derivatives the relations

$$\Gamma_k^{(2)} = z^T \Gamma_k^{(2)} z, \quad \bar{R}_k = z^T R_k z, \quad (\text{C3})$$

and inserting these in the flow equation (38) yields Eq. (C1) if in addition we replace the derivative with respect to t by the differential operator $\tilde{\partial}_t$ which is defined as

$$\tilde{\partial}_t \equiv \partial_t R_{k,\bar{k}} \partial_{R_{k,\bar{k}}} + \partial_t R_{k,\bar{k}}^* \partial_{R_{k,\bar{k}}^*}. \quad (\text{C4})$$

With this definition we may write $\partial_t \bar{R}_k = \tilde{\partial}_t \bar{R}_k$, which has the advantage that $\tilde{\partial}_t$ commutes with the multiplicative renormalization with Z (note that also Z is a running coupling and depends on t), i.e., we have

$$\tilde{\partial}_t \bar{R}_k = \tilde{\partial}_t (z^T R_k z) = z^T (\tilde{\partial}_t R_k) z. \quad (C5)$$

Furthermore, since $\tilde{\partial}_t$ acts only on the cutoff and not the inverse propagator $\Gamma_k^{(2)}$, we may rewrite the exact flow equation (C1) in the simple form

$$\partial_t \Gamma_k = \frac{i}{2} \text{Tr} \tilde{\partial}_t \ln (\Gamma_k^{(2)} + R_k). \quad (C6)$$

1. Expansion in fluctuations

According to its definition in Sec. III C, the effective action is a functional of the field expectation values, and also the flow equation (C6) can be evaluated for arbitrary field configurations. A particularly useful form of the flow equation can be obtained by decomposing the fields into homogeneous and frequency- and momentum-dependent fluctuation parts as $\chi(Q) = \chi \delta(Q) + \delta\chi(Q)$ and expanding the logarithm on the RHS of Eq. (C6) to second order in the fluctuations $\delta\chi(Q)$. Then, the zeroth order term determines the flow of the momentum-independent couplings whereas the β -functions for the wave-function renormalization and the gradient coefficient can be obtained from the second order contribution.

We begin by deriving an explicit expression for the full inverse propagator $\Gamma_k^{(2)}$ up to second order in $\delta\chi$. To this end we rewrite the effective action Eq. (44) in the form

$$\Gamma_k = \frac{1}{2} \int_Q \chi(-Q)^T D(Q) \chi(Q) - \int_X V, \quad (C7)$$

where $\int_Q = \int \frac{d\omega d^d \mathbf{q}}{(2\pi)^{d+1}}$, is the frequency- and momentum-dependent part of the inverse propagator Eq. (48) is denoted

$$\begin{aligned} V_{cq,11}^{(2)H} &= [(\rho_{cq} + \rho_{qc}) U_H^{(3)} + i(\rho_{cq} - \rho_{qc}) U_D^{(3)}] \chi_{c,1}^2 + (\rho_{cq} + \rho_{qc} + 2\chi_{c,1} \chi_{q,1}) U_H'' + i(\rho_{cq} - \rho_{qc} + i2\chi_{c,1} \chi_{q,2}) U_D'', \\ V_{cq,12}^{(2)H} &= V_{cq,21}^{(2)H} = (\chi_{c,2} \chi_{q,1} + \chi_{c,1} \chi_{q,2}) U_H'' + (\chi_{c,1} \chi_{q,1} - \chi_{c,2} \chi_{q,2}) U_D'' + \chi_{c,1} \chi_{c,2} [(\rho_{cq} + \rho_{qc}) U_H^{(3)} + i(\rho_{cq} - \rho_{qc}) U_D^{(3)}], \\ V_{cq,22}^{(2)H} &= [(\rho_{cq} + \rho_{qc}) U_H^{(3)} + i(\rho_{cq} - \rho_{qc}) U_D^{(3)}] \chi_{c,2}^2 + (\rho_{cq} + \rho_{qc} + 2\chi_{c,2} \chi_{q,2}) U_H'' + i(\rho_{cq} - \rho_{qc} - i2\chi_{c,2} \chi_{q,1}) U_D'', \end{aligned} \quad (C14)$$

the retarded and advanced components only contain classical background fields (hence we omit the index q),

$$V_c^{(2)R} = \begin{pmatrix} U_H' + \chi_{c,1} (\chi_{c,2} U_D'' + \chi_{c,1} U_H'') & U_D' + \chi_{c,2} (\chi_{c,2} U_D'' + \chi_{c,1} U_H'') \\ \chi_{c,1} (\chi_{c,2} U_H'' - \chi_{c,1} U_D'') - U_D' & U_H' + \chi_{c,2} (\chi_{c,2} U_H'' - \chi_{c,1} U_D'') \end{pmatrix}, \quad V_c^{(2)A} = (V_c^{(2)R})^\dagger, \quad (C15)$$

and the Keldysh component is field-independent and given by $V^{(2)K} = -i\gamma \mathbb{1}$. In Eq. (C6), the inverse propagator is supple-

mented by the cutoff to yield the regularized propagator

$$V = U' \rho_{cq} + U'^* \rho_{qc} - i\gamma \rho_q. \quad (C8)$$

by $D(Q) = P(Q) - P(0)$, and the effective potential V that contains all momentum-independent couplings is given by

$$\Gamma_k^{(2)}(Q, Q') = D(Q) \delta(Q - Q') - \mathcal{V}^{(2)}(Q, Q'), \quad (C9)$$

where the second term is just the functional derivative of the effective potential,

$$\mathcal{V}_{ij}^{(2)}(Q, Q') = \frac{\delta^2}{\delta\chi_i(-Q) \delta\chi_j(Q')} \int_X V = \int_X e^{i(Q-Q')X} V_{ij}^{(2)}, \quad (C10)$$

which can be reduced to ordinary (i.e., not functional) partial derivatives with respect to the fields in the time domain and real space,

$$V_{ij}^{(2)} = \frac{\partial^2}{\partial\chi_i \partial\chi_j} V. \quad (C11)$$

Setting the fluctuation components of the fields to zero in Eq. (C9) we obtain the inverse propagator in the presence of homogeneous classical and quantum background fields,

$$P_{cq}(Q) \delta(Q - Q') \equiv \Gamma_k^{(2)}(Q, Q') \Big|_{\delta\chi=0} = (D(Q) - V_{cq}^{(2)}) \delta(Q - Q'). \quad (C12)$$

Note that the difference between $P_{cq}(Q)$ and the inverse propagator Eq. (48) is that in the latter the background fields are set to their stationary values while in the former they remain unspecified. The background fields are all contained in the second contribution $V_{cq}^{(2)}$ which we split into 2×2 blocks according to

$$V_{cq}^{(2)} = \begin{pmatrix} V_{cq}^{(2)H} & V_c^{(2)A} \\ V_c^{(2)R} & V_{cq}^{(2)K} \end{pmatrix}. \quad (C13)$$

While the upper left block $V_{cq}^{(2)H}$ is linear in the quantum fields (and, therefore, vanishes when we set these to zero, giving rise to the causality structure of the inverse propagator Eq. (48)),

mented by the cutoff to yield the regularized propagator

$$P_{k,cq}(Q) = P_{cq}(Q) + R_k(q^2), \quad (C16)$$

which determines the zeroth order contribution in the fluctuation expansion of the flow equation.

We proceed by expanding the inverse propagator Eq. (C9) to second order in the fluctuations $\delta\chi$. With Eq. (C12) we may write

$$\Gamma_k^{(2)}(Q, Q') = P_{cq}(Q)\delta(Q - Q') + \mathcal{F}(Q, Q') + O(\delta\chi^3), \quad (\text{C17})$$

where the matrix \mathcal{F} is given by the sum $\mathcal{F} = \mathcal{F}_1 + \mathcal{F}_2$ with $\mathcal{F}_{1,2}$ being of first and second order in $\delta\chi$. The explicit dependence of these matrices on the fluctuations reads

$$\mathcal{F}_1(Q, Q') = - \sum_i V_i^{(3)} \delta\chi_i(Q - Q'), \quad (\text{C18})$$

$$\mathcal{F}_2(Q, Q') = - \frac{1}{2} \sum_{ij} V_{ij}^{(4)} \int_P \delta\chi_i(-P) \delta\chi_j(P + Q - Q'). \quad (\text{C19})$$

Here, for given values of i and j the quantities $V_i^{(3)}$ and $V_{ij}^{(4)}$ are 4×4 matrices defined as the partial derivatives of $V^{(2)}$,

$$V_i^{(3)} = \frac{\partial V^{(2)}}{\partial \chi_i}, \quad V_{ij}^{(4)} = \frac{\partial V^{(2)}}{\partial \chi_i \partial \chi_j}. \quad (\text{C20})$$

Inserting the decomposition Eq. (C17) in Eq. (C6) and expanding the logarithm in the fluctuations $\delta\chi$ yields

$$\partial_t \Gamma_k = \frac{i}{2} \left[\text{Tr} \tilde{\partial}_t \ln P_{k,cq} - \frac{1}{2} \tilde{\partial}_t \text{Tr} (G_{k,cq} \mathcal{F}_1)^2 \right], \quad (\text{C21})$$

where $G_{k,cq}(Q) = P_{k,cq}(Q)^{-1}$ is the propagator in the presence of classical and quantum background fields. Note that the appearance of $G_{k,cq}^2$ makes the trace in the last term UV-convergent and thereby allowed us to commute $\tilde{\partial}_t$ with Tr . In the expansion Eq. (C21) we are keeping only terms of zeroth and second order, as these determine, respectively, the flow of the effective potential and the frequency- and momentum-dependent contributions to the inverse propagator. We also omit a term $\tilde{\partial}_t \text{Tr} G_{k,cq} \mathcal{F}_2$ which in our truncation with momentum-independent vertices does not contribute to the flow of Z and \bar{K} .

2. Flow equation for the effective potential

Equation (C21) reduces to the flow equation for the effective potential if we set the fluctuations $\delta\chi$ to zero. Then the second term on the RHS vanishes and we have

$$\frac{1}{\Omega} \partial_t \Gamma_{k,cq} = \frac{i}{2} \int_Q \tilde{\partial}_t \ln \det_{cq}(\omega, q^2) \quad (\text{C22})$$

where $\det_{cq}(\omega, q^2) = \det P_{k,cq}(Q)$ denotes the determinant of the regularized inverse propagator Eq. (C16) in the presence of classical and quantum background fields. Since our model is symmetric under simultaneous phase rotations $\phi_v \rightarrow e^{i\alpha} \phi_v$ of the classical and quantum fields, the determinant $\det_{cq}(\omega, q^2)$ can be expressed as a function of the $U(1)$ -invariant field combinations $\rho_c, \rho_{cq}, \rho_{qc}$, and ρ_q . It can not

be written as a function of these invariants without ambiguity though, as can be seen by noting that the product of four fields $\phi_c^* \phi_q^* \phi_c \phi_q$ equals both $\rho_c \rho_q$ and $\rho_{cq} \rho_{qc}$. However, the form of the field-dependent contribution Eq. (C13) to the inverse propagator implies that $\det_{cq}(\omega, q^2)$ contains terms that are at most quadratic in the quantum fields and that there is no contribution that contains $\phi_q^* \phi_q$ but no classical fields. All contributions containing quantum *and* classical fields can be expressed in powers of ρ_c, ρ_{cq} , and ρ_{qc} . Therefore, in the following we will consider $\det_{cq}(\omega, q^2)$ to be a function of this reduced set of invariants. Then, inserting Eq. (C22) in the definition of ζ' in Eq. (80) we find

$$\zeta' = - \frac{i}{2} \int_Q \tilde{\partial}_t \left\{ \frac{1}{\det_c(\omega, q^2)} \left[\partial_{\rho_{cq}} \det_{cq}(\omega, q^2) \right]_{\rho_{cq}=\rho_{qc}=0} \right\}, \quad (\text{C23})$$

where $\det_c(\omega, q^2) = \det P_{k,c}(Q)$ is the determinant of the regularized propagator with only classical background fields,

$$P_{k,c}(Q) = P_{k,cq}(Q) \Big|_{\phi_q=\phi_q^*=0}, \quad (\text{C24})$$

which differs from $P_{k,cq}(Q)$ only in the block $V_{cq}^{(2)H}$ (note that the other blocks in Eq. (C13) do not contain quantum fields) which vanishes for $\phi_q = \phi_q^* = 0$. Accordingly the inverse propagator $P_{k,c}(Q)$ acquires the causality structure Eq. (50) which implies that the determinant $\det_c(\omega, q^2)$ factorizes into retarded and advanced contributions,

$$\det_c(\omega, q^2) = \det_c^R(\omega, q^2) \det_c^A(\omega, q^2). \quad (\text{C25})$$

These are simply related by a change of the sign of the frequency variable, $\det_c^R(\omega, q^2) = \det_c^A(-\omega, q^2)$. Inserting Eq. (C25) in Eq. (C23) we can rewrite the latter as

$$\zeta' = 2v_d \int_0^\infty dx x^{d/2-1} \tilde{\partial}_t \zeta'(x), \quad (\text{C26})$$

where $v_d = (2^{d+1} \pi^{d/2} \Gamma(d/2))^{-1}$ and we introduced a new integration variable $x = q^2$; the function appearing in the integrand is given by the integral over frequencies

$$\zeta'(q^2) = - \frac{i}{4\pi} \int_{-\infty}^\infty d\omega \frac{\left[\partial_{\rho_{cq}} \det_{cq}(\omega, q^2) \right]_{\rho_{cq}=\rho_{qc}=0}}{\det_c^A(\omega, q^2) \det_c^A(-\omega, q^2)}, \quad (\text{C27})$$

which can be performed with the aid of Ref.⁷⁵, p. 308, 18. (where a factor of $(-1)^{n+1}$ is missing⁷⁶). We omit the rather lengthy result.

Let us proceed by specifying the action of $\tilde{\partial}_t$ in Eq. (C26). The function $\zeta'(x)$ depends on the cutoff via its dependence on $p_a(x)$ for which we have $\tilde{\partial}_t p_a(x) = -\tilde{\partial}_t R_{k,a}(x)$, see Eq. (57), and thus

$$\tilde{\partial}_t \zeta'(x) = - \sum_{a=A,D} \tilde{\partial}_t R_{k,a}(x) \partial_{p_a(x)} \zeta'(x). \quad (\text{C28})$$

Recalling the definition Eq. (C4) of the differential operator $\tilde{\partial}_t$ according to which it effectively acts as a scale derivative of the bare cutoff, we find

$$\begin{aligned} \tilde{\partial}_t R_{k,A}(x) &= \text{Re} \left(\partial_t R_{k,\bar{K}}(x) / Z \right), \\ \tilde{\partial}_t R_{k,D}(x) &= \text{Im} \left(\partial_t R_{k,\bar{K}}(x) / Z \right). \end{aligned} \quad (\text{C29})$$

Inserting here the expression

$$\partial_t R_{k,\bar{K}}(x) = - \left[(2\bar{K} + \partial_t \bar{K}) k^2 - \partial_t \bar{K} x \right] \theta(k^2 - x), \quad (\text{C30})$$

we end up with

$$\tilde{\partial}_t R_{k,a}(x) = - \left[(2 - \bar{\eta}_a) k^2 + \bar{\eta}_a x \right] a \theta(k^2 - x), \quad (\text{C31})$$

where we defined

$$\bar{\eta}_A = -\frac{1}{A} \text{Re}(\partial_t \bar{K}/Z), \quad \bar{\eta}_D = -\frac{1}{D} \text{Im}(\partial_t \bar{K}/Z). \quad (\text{C32})$$

Plugging these results in Eq. (C26) and using that the θ -function restricts the range of integration over x to the interval $[0, k^2]$, where $p_a(x) = ak^2$ (cf. Eq. (57)) and therefore $\zeta'(x) = \zeta'(k^2)$ does not depend on x , we get

$$\zeta' = \frac{8v_d k^{d+2}}{d} \sum_a \left(1 - \frac{\bar{\eta}_a}{d+2} \right) a \left[\partial_{p_a(x)} \zeta'(x) \right]_{p_A(x)=Ak^2, p_D(x)=Dk^2}. \quad (\text{C33})$$

The further evaluation of this expression is most conveniently performed on the computer using `MATHEMATICA`.

In Sec. V we specified prescriptions that allow us to obtain flow equations for the complex two- and three-body couplings from the flow equation for the effective potential, cf. Eqs. (82) and (83). When we switch to `MATHEMATICA` for an explicit evaluation of the flow equations, however, it is more convenient to work with real couplings. The flow equations for the quartic and sextic couplings are then given by

$$\begin{aligned} \partial_t \lambda &= \beta_\lambda = \eta_{ZR} \lambda - \eta_{ZI} \kappa + \lambda_3 \partial_t \rho_0 + \partial_{\rho_c} \zeta'_H \Big|_{\text{ss}}, \\ \partial_t \kappa &= \beta_\kappa = \eta_{ZR} \kappa + \eta_{ZI} \lambda + \kappa_3 \partial_t \rho_0 + \partial_{\rho_c} \zeta'_D \Big|_{\text{ss}}, \\ \partial_t \lambda_3 &= \beta_{\lambda_3} = \eta_{ZR} \lambda_3 - \eta_{ZI} \kappa_3 + \partial_{\rho_c}^2 \zeta'_H \Big|_{\text{ss}}, \\ \partial_t \kappa_3 &= \beta_{\kappa_3} = \eta_{ZR} \kappa_3 + \eta_{ZI} \lambda_3 + \partial_{\rho_c}^2 \zeta'_D \Big|_{\text{ss}}, \end{aligned} \quad (\text{C34})$$

where we decompose $\zeta' = \zeta'_H + i\zeta'_D$ and $\eta_Z = \eta_{ZR} + i\eta_{ZI}$ into real and imaginary parts. For completeness we also state the flow equation of ρ_0 in terms of these quantities:

$$\partial_t \rho_0 = \beta_{\rho_0} = -\zeta'_D \Big|_{\text{ss}} / \kappa. \quad (\text{C35})$$

To conclude this section let us specify the flow equation for γ . Similar to Eq. (C26) we can express the quantity ζ_γ defined in Eq. (86) as

$$\zeta_\gamma = 2v_d \int_0^\infty dx x^{d/2-1} \tilde{\partial}_t \zeta_\gamma(x). \quad (\text{C36})$$

As anticipated in the paragraph following Eq. (C22), the determinant $\det_{c,q}(\omega, q^2)$ can be expressed in terms of $\rho_c, \rho_{c,q}$, and $\rho_{q,c}$ solely. Therefore, the term that is proportional to $\phi_q^* \phi_q$ and determines the flow of γ can then be found taking the derivative

$$\frac{\partial^2}{\partial \phi_q^* \partial \phi_q} = \frac{\partial \rho_{c,q}}{\partial \phi_q} \frac{\partial \rho_{q,c}}{\partial \phi_q^*} \frac{\partial^2}{\partial \rho_{c,q} \partial \rho_{q,c}} = \rho_c \frac{\partial^2}{\partial \rho_{c,q} \partial \rho_{q,c}}, \quad (\text{C37})$$

and we find for the integrand in Eq. (C36) the expression

$$\zeta_\gamma(q^2) = \frac{\rho_0}{4\pi} \int_{-\infty}^\infty d\omega \left[\frac{\partial_{\rho_{c,q} \rho_{q,c}}^2 \det_{c,q}(\omega, q^2)}{\det_c(\omega, q^2)} - \frac{\partial_{\rho_{c,q}} \det_{c,q}(\omega, q^2) \partial_{\rho_{q,c}} \det_{c,q}(\omega, q^2)}{\det_c^2(\omega, q^2)} \right]_{\text{ss}}. \quad (\text{C38})$$

This can be treated in the same way as Eq. (C27) above.

3. Flow equation for the inverse propagator

The second term on the RHS of Eq. (C21) determines the flow of both the wave-function renormalization and the gradient coefficient. It is quadratic in the fluctuations $\delta\chi$, hence we can write it as

$$\text{Tr} \left(G_{k,cq} \mathcal{F}_1 \right) \Big|_{\text{ss}} = -i2 \int_Q \delta\chi(-Q)^T \Sigma(Q) \delta\chi(Q), \quad (\text{C39})$$

where we set the fields to their stationary values. $\Sigma(Q)$ can be visualized as consisting of one-loop diagrams with four external legs two of which are attached to the condensate (cf. the second diagram on the RHS of Eq. (32)) and is given by

$$\Sigma_{ij}(Q) = \frac{i}{2} \int_P \text{tr} \left(G_k(P) V_i^{(3)} G_k(P+Q) V_j^{(3)} \right), \quad (\text{C40})$$

where $G_k(Q) = P_k(Q)^{-1}$ with the inverse propagator given by Eqs. (50) and (51) to which the cutoff $R_k(q^2)$ has to be added. For $\phi_c = \phi_c^* = \phi_0$ and $\phi_q = \phi_q^* = 0$ the matrices $V_i^{(3)}$ have the structure

$$V_i^{(3)} = \begin{pmatrix} v_{3,i}^H & v_{3,i}^A \\ v_{3,i}^R & 0 \end{pmatrix}, \quad v_{3,1}^H = v_{3,2}^H = 0, \quad v_{3,3}^{R/A} = v_{3,4}^{R/A} = 0. \quad (\text{C41})$$

Inserting this expression in Eq. (C40) above and taking the causality structure of the propagator into account, we can rewrite the integrand in the form ($P_+ \equiv P + Q$)

$$\begin{aligned} \text{tr} \left(G_k(P) V_i^{(3)} G_k(P_+) V_j^{(3)} \right) &= \text{tr} \left(G_k^K(P) v_{3,i}^H G_k^K(P_+) v_{3,j}^H \right) \\ &+ \text{tr} \left(G_k^K(P) v_{3,i}^H G_k^R(P_+) v_{3,j}^R \right) + \text{tr} \left(G_k^R(P) v_{3,i}^R G_k^K(P_+) v_{3,j}^H \right) \\ &+ \text{tr} \left(G_k^K(P) v_{3,i}^A G_k^A(P_+) v_{3,j}^H \right) + \text{tr} \left(G_k^A(P) v_{3,i}^H G_k^K(P_+) v_{3,j}^A \right). \end{aligned} \quad (\text{C42})$$

Then the second and third equalities in Eq. (C41) imply that $\Sigma(Q)$ has the same causality structure as the inverse propagator. For the retarded block we find

$$\begin{aligned} \Sigma_{ij}^R(Q) &= \frac{i}{2} \int_P \left[\text{tr} \left(G_k^K(P) v_{3,i+2}^H G_k^K(P_+) v_{3,j}^R \right) \right. \\ &\quad \left. + \text{tr} \left(G_k^A(P) v_{3,i+2}^H G_k^K(P_+) v_{3,j}^A \right) \right], \end{aligned} \quad (\text{C43})$$

where now the indices i and j take the values 1, 2, and the Keldysh component is given by

$$\Sigma_{ij}^K(Q) = \frac{i}{2} \int_P \text{tr} \left(G_k^K(P) v_{3,i+2}^H G_k^K(P_+) v_{3,j+2}^H \right). \quad (\text{C44})$$

The frequency integrals appearing in Eqs. (C43) and (C44) can be evaluated by straightforward application of the residue theorem: $G_k^R(Q)$ has simple poles $\omega_{1,2}^R$ given by Eq. (53) with Aq^2 and Dq^2 replaced by $p_A(q^2)$ and $p_D(q^2)$ respectively. While the poles of the advanced propagator $\omega_{1,2}^A$ are complex conjugate to the poles of the retarded propagator, $G_k^K(Q)$ has poles at both $\omega_{1,2}^R$ and $\omega_{1,2}^A$. We omit the lengthy expression for $\Sigma(Q)$ after frequency integration.

Combining Eqs. (87) and (C21), the flow equation for frequency- and momentum-dependent part of the the bare inverse propagator can be written as

$$\partial_t (\bar{P}(Q) - \bar{P}(0)) = -z^T (\tilde{\partial}_t \Sigma(Q)) z, \quad (\text{C45})$$

with the matrix z defined in Eq. (C2). Inserting this expression in the flow equations for the wave-function renormalization Z and the gradient coefficient \bar{K} , Eqs. (90) and (89) respectively, we find after some algebra,

$$\eta_Z = -\frac{1}{2} \partial_\omega \text{tr} \left[(\mathbb{1} + \sigma_y) \tilde{\partial}_t \Sigma^R(Q) \right] \Big|_{Q=0}, \quad (\text{C46})$$

$$\partial_t \bar{K}/Z = \partial_{q^2} (\tilde{\partial}_t \Sigma_{22}^R(Q) + i \tilde{\partial}_t \Sigma_{12}^R(Q)) \Big|_{Q=0}. \quad (\text{C47})$$

The real and imaginary parts of the anomalous dimension η_Z , which appear in the flow equations (C34) of the real quartic and sextic couplings, are then given by

$$\eta_{ZR} = \text{Re } \eta_Z = -\frac{1}{2} \partial_\omega \text{tr} (\sigma_y \tilde{\partial}_t \Sigma^R(Q)) \Big|_{Q=0}, \quad (\text{C48})$$

$$\eta_{ZI} = \text{Im } \eta_Z = -\frac{i}{2} \partial_\omega \text{tr} (\tilde{\partial}_t \Sigma^R(Q)) \Big|_{Q=0}. \quad (\text{C49})$$

Here we used the relation $\Sigma^R(Q) = \Sigma^R(-Q)^*$ which implies $\partial_\omega \Sigma^R(0) = -\partial_\omega \Sigma^R(0)^*$. To further evaluate η_{ZR} and η_{ZI} we switch to MATHEMATICA. The derivatives with respect to the frequency can be carried out without any difficulty and $\tilde{\partial}_t$ can be calculated as in Eq. (C28) above. Again the integral over spatial momenta is facilitated by the θ -function contained in $\tilde{\partial}_t R_{k,a}(x)$ and can be carried out analytically.

Finally, for the real and imaginary parts of the renormalized kinetic coefficient $K = \bar{K}/Z = A + iD$ we have

$$\partial_t A = \beta_A = \text{Re } \partial_t K = \eta_{ZR} A - \eta_{ZI} D - \bar{\eta}_A A, \quad (\text{C50})$$

$$\partial_t D = \beta_D = \text{Im } \partial_t K = \eta_{ZR} D + \eta_{ZI} A - \bar{\eta}_D D, \quad (\text{C51})$$

where using $\partial_{q^2} \Sigma^R(0) = \partial_{q^2} \Sigma^R(0)^*$ (note that $\Sigma(Q)$ depends only on the norm squared q^2 of the spatial momentum) we may express the quantities $\bar{\eta}_A$ and $\bar{\eta}_D$ defined in Eq. (C32) as

$$\bar{\eta}_A = -\frac{1}{A} \partial_{q^2} \tilde{\partial}_t \Sigma_{22}^R(Q) \Big|_{Q=0} = -\frac{1}{2A} \partial_{q^2}^2 \tilde{\partial}_t \Sigma_{22}^R(Q) \Big|_{Q=0}, \quad (\text{C52})$$

$$\bar{\eta}_D = -\frac{1}{D} \partial_{q^2} \tilde{\partial}_t \Sigma_{12}^R(Q) \Big|_{Q=0} = -\frac{1}{2D} \partial_{q^2}^2 \tilde{\partial}_t \Sigma_{12}^R(Q) \Big|_{Q=0}.$$

We will proceed with the evaluation of these expressions in the next section.

4. Computation of gradient coefficient anomalous dimensions

As the cutoff Eq. (54) is a non-analytic function of the momentum, the evaluation of the derivatives in Eq. (C52) requires some care. In this section we present two approaches to this problem: The first one was introduced by Wetterich in Ref.⁷² and the second one makes use of Morris' lemma.⁷⁷ Our starting point is Eq. (C43) in which we set the external frequency ω to zero. Using the shorthand $\int_{\mathbf{p}} = \int \frac{d^d \mathbf{p}}{(2\pi)^d}$ we may write

$$\Sigma^R(0, \mathbf{q}) = \int_{\mathbf{p}} \sigma^R(p_A, p_D, p_{A+}, p_{D+}). \quad (\text{C53})$$

Here and in the following for the sake of brevity we will omit the arguments in $p_a \equiv p_a(x)$ and $p_{a\pm} \equiv p_a(x_{\pm})$ for $a = A, D$, $x = q^2$ and $x_{\pm} = |\mathbf{p} \pm \mathbf{q}|^2$. The integrand in the above expression is given by the integral over the frequency component of the internal momentum $P = (\nu, \mathbf{p})$,

$$\sigma_{ij}^R(p_A, p_D, p_{A+}, p_{D+}) = \frac{i}{2} \int \frac{d\nu}{2\pi} \left[\text{tr} \left(G_k^K(P) v_{i+2}^H G_k^R(P_+) v_{3,j}^R \right) + \text{tr} \left(G_k^A(P) v_{3,i+2}^H G_k^K(P_+) v_{3,j}^A \right) \right]. \quad (\text{C54})$$

Our notation makes explicit that the momentum dependence of the regularized propagator $G_k(Q)$ is contained in the functions $p_a(q^2)$ introduced in Eq. (57). Inserting Eq. (C54) in the expressions for the anomalous dimensions Eq. (C52) we find

$$\bar{\eta}_A = -\frac{1}{2A} \partial_q^2 \Big|_{q=0} \int_{\mathbf{p}} \tilde{\partial}_t \sigma_{22}^R(p_A, p_D, p_{A+}, p_{D+}), \quad (\text{C55})$$

$$\bar{\eta}_D = -\frac{1}{2D} \partial_q^2 \Big|_{q=0} \int_{\mathbf{p}} \tilde{\partial}_t \sigma_{12}^R(p_A, p_D, p_{A+}, p_{D+}).$$

In the following we will discuss the evaluation of $\bar{\eta}_A$ while we will only state the result for $\bar{\eta}_D$. Let us begin by introducing the abbreviations $\partial_a \equiv \partial_{p_a(x)}$ and $\partial_{a\pm} \equiv \partial_{p_a(x_{\pm})}$. In the integrand we omit the arguments and write $\sigma_{22+}^R \equiv \sigma_{22}^R(p_A, p_D, p_{A+}, p_{D+})$ and $\sigma_{22-}^R \equiv \sigma_{22}^R(p_{A-}, p_{D-}, p_A, p_D)$. We recall that the derivative $\tilde{\partial}_t$ acts only on the cutoff, hence we have

$$\bar{\eta}_A = \frac{1}{2A} \partial_q^2 \Big|_{q=0} \int_{\mathbf{p}} \sum_a \tilde{\partial}_t R_{k,a}(x) \partial_a (\sigma_{22+}^R + \sigma_{22-}^R), \quad (\text{C56})$$

where we performed a change of integration variables $\mathbf{p} \rightarrow \mathbf{p} + \mathbf{q}$ in the second term.

a. Wetterich's method

Following Ref.⁷² we introduce new variables: With $y = x - k^2$ and $z = (x - k^2) \theta(x - k^2) = y \theta(y)$ we have

$$p_a(x) = a(k^2 + z). \quad (\text{C57})$$

We now use the fact that an expansion of the integrand in Eq. (C56) in powers of z_{\pm} is effectively equivalent to an expansion in q^2 : Below we will see that due to the θ -functions

contained in z_{\pm} and $\tilde{\partial}_t R_{k,a}(x)$ the integration over \mathbf{p} is restricted to a region that is $O(q)$ for $q \rightarrow 0$. In this region $p \approx k$ and the prefactor of the θ -function in the definition of z_{\pm} , therefore, is also $O(q)$. Hence we may restrict ourselves to the first order in the expansion

$$a\partial_a\sigma_{22\pm}^R = a\partial_a\sigma_{22\pm}^R|_{z_{\pm}=0} + A_{\pm}z_{\pm} + O(z_{\pm}^2), \quad (\text{C58})$$

where the coefficient of the linear term is

$$A_{\pm} = a\partial_a \sum_b b\partial_{b\pm}\sigma_{22\pm}^R|_{z_{\pm}=0}. \quad (\text{C59})$$

The zeroth order term does not depend on q and can be discarded from the expression for $\bar{\eta}_A$ which now becomes

$$\bar{\eta}_A = \frac{1}{2A} \partial_q^2|_{q=0} \int_{\mathbf{p}} \sum_a \frac{1}{a} \tilde{\partial}_t R_{k,a}(x) (A_+ z_+ + A_- z_-). \quad (\text{C60})$$

Inserting here the explicit expressions for $z_{\pm} = y_{\pm}\theta(y_{\pm})$ we find

$$\bar{\eta}_a = -\frac{1}{2A} \partial_q^2|_{q=0} (B_+ + B_-), \quad (\text{C61})$$

where using Eq. (C31) we have

$$B_{\pm} = \sum_a \int_{\mathbf{p}} \left[(2 - \bar{\eta}_a) k^2 + \bar{\eta}_a x \right] \theta(k^2 - x) \theta(y_{\pm}) A_{\pm} y_{\pm}. \quad (\text{C62})$$

Due to the first θ -function only momenta \mathbf{p} within a circle of radius k centered at the origin contribute to the integral (hence we may set $p_a(x) = ak^2$ in A_{\pm}), while the second θ -function excludes all \mathbf{p} inside a circle of radius k centered at $\mp\mathbf{q}$. In the resulting area of integration – which is itself $O(q)$ as anticipated above – we have $p \approx k$ for $q \rightarrow 0$. Without loss of generality we choose $\mathbf{q} = (q, 0, \dots)$ and decompose the integral as $\int_{\mathbf{p}} = \int_{\mathbf{p}_t} \int_{-\infty}^{\infty} \frac{dp_1}{2\pi}$, where p_1 is the component in the direction of \mathbf{q} , i.e., $\mathbf{p} = (p_1, \mathbf{p}_t)$, and $\mathbf{p}_t \in \mathbb{R}^{d-1}$. The integrand does not depend on the direction of \mathbf{p}_t , hence, using (this relation holds for $d \geq 2$; for $d = 1$ there is no integration over \mathbf{p}_t)

$$\int_{\mathbf{p}_t} f(x_t) = 2v_{d-1} \int_0^{\infty} dx_t x_t^{(d-3)/2}, \quad (\text{C63})$$

where the integration variable on the RHS is $x_t = p_t^2$, we have

$$B_{\pm} = \int_0^{\infty} dx_t \int_{-\infty}^{\infty} dp_1 \theta(k^2 - x) \theta(y_{\pm}) b_{\pm}, \quad (\text{C64})$$

where

$$b_{\pm} = \frac{v_{d-1}}{\pi} x_t^{(d-3)/2} \sum_a \left[(2 - \bar{\eta}_a) k^2 + \bar{\eta}_a x \right] A_{\pm} y_{\pm}. \quad (\text{C65})$$

In Eq. (C64) the θ -functions restrict the range of integration to

$$k^2 - p_1^2 - x_t > 0, \quad (p_1 \pm q)^2 + x_t - k^2 > 0. \quad (\text{C66})$$

The first of these inequalities allows for a solution for p_1 only if $0 < x_t < k^2$. Then it implies

$$-\alpha < p_1 < \alpha. \quad (\text{C67})$$

where $\alpha = \sqrt{k^2 - x_t}$. The second inequality is equivalent to

$$p_1 > \alpha \mp q \quad \vee \quad p_1 < -\alpha \mp q. \quad (\text{C68})$$

For B_+ we have to consider the upper sign. Then Eq. (C67) and the first inequality Eq. (C68) have the joint solution

$$\max\{-\alpha, \alpha - q\} < p_1 < \alpha. \quad (\text{C69})$$

Splitting the integration over x_t into two ranges $0 < x_t < x_{t0}$ where $x_{t0} = k^2 - q^2/4$ and $x_{t0} < x_t < k^2$ we can specify the maximum explicitly as

$$\max\{-\alpha, \alpha - q\} = \begin{cases} \alpha - q & \text{for } 0 < x_t < x_{t0}, \\ -\alpha & \text{for } x_{t0} < x_t < k^2. \end{cases} \quad (\text{C70})$$

The second inequality Eq. (C68) and Eq. (C67) do not have a common region of validity, and we find

$$B_+ = \int_0^{x_{t0}} dx_t \int_{\alpha-q}^{\alpha} dp_1 b_+ + \int_{x_{t0}}^{k^2} dx_t \int_{-\alpha}^{\alpha} dp_1 b_+. \quad (\text{C71})$$

Let us now consider B_- : Eq. (C67) and the second inequality Eq. (C68) are solved by

$$-\alpha < p_1 < \min\{\alpha, -\alpha + q\}. \quad (\text{C72})$$

where in the same ranges of x_t as above the minimum is

$$\min\{\alpha, -\alpha + q\} = \begin{cases} -\alpha + q & \text{for } 0 < x_t < x_{t0}, \\ \alpha & \text{for } x_{t0} < x_t < k^2. \end{cases} \quad (\text{C73})$$

The first inequality Eq. (C68) and Eq. (C67) can not be fulfilled at the same time. Thus we have

$$B_- = \int_0^{x_{t0}} dx_t \int_{-\alpha}^{-\alpha+q} dp_1 b_- + \int_{x_{t0}}^{k^2} dx_t \int_{-\alpha}^{\alpha} dp_1 b_-. \quad (\text{C74})$$

Now it is straightforward to carry out the integral over x_t in both B_+ and B_- and we obtain the result

$$B_{\pm} = \frac{4v_d}{d} k^{d+2} q^2 \sum_a A_{\pm}. \quad (\text{C75})$$

Inserting this in Eq. (C61) and carrying out a similar analysis for $\bar{\eta}_D$ we find

$$\begin{aligned} \bar{\eta}_A &= -\frac{4v_d}{dA} k^{d+2} \sum_{a,b} ab\partial_a \left[\partial_{b+}\sigma_{22+}^R + \partial_{b-}\sigma_{22-}^R \right]_{q=0,p=k}, \\ \bar{\eta}_D &= -\frac{4v_d}{dD} k^{d+2} \sum_{a,b} ab\partial_a \left[\partial_{b+}\sigma_{12+}^R + \partial_{b-}\sigma_{12-}^R \right]_{q=0,p=k}, \end{aligned} \quad (\text{C76})$$

where we used that setting $z_{\pm} = 0$ in these expressions is the same as setting $q = 0$ and $p = k$. The remaining derivatives can straightforwardly be performed using MATHEMATICA.

b. *Morris' lemma*

The same results can also be obtained by a direct evaluation of the derivatives in Eq. (C56),

$$\bar{\eta}_A = \frac{1}{2A} \int_{\mathbf{p}} \sum_{a,b} \tilde{\partial}_t R_{k,a}(x) \partial_a \left\{ \sum_c \partial_{b_+,c}^2 \sigma_{22+}^R p'_{b_+} p'_{c_+} (\partial_q x_+)^2 + \partial_{b_+} \sigma_{22+}^R \left[p''_{b_+} (\partial_q x_+)^2 + p'_{b_+} \partial_q^2 x_+ \right] + (+ \rightarrow -) \right\} \Big|_{q=0} \quad (\text{C77})$$

Upon setting $q = 0$ in the terms in braces, x_{\pm} are replaced by x . Then we may drop all terms that include the product $\tilde{\partial}_t R_{k,a}(x) p'_b$ as it contains θ -functions that do not have a common support: According to Eq. (C31) $\tilde{\partial}_t R_{k,a}(x)$ is proportional to $\theta(k^2 - x)$, while $p'_b(x) = b\theta(x - k^2)$. With $\partial_q x_{\pm}|_{q=0} = \pm 2\mathbf{p} \cdot \hat{\mathbf{q}}$ (here $\hat{\mathbf{q}}$ denotes the vector of unit length in the direction of \mathbf{q})

we find

$$\bar{\eta}_A = \frac{2}{dA} \int_{\mathbf{p}} x \sum_{a,b} \tilde{\partial}_t R_{k,a}(x) p''_b \partial_a \left[\partial_{b_+} \sigma_{22+}^R + \partial_{b_-} \sigma_{22-}^R \right]_{q=0}, \quad (\text{C78})$$

where we used

$$\int_{\mathbf{p}} (\mathbf{p} \cdot \hat{\mathbf{q}})^2 f(p) = \frac{1}{d} \int_{\mathbf{p}} p^2 f(p) \quad (\text{C79})$$

The second derivative $p''_b(x) = b\delta(x - k^2)$ contains a δ -function and therefore we may set $p = k$ in the terms in brackets. (Note that $p_a(x)$ is continuous at $x = k^2$.) Then, Using Morris' lemma according to which $\delta(x)\theta(x) = \frac{1}{2}\delta(x)$, we have

$$\tilde{\partial}_t R_{k,a}(x) p''_b(x) = -\frac{abk}{2} \delta(p - k). \quad (\text{C80})$$

Evaluating the integral over p with the aid of the δ -function reproduces the result Eq. (C76).

-
- ¹ I. Carusotto and C. Ciuti, *Rev. Mod. Phys.* **85**, 299 (2013).
² K. Baumann, C. Guerlin, F. Brennecke, and T. Esslinger, *Nature* **464**, 1301 (2010).
³ F. Brennecke, F. R. Mottl, K. Baumann, R. Landig, T. Donner, and T. Esslinger, *PNAS* **110**, 11763 (2013).
⁴ H. Ritsch, P. Domokos, F. Brennecke, and T. Esslinger, *Rev. Mod. Phys.* **85**, 553 (2013).
⁵ J. Kasprzak, M. Richard, S. Kundermann, A. Baas, P. Jeambrun, J. M. J. Keeling, F. M. Marchetti, M. H. Szymanska, R. Andre, J. L. Staehli, V. Savona, P. B. Littlewood, B. Deveaud, and L. S. Dang, *Nature* **443**, 409 (2006).
⁶ K. G. Lagoudakis, M. Wouters, M. Richard, A. Baas, I. Carusotto, R. Andre, L. S. Dang, and B. Deveaud-Pledran, *Nat. Phys.* **4**, 706 (2008).
⁷ G. Roumpos, M. Lohse, W. H. Nitsche, J. Keeling, M. H. Szymanska, P. B. Littlewood, A. Löffler, S. Höfling, L. Worschech, A. Forchel, and Y. Yamamoto, *PNAS* **109**, 6467 (2012).
⁸ S. A. Moskalenko and D. Snoke, *Bose-Einstein Condensation of Excitons and Biexcitons* (Cambridge Univ. Press, 2000).
⁹ J. Keeling, M. H. Szymanska, and P. B. Littlewood, in: *Nanoscience and Technology*, edited by G. Slavcheva and P. Roussignol (2010).
¹⁰ J. Clarke and F. K. Wilhelm, *Nature* **453**, 1031 (2008).
¹¹ M. Hartmann, F. Brandao, and M. Plenio, *Laser & Photonics Reviews* **2**, 527 (2008).
¹² A. A. Houck, H. E. Tureci, and J. Koch, *Nat. Phys.* **8**, 292 (2012).
¹³ J. Koch and S. Schmidt, *Ann. Phys.* **525**, 395 (2013).
¹⁴ R. Blatt and C. Roos, *Nat. Phys.* **8**, 227 (2012).
¹⁵ J. W. Britton, B. C. Sawyer, A. C. Keith, C.-C. J. Wang, J. K. Freericks, H. Uys, M. J. Biercuk, and J. J. Bollinger, *Nature* **484**, 489 (2012).
¹⁶ F. Marquardt and S. M. Girvin, *Physics* **2**, 40 (2009).
¹⁷ D. E. Chang, A. H. Safavi-Naeini, M. Hafezi, and O. Painter, *New J. Phys.* **13**, 023003 (2011).
¹⁸ M. Ludwig and F. Marquardt, *Phys. Rev. Lett.* **111**, 073603 (2013).
¹⁹ L. M. Sieberer, S. D. Huber, E. Altman, and S. Diehl, *Phys. Rev. Lett.* **110**, 195301 (2013).
²⁰ S. Utsunomiya, L. Tian, G. Roumpos, C. W. Lai, N. Kumada, T. Fujisawa, M. Kuwata-Gonokami, A. Löffler, S. Höfling, A. Forchel, and Y. Yamamoto, *Nat. Phys.* **4**, 700 (2008).
²¹ C. Ates, B. Olmos, J. P. Garrahan, and I. Lesanovsky, *Phys. Rev. A* **85**, 043620 (2012).
²² B. Olmos, D. Yu, and I. Lesanovsky, arXiv:1308.3967 (2013).
²³ T. E. Lee, S. Gopalakrishnan, and M. D. Lukin, *Phys. Rev. Lett.* **110**, 257204 (2013).
²⁴ S. De Sarkar, R. Sensarma, and K. Sengupta, arXiv:1308.4689 (2013).
²⁵ A. Janot, T. Hyart, P. R. Eastham, and B. Rosenow, arXiv:1307.1407 (2013).
²⁶ J. Berges, A. Rothkopf, and J. Schmidt, *Phys. Rev. Lett.* **101**, 041603 (2008).
²⁷ C. Scheppach, J. Berges, and T. Gasenzer, *Phys. Rev. A* **81**, 033611 (2010).
²⁸ J. Schole, B. Nowak, and T. Gasenzer, *Phys. Rev. A* **86**, 013624 (2012).
²⁹ M. Karl, B. Nowak, and T. Gasenzer, arXiv:1307.7368 (2013).
³⁰ C. Wetterich, *Phys. Lett. B* **301**, 90 (1993).
³¹ M. Wouters and I. Carusotto, *Phys. Rev. Lett.* **99**, 140402 (2007).
³² J. Keeling, P. R. Eastham, M. H. Szymanska, and P. B. Littlewood, *Phys. Rev. Lett.* **93**, 226403 (2004).
³³ M. H. Szymańska, J. Keeling, and P. B. Littlewood, *Phys. Rev. Lett.* **96**, 230602 (2006).
³⁴ J. Keeling and N. G. Berloff, *Phys. Rev. Lett.* **100**, 250401 (2008).
³⁵ M. Wouters and I. Carusotto, *Phys. Rev. Lett.* **105**, 020602 (2010).
³⁶ M. Wouters, T. C. H. Liew, and V. Savona, *Phys. Rev. B* **82**, 245315 (2010).
³⁷ P. C. Hohenberg and B. I. Halperin, *Rev. Mod. Phys.* **49**, 435 (1977).
³⁸ J. Zinn-Justin, *Quantum Field Theory and Critical Phenomena*, 4th ed. (World Scientific, Singapore, 2005).
³⁹ D. J. Amit and V. Martin-Mayor, *Field Theory, the Renormalization Group, and Critical Phenomena*, 3rd ed. (World Scientific, Singapore, 2005).
⁴⁰ S. Coleman and E. Weinberg, *Phys. Rev. D* **7**, 1888 (1973).

- ⁴¹ B. I. Halperin, T. C. Lubensky, and S.-k. Ma, Phys. Rev. Lett. **32**, 292 (1974).
- ⁴² The continuous planar rotations of $O(2)$ reflect the continuous phase rotation symmetry $U(1) \cong SO(2)$ of the driven open Bose system.
- ⁴³ N. Goldenfeld, *Lectures on Phase Transitions and the Renormalization Group*, Frontiers in Physics (Perseus Books, Reading, Massachusetts, 1992).
- ⁴⁴ It may – and does – occur as a regularization, meaning however that it has to be sent to zero in such a way that it does not affect any physical result.
- ⁴⁵ J. T. Stewart, J. P. Gaebler, and D. S. Jin, Nature **454**, 744 (2008).
- ⁴⁶ J. Berges, N. Tetradis, and C. Wetterich, Phys. Rept. **363**, 223 (2002).
- ⁴⁷ M. Salmhofer and C. Honerkamp, Progress of Theoretical Physics **105**, 1 (2001).
- ⁴⁸ J. M. Pawłowski, Annals of Physics **322**, 2831 (2007).
- ⁴⁹ B. Delamotte, arXiv:0702365 (2008).
- ⁵⁰ O. J. Rosten, Physics Reports **511**, 177 (2012).
- ⁵¹ I. Boettcher, J. M. Pawłowski, and S. Diehl, Nuclear Physics B - Proceedings Supplements **228**, 63 (2012).
- ⁵² A. Kamenev and A. Levchenko, Adv. Phys. **58**, 197 (2009).
- ⁵³ A. Altland and B. Simons, *Condensed Matter Field Theory*, 2nd ed. (Cambridge University Press, Cambridge, 2010).
- ⁵⁴ E. M. Lifshitz and L. P. Pitaevskii, *Statistical Physics, Part 2: Theory of the Condensed State*, 2nd ed., Course of Theoretical Physics, Vol. 9 (Pergamon Press, New York, 1980).
- ⁵⁵ M. Wouters and I. Carusotto, Phys. Rev. B **74**, 245316 (2006).
- ⁵⁶ T. Gasenzer and J. M. Pawłowski, Phys. Lett. B **670**, 135 (2008).
- ⁵⁷ J. Berges and G. Hoffmeister, Nucl. Phys. B **813**, 383 (2009).
- ⁵⁸ J. Berges and D. Mesterhazy, Nuclear Physics B - Proceedings Supplements **228**, 37 (2012).
- ⁵⁹ D. Mesterhazy, J. H. Stockemer, L. F. Palhares, and J. Berges, arXiv:1307.1700 (2013).
- ⁶⁰ J. Cardy, *Scaling and Renormalization in Statistical Physics* (Cambridge University Press, Cambridge, 1996).
- ⁶¹ N. Tetradis and C. Wetterich, Nucl. Phys. B **422**, 541 (1994).
- ⁶² D. F. Litim, Phys. Lett. B **486**, 92 (2000).
- ⁶³ H. Janssen, in *Dynamical Critical Phenomena and Related Topics*, Lecture Notes in Physics, Vol. 104, edited by C. Enz (Springer-Verlag, Berlin, 1979) pp. 25–47.
- ⁶⁴ C. Aron, G. Biroli, and L. F. Cugliandolo, J. Stat. Mech. **2010**, P11018 (2010).
- ⁶⁵ L. Canet, H. Chaté, and B. Delamotte, J. Phys. A: Math. Theor. **44**, 495001 (2011).
- ⁶⁶ Due to the relation $\hat{G}^K(\omega, \mathbf{q}) = -\hat{G}^R(\omega, \mathbf{q})\hat{P}^K\hat{G}^A(\omega, \mathbf{q})$, in Eq. (71) the propagators can be replaced by the inverse propagators.
- ⁶⁷ Here we denote the couplings that are not divided by Z as bare.
- ⁶⁸ R. Dashen and D. J. Gross, Phys. Rev. D **23**, 2340 (1981).
- ⁶⁹ D. F. Litim, Nuclear Physics B **631**, 128 (2002).
- ⁷⁰ R. Guida and J. Zinn-Justin, Journal of Physics A: Mathematical and General **31**, 8103 (1998).
- ⁷¹ The cancellation of η_{ZR} and η_Y can be made explicit by inserting the β -functions for κ and κ_3 , Eqs. (C55) and (C56) respectively, as well as the expression for η_D that follows from Eq. (C51), in the flow equations for $\tilde{\kappa}$ and $\tilde{\kappa}_3$. In the resulting expressions the anomalous dimensions η_{ZR} and η_Y appear only as the sum $\eta_{ZR} + \eta_Y$.
- ⁷² C. Wetterich, Phys. Rev. B **77**, 064504 (2008).
- ⁷³ D. Porras and J. I. Cirac, Phys. Rev. Lett. **92**, 207901 (2004).
- ⁷⁴ For fermions, additional signs arise due to the Grassmann nature of the fermion field, but a similar translation table exists.
- ⁷⁵ A. P. Prudnikov, Y. A. Brychkov, and O. I. Marichev, *Integrals and Series, Volume 1: Elementary Functions*, 4th ed. (Taylor & Francis, London, 1998).
- ⁷⁶ S. G. Hofer, private communication (2013).
- ⁷⁷ T. R. Morris, International Journal of Modern Physics A **09**, 2411 (1994).